Investigation of time-lapse 4D seismic tuning and spectral responses to CO_2-EOR for enhanced characterization and monitoring of a thin carbonate reservoir

by

Austin Krehel

B.S., Hope College, 2014

A THESIS

submitted in partial fulfillment of the requirements for the degree

MASTER OF SCIENCE

Department of Geology
College of Arts and Science

KANSAS STATE UNIVERSITY
Manhattan, Kansas

2017

Approved by:

Major Professor
Dr. Abdelmoneam Raef

Copyright

Abstract

Advancements, applications, and success of time-lapse (4D) seismic monitoring of carbonate reservoirs is limited by these systems' inherent heterogeneity and low compressibility relative to siliciclastic systems. To contribute to the advancement of 4D seismic monitoring in carbonates, an investigation of amplitude envelope across frequency sub-bands was conducted on a high-resolution 4D seismic data set acquired in fine temporal intervals between a baseline and eight monitor surveys to track CO_2-EOR from 2003-2005 in the Hall-Gurney Field, Kansas. The shallow (approximately 900 m) Plattsburg 'C Zone' target reservoir is an oomoldic limestone within the Lansing-Kansas City (LKC) supergroup – deposited as a sequence of high-frequency, stacked cyclothems. The LKC reservoir fluctuates around thin-bed thickness within the well pattern region and is susceptible to amplitude tuning effects, in which CO_2 replacement of initial reservoir fluid generates a complex tuning phenomena with reduction and brightening of amplitude at reservoir thickness above and below thin-bed thickness, respectively.

A thorough analysis of horizon snapping criteria and parameters was conducted to understand the sensitivity of these autonomous operations and produce a robust horizon tracking workflow to extend the Baseline Survey horizon data to subsequent Monitor Surveys. This 4D seismic horizon tracking workflow expedited the horizon tracking process across monitor surveys, while following a quantitative, repeatable approach in tracking the LKC and maintaining geologic integrity despite low signal-to-noise ratio (SNR) data and misties between surveys. Analysis of amplitude envelope data across frequency sub-bands (30-80 Hz) following spectral decomposition identified geometric features of multiple LKC shoal bodies at the reservoir interval. In corroboration with prior geologic interpretation, shoal boundaries, zones of overlap between stacked shoals, thickness variation, and lateral changes in lithofacies were

delineated in the Baseline Survey, which enhanced detail of these features' extent beyond capacity offered from well log data. Lineaments dominated by low-frequency anomalies within regions of adjacent shoals' boundaries suggest thicker zones of potential shoal overlap. Analysis of frequency band-to-band analysis reveals relative thickness variation. Spectral decomposition of the amplitude envelope was analyzed between the Baseline and Monitor Surveys to identify spectral and tuning changes to monitor CO_2 migration. Ambiguity of CO_2 effects on tuning phenomena was observed in zones of known CO_2 fluid replacement. A series of lineaments highlighted by amplitude brightening from the Baseline to Monitor Surveys is observed, which compete with a more spatially extensive effect of subtle amplitude dimming. These lineaments are suggestive of features below tuning thickness, such as stratigraphic structures of shoals, fractures, and/or thin shoal edges, which are highlighted by an increased apparent thickness and onset of tuning from CO_2.

Detailed analysis of these 4D seismic data across frequency sub-bands provide enhanced interpretation of shoal geometry, position, and overlap; identification of lateral changes in lithofacies suggestive of barriers and conduits; insight into relative thickness variation; and the ability of CO_2 tuning ambiguity to highlight zones below tuning thickness and improve reservoir characterization. These results suggest improved efficiency of CO_2 -EOR reservoir surveillance in carbonates, with implications to ensure optimal field planning and flood performance for analogous targets.

Table of Contents

List of Figures

List of Tables

Nomenclature

Acronyms & Abbreviations

AI	Acoustic Impedance
°API	API Gravity
bbl	Barrel
BHP	Bottom-Hole Pressure
CO_2	Carbon Dioxide
CO_2 -EOR	CO_2 Enhanced Oil Recovery
cP	Centipoise
DOE	Department of Energy
EOR	Enhanced Oil Recovery
GOR	Gas-Oil-Ratio
GR	Gamma Ray
GW	Guided Window
KGS	Kansas Geological Survey
LKC	Lansing-Kansas City Supergroup
LKCC	Lansing-Kansas City Supergroup Plattsburg Limestone 'C Zone'
LKCD	Lansing-Kansas City Supergroup 'D Zone'
M1	Seismic Monitor Survey #1
M2	Seismic Monitor Survey #2
M3	Seismic Monitor Survey #3
M4	Seismic Monitor Survey #4
M5	Seismic Monitor Survey #5
M6	Seismic Monitor Survey #6
Ma	Mega Annum (million years before present)
MCF	Thousand Cubic Feet
mD	Millidarcy
MMbbl	Million Barrels
MMCF	Million Cubic Feet
MMP	Minimum Miscibility Pressure
MPa	Megapascals
ms	Milliseconds
OOIP	Original Oil In Place
PPB	Parallel Progressive Blanking
RAI	Relative Acoustic Impedance
$scCO_2$	Supercritical CO_2
SNR	Signal-to-Noise Ratio
Sorw	Residual Oil Saturation after Waterflood
T-D	Time-Depth
TSS	Trace Search Shortcut
TWT	Two-Way Time
UWI	Unique Well Identifier (United States)
Vp	Compressional (P) Wave Velocity

VSP	Vertical Seismic Profile
WAG	Water Alternating Gas

Symbols

λ	Wavelength
ϕ	Porosity

Acknowledgements

I acknowledge the following people for their role in shaping my academic and professional career – directly and indirectly, and before and during my time at Kansas State University:

- **Dr. Raef** – for introducing me to the field of geophysics through interesting, challenging, and rewarding coursework. A massive thank-you for accepting me as a graduate student with short notice when I wanted and needed a change from the direction I was heading, and taking a risk with my lack of geophysics background. I appreciate the challenging, multidisciplinary thesis topic you provided me, and for all your help along the way.
- **MS thesis committee** – Dr. Totten and Dr. Chaudhuri – for their support and guidance through my MS thesis research.
- **Paul and Deana Strunk** – for their financial support to help complete my degree at Kansas State University.
- **Hope College Geology professors –** who drew my interest to pursue a career in the geosciences, laid a solid foundation of undergraduate research, provided outstanding fieldwork instruction and experience, and who were all a pleasure to learn from and work with.
- **Elizabeth Ramsey –** for her career mentorship, technical material and advice, and her contagious fascination with wavelets…but certainly not for the terrible puns she promotes.
- **The DOE and Kansas Geological Survey** – for making the extensive data set for the Hall-Gurney CO_2-EOR pilot project possible, and available. Special thanks to Paul Willhite and Lynn Watney of KGS for providing additional data upon request.

- **Ikon Science** – for their university outreach and excellent customer service, which includes their dedication and willingness to help students. Amazing company and employees – I love this software and the direction this company is going!
- **Society of Exploration Geophysicists, Chevron, and ExxonMobil** – for sponsoring student participation to educational programs (Student Education Program, Student Leadership Symposium) in addition to the SEG Annual Meeting, and providing the opportunity to gain experience outside of the classroom, and into the energy industry sector of the geosciences.
- **Chevron, Statoil, and CGG** – for continuing to sponsor SEG and AAPG student memberships.

Dedication

This work is dedicated to my parents – whose support made it possible to pursue a college education and complete Bachelor's and Master's degrees in the geosciences.

Preface

Oil and natural gas constitute the fundamental backbone of energy which has industrialized modern society. Contrary to popular ignorance, humanity will continue to demand petroleum for decades-centuries to come. Emerging global economies and continued population growth will require more oil and gas, as renewables prove to be largely uneconomic and inefficient, not to mention the fact that many renewables require petroleum. Despite the fact petroleum is a finite resource, technological advances continue to diversify assets and augment reserves as deeper, tighter, thinner reservoirs with smaller hydrocarbon saturations emerge as conventional targets to explore for, develop, and produce. The oil and gas industry is here to stay, and will continue to serve as a pinnacle of geoscience advancement.

Motivation to pursue this thesis included the opportunity to tackle a multidisciplinary problem - spanning geophysics, geology, and petroleum engineering domains - with relevancy of future business interest to the petroleum industry. Challenges of this project (onshore surveys; low SNR data; shallow, thin, oomoldic limestone reservoir) provide a unique, end-member case study of difficulty compared with conventional 4D seismic monitoring programs. Relative to siliciclastics, carbonates are less understood even though they represent a significant portion of global hydrocarbon reserves. Application of EOR methods to known carbonate targets will gain importance as easier targets become depleted.

Chapter 1 (**Introduction**) provides a brief review of the major topics for this project, including CO_2-EOR, time-lapse 4D seismic, challenges of carbonate seismology, and aspects of resolution including tuning and spectral decomposition.

Chapter 2 (**Background**) outlines details of the Hall-Gurney Field (setting, petroleum system, and production history), a characterization of the CO_2-EOR Lansing-Kansas City Plattsburg Limestone target reservoir, and covers the CO_2-EOR pilot demonstration project.

Chapter 3 (**Project Creation and Data Upload Parameters**) describes the data used and how the project was created, which may be useful in understanding the results, replicating this study, or continuing this project for future research.

Chapter 4 (**Methodology**) includes a step-by-step description of the methods employed to prepare the data for interpretation, as well as approaches taken in interpretation.

Chapter 5 (**Baseline Seismic Reservoir Characterization**) reviews the results and interpretation of the Baseline seismic survey, largely focused on spectral decomposition data. Objectives were to enhance reservoir characterization beyond detail offered from well log data in prior geological interpretations, including identification of shoal and/or facies boundaries and determination of thickness variation. Establishing a thorough Baseline Survey characterization was essential prior to investigating 4D seismic anomalies.

Chapter 6 (**CO2 Impact on Spectral Components**) covers a preliminary spatiotemporal analysis of potential 4D anomalies to expect, ambiguity of tuning introduced from CO_2 fluid replacement with reservoir thickness variation, and the results and interpretation of changes in spectral and tuning effects from the Baseline to Monitor Surveys.

Chapter 1 - Introduction

CO_2-Enhanced Oil Recovery

Once primary and secondary production of a reservoir becomes uneconomic, enhanced oil recovery (EOR) can be applied as a tertiary stage to mobilize bypassed and residual oil remaining in the reservoir. EOR can significantly extend the economic life of a field and maximize ultimate recovery of original oil in place (OOIP) beyond primary and secondary production stages. EOR methods range from gas (CO_2, N_2, CH_4), chemical (acid, surfactant, polymer), and thermal (steam, fire) stimulation methods. CO_2-EOR is attractive due to high supply, low cost relative to other solvents, and CO_2 behavior with hydrocarbons. Typical CO_2-EOR operations inject CO_2 into a pressurized reservoir with the aim of achieving miscibility between oil and CO_2. Re-pressurizing a reservoir is commonly conducted through waterflooding, or secondary recovery, following primary production. Waterflooding provides insight into CO_2-EOR feasibility, as reservoirs successful with waterflooding are typically prime candidates for CO_2-EOR flooding (DOE/NETL, 2010).

CO_2 has potential to exist in gas, liquid, and supercritical fluid phases in the subsurface, which is largely dependent on temperature and pressure. The objective of most CO_2-EOR operations is to inject supercritical CO_2 ($scCO_2$) into a reservoir at pressures and temperatures which allow CO_2 to persist in the supercritical fluid phase. CO_2 exists as a supercritical fluid phase above its critical pressure (7.4 MPa) and critical temperature (31°C), as shown with bulk modulus and density relations in Figure 1.1 (Yam and Schmitt, 2011). Exhibiting properties between gas and liquid phases, $scCO_2$ behaves with gas mobility, and fluid density and miscibility. This advantageous combination of properties allows CO_2 to disperse throughout the EOR target and mobilize bypassed and residual oil. Low surface tension and viscosity of $scCO_2$

lowers oil viscosity once CO_2-oil miscibility is achieved (Verma, 2015), which eliminates interfacial tension between the oil and reservoir and increases oil's effective permeability. Assuming relatively stable reservoir temperatures, pressure decline is the most concerning factor in maintaining CO_2 in a supercritical fluid phase, and ultimately allowing CO_2-oil miscibility.

Miscibility of $scCO_2$ with hydrocarbons requires meeting or exceeding the minimum miscibility pressure (MMP), which varies as a function of temperature and fluid properties. Factors which contribute to a lower effective MMP include higher °API oil and higher temperatures. Above the MMP, dynamic miscibility is achieved through vaporization and condensation gas-drive processes in which hydrocarbons vaporize into the CO_2 and CO_2 dissolves into hydrocarbons, respectively, to create a single-phase homogeneous fluid (Verma, 2015). In theory, these phenomena create transition zones within the reservoir where vaporization gas-drive processes dominate near CO_2 injectors and condensation gas-drive processes dominate near producing wells (Verma, 2015). This strategy aims to produce an oil bank at the flood front, which is driven toward producing wells. Determining CO_2-EOR reservoir candidates therefore requires screening to ensure CO_2 can sustain in a supercritical phase, and MMP can be reached between CO_2 and oil.

Designing a CO_2-EOR program requires configuration of a well pattern and injection scheme. Well pattern design must consider well spacing and the number of wells on board for injection, production, and monitoring. Injection considerations include timing of injected fluid(s) within the well pattern, alternating fluid injected by well, and injectivity. CO_2 is injected either continuously or alternated with slugs of water injection, known as water-alternating-gas (WAG) injection. WAG is carried out in order to reduce the effect of CO_2 fingering. These criteria can be adjusted following the commencement of CO_2-EOR operations to optimize recovery. Applying

various geophysical, geological, geochemical, and engineering methods has proven powerful in monitoring subsurface fluid response to injection and production, which can provide insight into mechanisms controlling fluid flow and allow adjustments for CO_2-EOR optimization.

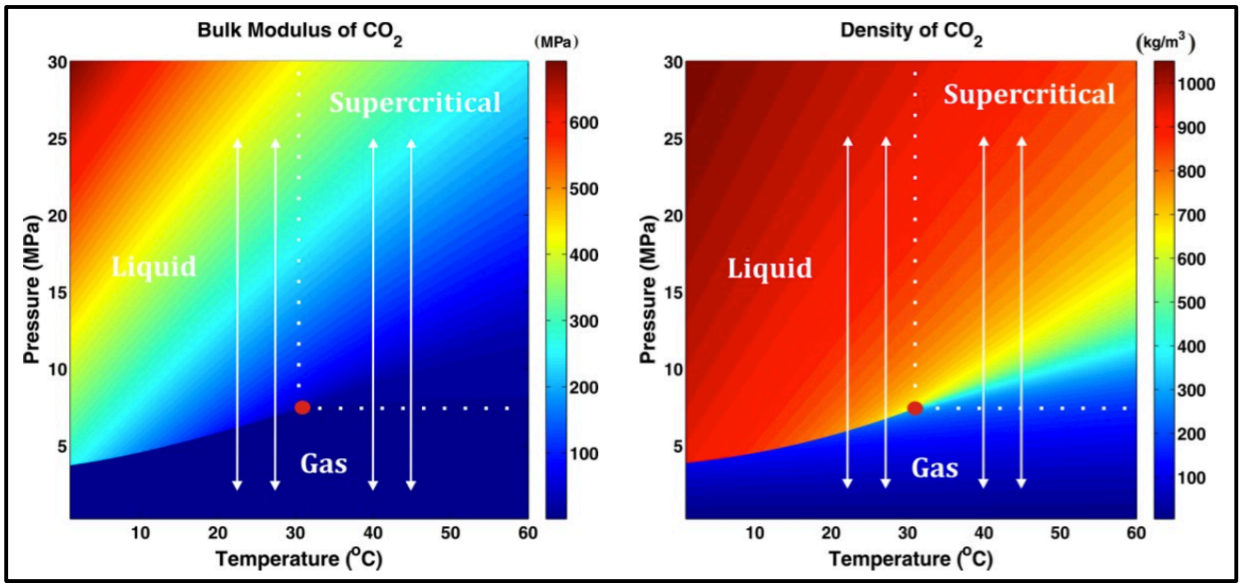

Figure 1.1: CO_2 phase, bulk modulus, and density as a function of pressure and temperature, CO_2 exists as a supercritical fluid at temperatures and pressures exceeding the dotted white lines extending from the critical point (red dot). After Figure 1 in: Yam and Schmitt (2011).

Time-Lapse 4D Seismic

In the petroleum industry, time-lapse seismic is a surveillance tool to detect, monitor, and verify subsurface changes over calendar time associated with injection and production activity in reservoirs. Time-lapse seismic surveying requires the acquisition of an initial baseline survey to capture subsurface properties prior to the onset of production and/or injection, with at least one monitor survey obtained in replication of baseline acquisition criteria to determine changes in the seismic data caused by altered rock, fluid, or environmental variables. Although time-lapse seismic studies can be conducted with vertical seismic profiles (VSP) and 2D seismic surveys, the majority of time-lapse application includes repeated 3D seismic reflection surveys. The

additional dimension of elapsed calendar time between 3D seismic surveys gives rise to the term '4D seismic'.

Since seismic data are composed entirely of amplitude, frequency, phase, and two-way time (TWT) arrival, at least one of these fundamental attributes requires alteration between surveys to yield an observed difference. Changes in seismic data character between data sets give rise to 4D seismic anomalies, which can provide valuable insight into subsurface changes occurring over calendar time. 4D seismic anomalies are not entirely indicative of physical changes occurring in the subsurface, as non-repeatable noise may contribute to 'observed' changes in the seismic character between surveys. Environmental factors, along with rock and fluid properties capable of influencing the reflective character of sedimentary rocks at depth, are included in Table 1.1, modified after Wang (2001) and Johnston (2013), wherein relationships of these rock-fluid-environmental criteria with seismic data are included. It is important to note the inherent complexity in delineating the primary variable(s) generating a 4D seismic anomaly, based on the interplay between these criteria. Furthermore, the responses of 4D seismic anomalies to actual subsurface physical changes are not necessarily linear.

4D seismic anomalies can be observed through simple qualitative comparison, quantitative differencing of data, and normalization of data sets. Qualitative comparison between surveys of seismic events' attributes, spatial and temporal position, and TWT thickness can be especially powerful where significant 4D seismic anomalies exist. Quantitative differencing of 4D seismic surveys removes overlap of invariable static data, resulting in a residual dataset characteristic of spatial and temporal anomalies attributed to injection and production activity, and non-repeatable noise. Normalizing the data sets can provide similar results to differencing without actually removing components of the data. Common 4D seismic anomalies produced

from CO_2 fluid replacement include increased apparent temporal thickness of seismic reflectors, apparent time-depth (T-D) shift of seismic reflectors beneath the CO_2 plume, and attenuation of higher frequencies in the seismic data.

To assess 4D seismic feasibility, a multitude of reservoir and seismic criteria should be considered to ensure 4D seismic anomalies are seismically representative of changes onset by injection and production. These subsurface changes must be detectable, and the monitor survey(s) must be repeatable in order to justify a 4D seismic survey. Lumley et al. (1997) provide a '4-D Technical Risk Spreadsheet', which assembles the principal variables which affect 4D seismic data (Table 1.2), and scores these criteria. Additional factors to consider are turnaround time expected between seismic acquisition and processed data, and how the data are to be implemented for reservoir modeling. Ultimately, 4D seismic programs are time- and cost-intensive, and must make economic sense to implement.

Determining when and where subsurface changes are occurring in response to production and/or injection is the ultimate goal of 4D seismic surveying, which is dependent on detectability potential. Between surveys, at least one rock, fluid, or environmental criterion influencing the seismic character must undergo a sufficient magnitude of change to produce a meaningful and detectible 4D seismic anomaly. Although a change in one of these criteria between surveys may exceed the threshold to be detected, changes in other criteria may interfere with, and neutralize, the capacity of detection. Furthermore, detectable changes are not always resolvable with conventional seismic interpretation, and may require a deeper investigation of the data with more quantitative scrutiny.

In addition to detectability, repeatability is a critical element in 4D seismic surveying. In order to image 4D seismic anomalies representative of subsurface changes onset by production

and/or injection, a multitude of acquisition variables must be reproduced in each 3D seismic survey, with minimal variance. For onshore 4D seismic surveys, these variables include acquisition geometry, near surface factors, noise, and geologic considerations (Johnston, 2013), which are displayed in Table 1.3.

Observing subsurface changes through 4D seismic surveying has applications in monitoring primary, secondary, and tertiary production, constraining reservoir models via history matching, and enhancing reservoir characterization in areas with sparse or absent well data. 4D seismic monitoring during all stages of hydrocarbon production can effectively detect and track subsurface fluid movement, delineate mechanism(s) controlling fluid flow, predict future movement and breakthrough at wells, and identify un-swept, compartmentalized zones which may hold significant infill drilling potential. O'Brien et al. (2010) demonstrate the value of 4D seismic surveying with a multitude of monitor surveys acquired in fine time steps, which can add significant potential in tracking reservoir changes, predicting future flow, determining sweep efficiency, and improving reservoir characterization. 4D seismic is proven effective in monitoring CO_2-EOR, and attaining additional knowledge of – and certainty within – the reservoir required to modify well patterns and/or adjust injectivity to optimize recovery. 4D seismic technology is, however, largely applied to prolific siliciclastic targets located in offshore fields. In contrast, application of 4D seismic monitoring to shallow, onshore, thin, carbonate reservoirs is inherently challenging. These elements, alone or in combination, generally drive a 4D seismic monitoring program outside of the justifiable risk envelope.

ROCKS	FLUIDS	ENVIRONMENTAL
Compaction	Viscosity	Frequency
Consolidation	Density	Stress history
Age	Wettability	Depositional environment
Cementation	Composition	Temperature
Texture	Phase	Reservoir process
Density	Gas-Oil, Gas-Water ratios	Production history
Clay content	Saturation	Layer geometry
Anisotropy		Net reservoir pressure
Fractures		
Porosity		
Lithology		
Pore shape		

Table 1.1: Rock, fluid, and environmental parameters which influence the character of seismic reflectivity. Modified after Wang (2001) and Johnston (2013).

VARIABLE	IDEAL
Reservoir	
Depth	Shallow
Overburden Pressure	Low
Pore Pressure	High
Net Pressure	Low
Temperature	High
Unit Thickness	High
Seismic	
Dominant Frequency	High
Average Resolution (ft)	Low
Image Quality	High
Repeatability	High
Fluid Contact Visibility	High
Predicted Travel Time Change	High
Predicted Impedance Change	High
Fluids	
Fluid Saturation Change	High
Fluid Compression Contrast	High
Rock	
Dry Bulk Fluid Modulus	Low
Dry Density	Low
Porosity	High
Oil	
Solution GOR	High
API Gravity	High
Density	Low
Bulk Modulus	Low
Water	
Salinity	High
Density	High
Bulk Modulus	High
Gas	
Density	Low
Bulk Modulus	Low

Table 1.2: Ideal relative properties of key variables to consider when assessing 4D seismic feasibility, modified after Lumley et al. (1997).

Category	Repeatability Variables
Acquisition-geometry	Source-receiver spacing
	Coverage obstructions
Near-surface	Statics
	Receiver coupling
Noise	Ambient
	Shot-generated
	Residual multiples
Geologic	Shallow gas
	Steep dips
	Fault shadows
	Producing reservoirs

Table 1.3: Variables affecting repeatability of onshore 4D seismic surveys, modified after Johnston (2013).

Seismic Expression of Carbonates

After nearly one century of development in acquisition, processing, and interpretation, the application of reflection seismology for petroleum exploration and exploitation remains better understood in siliciclastic systems than carbonates, despite the latter exceeding half of worldwide hydrocarbon reserves (Palaz and Marfurt, 1997). The complex nature of carbonate systems can pose significant difficulty with identifying and characterizing carbonate reservoirs in 2D and 3D seismic data. 4D seismic programs applied to carbonate reservoirs bear greater challenges than siliciclastics since velocity changes in carbonates are less sensitive to saturation and pressure changes onset by production and/or injection activity. The uncertainties inherent with 4D seismic anomalies in carbonates yield observations more difficult to understand and classify with confidence during reservoir monitoring.

Relative to siliciclastics, carbonates contain greater diversity with respect to mineralogy, facies, pore type, and diagenetic alteration, which creates complexity with understanding and quantifying petrophysical properties. Porosity and permeability distribution can differ greatly from the distribution of carbonate depositional facies, especially when exposed to diagenetic and

overprinting phenomena (Skirius et al., 1999). Carbonates are characteristic of small acoustic impedance (AI) contrasts, which occur between carbonates containing similar mineralogy, as well as between hydrocarbon-bearing carbonate reservoirs and the overlying seal (Skirius et al., 1999). Carbonates typically contain higher interval velocities than siliciclastics, which creates multiples in the data in addition to reducing resolution (Sarg and Schuelke, 2003). Carbonate deposition can produce much steeper slopes than siliciclastics, which is problematic for seismic imaging (Sarg and Schuelke, 2003). Evaporites associated with carbonate depositional environments can create complex structures and reduce resolution beneath evaporites (Sarg and Schuelke, 2003). The inherent heterogeneity of carbonates generates uncertainty, especially when attempting to determine porosity and permeability distribution, and can render reservoir characterization and prediction unattainable.

Beyond the complexity diagenesis can impose on secondary porosity, carbonates contain a greater variety of pore types than siliciclastics. Whereas siliciclastics are dominated by intergranular porosity, carbonates contain moldic, vuggy, interparticle, and intraparticle pore types (Xu and Payne, 2009). Results from Xu and Payne (2009) indicate for a given porosity, 40% difference in P-wave velocity (Vp) can occur from variance in pore shape alone. Pore aspect ratio – the ratio of a pore's short axis to long axis – provides a quantitative classification of pore shape which can be used to explain velocity perturbations and allow pore shape to be inverted from seismic data. Moldic, intraframe, and vuggy pores have high pore aspect ratios, which contribute to a stronger rock frame and allow propagation of higher seismic velocities (Xu and Payne, 2009). Pores with small aspect ratios, such as microcracks and fractures, have the opposite effect and reduce seismic velocities (Xu and Payne, 2009). Since pore phenomena are fundamentally more complex in carbonates relative to siliciclastics, acoustic analysis of

carbonates should consider all pore types in a multi-pore system and associated shapes, in addition to porosity. Abrupt lateral and vertical pore type variation associated with rapid changes in carbonate lithofacies can create significant scatter in the velocity-porosity relationship, and linking the acoustic velocity response to lithofacies demands rock physics modeling with pore geometry and mineralogy considerations (Chen et al., 2008).

Resolution, Tuning, and Spectral Decomposition

The limit of minimum thickness to which layers are identified and distinguished from their confining layers varies between exploration methods. Principally, these include downhole well logging and seismic reflection techniques. While both methods depend on data quality to yield interpretable certainty, key differences separate their capacity to image thin layers. Whereas downhole methods' resolution is dependent upon length of sample interval, seismic resolution is dependent on temporal sampling interval, data bandwidth, dominant frequency, and depth, thickness, and acoustic properties of the target interval. Vertical seismic resolution is defined by the ability to distinguish adjacent stratigraphic units exhibiting a contrast in acoustic propagation from variance in rock and fluid properties.

In the seismic domain, conventional thickness is met when the T-D separation of amplitude events (peak, trough, zero-crossing) constituting a geologic layer's top and base are proportional to the layer's actual thickness – determined using interval velocity. The ability of a layer's top and base to be resolved and separated proportional to actual thickness is dependent on the signal wavelength (λ), which is proportional to velocity (v) and inversely proportional to frequency (f): ($\lambda = v/f$). In theory, the minimum limit to which conventional seismic thickness is sustained – the tuning thickness – is defined by one-quarter of the dominant wavelength ($\lambda_d/4$) for full-band data or a sub-band of the data, and one-quarter of the wavelength ($\lambda/4$) for a

discrete frequency. Tuning thickness may vary from this theoretical limit, and by the words of Yogi Berra, "in theory there is no difference between theory and practice; in practice there is." At tuning thickness, reflections from the layer's top and base interfaces undergo maximum constructive interference and create a composite response of the amplitude reflection event (peak, trough), typically on the order of 1.5 times the maximum amplitude achievable in absence of tuning impact. Tuning thickness is therefore the minimum thickness – in consideration of acoustic and reflected signal properties – to which measurements can be accurately made between two reflectors (Lee et al., 2009). For thickness below tuning thickness, T-D separation between adjacent reflectors overestimates actual thickness.

Tuning is a phenomenon which deviates the amplitude reflection response from the natural strength expected from an interface's AI contrast. In theory, the effect of tuning is maximized at the tuning thickness ($\lambda/4$) and reduced with thickening and thinning to $\lambda/2$ and $\lambda/8$, respectively. This means for a thinning layer, tuning effects onset at $\lambda/2$ and increase until a maximum response at $\lambda/4$, and then decrease via destructive interference until $\lambda/8$ – the theoretical threshold of resolution (Widess, 1973). Like the determination of tuning thickness, these tuning effects depend on interplay between interval velocity, thickness, and the bandwidth of the source signal. These criteria are theoretical, and the onset of tuning, transitions between constructive and destructive interference, and point of tuning thickness can vary based on wavelet stability, noise, and heterogeneity, amongst other variables.

Widess (1973) outlines the theoretical seismic context of thin beds. As destructive interference increases with thinning from tuning thickness ($\lambda/4$), the reflection properties from the layer's top and base progressively amalgamate until the theoretical threshold of resolution ($\lambda/8$) is reached (Widess, 1973). For beds equal to and less than $\lambda/8$ thickness, the reflection

properties from the top and base interfaces of a layer are combined, resulting in a composite, non-unique amplitude response which may apply to a variety of thin beds (Widess, 1973). These tuning relationships are represented through a wedge model in Figure 1.2, which reveals amplitude variation with bed thickness.

Spectral decomposition refers to a range of time-frequency analyses capable of converting seismic data from the time domain into the frequency domain by use of the Fourier Transform (Partyka et al., 1999). Applications of spectral decomposition in seismic interpretation include thickness estimation, identification of discontinuities, hydrocarbon detection, and stratigraphy prediction. Partitioning the full-band seismic data into discrete frequencies and/or frequency sub-bands allows amplitude tuning effects to be visualized in time-depth and spatially. With layer thickness and interval velocity information at a well, the observed tuning frequency at this location can be used to compare this with the theoretical tuning frequency expected. Based on the theoretical-observed relationship, tuning effects at discrete frequencies associated with the layer can be used to extrapolate layer thickness away from well control for relative and/or absolute thickness estimation. Differences between laterally-adjacent facies of the same thickness which may impact wave propagation, and therefore highlight discontinuities between the facies, including mineralogy, porosity and permeability (fractures), fluid(s) present and saturation, amongst other variables. The ratio of spectral components' data can provide insight into these discontinuities and highlight zones containing high- and low-frequency anomalies.

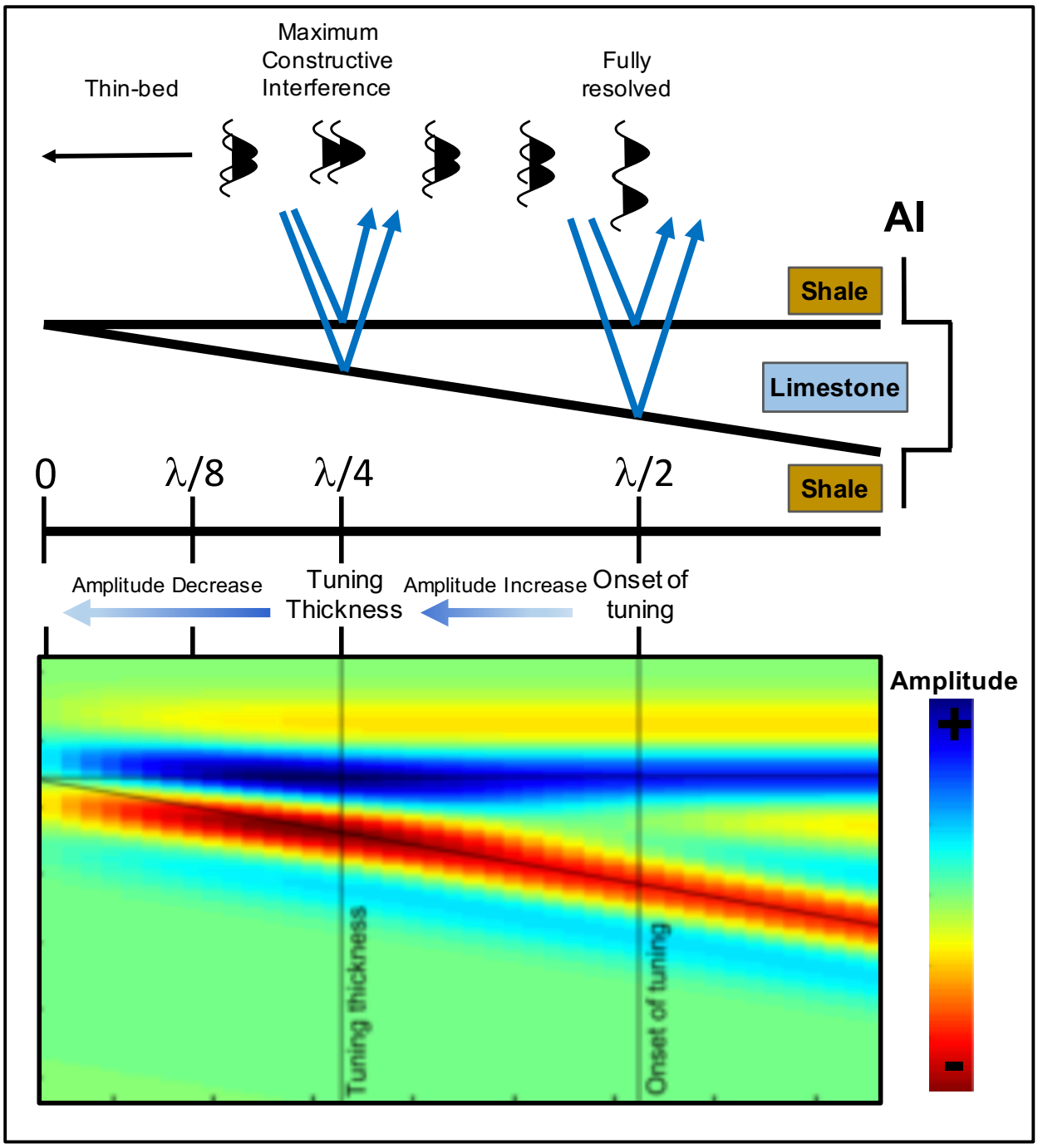

Figure 1.2: Relationship between layer thickness and tuning phenomena for an acoustically hard reservoir in a wedge model. The onset of tuning from a composite amplitude response occurs below λ/2, in which reflections from a layer's top and base interfaces undergo constructive interference. This tuning effect is maximized at λ/4, and the effect decreases until λ/8, the point of thin-bed thickness. Amplitude model modified after Agile Geoscience (2011).

Chapter 2 - Background

The Reservoir Depositional Classification System applied EOR technology - previously untested in the selected region - to one of 22 (16 siliciclastic, 6 carbonate) geologically-classified depositional plays, or reservoir classes, displayed in Figure 2.1 (DOE/NETL, 2008). This reservoir classification system categorizes sedimentary reservoirs by depositional environment, whose geologic variables provide a set of rock properties unique - and with definable limits - to each reservoir class (DOE/NETL, 2008). This initiative was funded by the Department of Energy (DOE) in response to rapid decline of domestic U.S. oil production over the late twentieth century. DOE funding allowed EOR methods to be tested in reservoir classes considered risky and/or uncertain by industry, with intent of exposing specific technologies' applicability to specific reservoir classes, and ultimately revealing recoverable potential in genetically similar reservoirs (DOE/NETL, 2008).

The Class Revisit project - "Field Demonstration of Carbon Dioxide Miscible Flooding in the Lansing-Kansas City Formation, central Kansas" (Project ID: DE-FC26-00BC15124) - was awarded in October 1999 to determine CO_2-EOR feasibility in a class II Shallow shelf carbonate reservoir (DOE/NETL, 2008). The Lansing-Kansas City (LKC) Supergroup's Plattsburg Limestone 'C Zone' was selected as the miscible CO_2-EOR target in the Carter-Colliver Lease of Hall-Gurney Field for the Class Revisit project**.** This project was completed between March 2000 and March 2010 in three phases – reservoir characterization, field implementation, and monitoring. Detailed reservoir characterization was conducted on historical data and additional data acquired prior to CO_2-EOR field implementation and 4D seismic monitoring, and saw progressive improvement throughout the project.

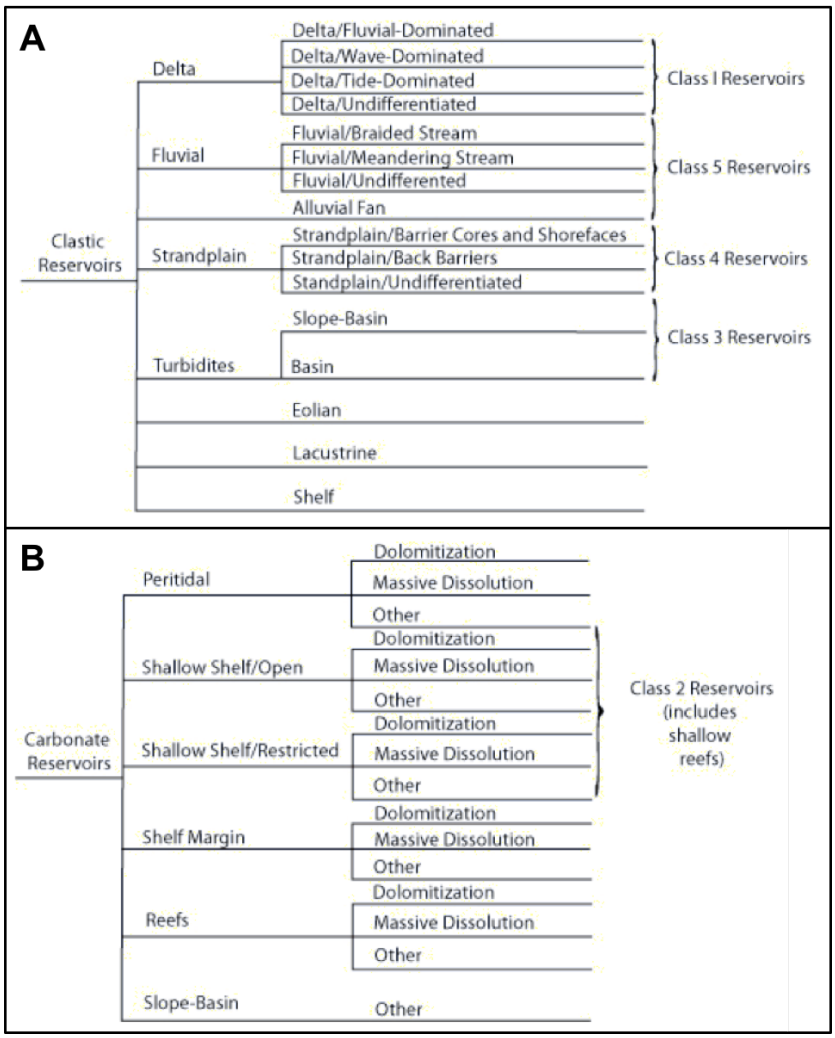

Figure 2.1: Categorization of 22 geologically defined reservoirs, with a class system (1=highest; 5=lowest) adopted to proportionally rank remaining OOIP in, at the time of publication, approximately two-thirds of domestic U.S. oil resources. (A) Siliciclastic reservoirs (n=16) include Class 1, 3, 4, and 5 Reservoirs, and are classified by mode of transport and deposition. (B) Carbonate reservoirs (n=6) include Class 2 Reservoirs, and are classified by depth of water and biogenic formation, and facies and diagenesis. (A) and (B) after Figure 1 and Figure 2, respectively, in: DOE/NETL (2008).

Hall-Gurney Field

Regional Context

The 24,299-acre Hall-Gurney Field is located in central Kansas within the Central Kansas Uplift geologic province (Figure 2.2). The Central Kansas Uplift is a major northwest-southeast trending structural feature, which likely formed between mid-Mississippian (post-Meramecian stage, 340-355 Ma) and mid-Pennsylvanian (between Morrowan and Desmoinesian stages, 310-330 Ma) (Merriam, 1963). A Mississippian-Pennsylvanian unconformity exists where Mississippian strata are absent beneath Pennsylvanian strata on the Central Kansas Uplift, in addition to other structural highs as seen in Figure 2.3 (Merriam, 1963). Merriam (1963) indicates Mississippian strata once completely covered Kansas, but were eroded from these uplifted areas. As the largest positive structural feature in Kansas, the Central Kansas Uplift occupies approximately 5,700 square miles and contains a maximum post-Precambrian sedimentary thickness of 5,000 feet (Merriam, 1963). The majority of Hall-Gurney Field lies within Russell County (T14S-R14W; T14S-R13W; T14S-R12W; T15S-R14W; T15S-R13W; T15S-R12W;), with a small southeastern portion of the field extending into Barton County (T16S-R12W), as seen in Figure 2.4 (KGS, 2011).

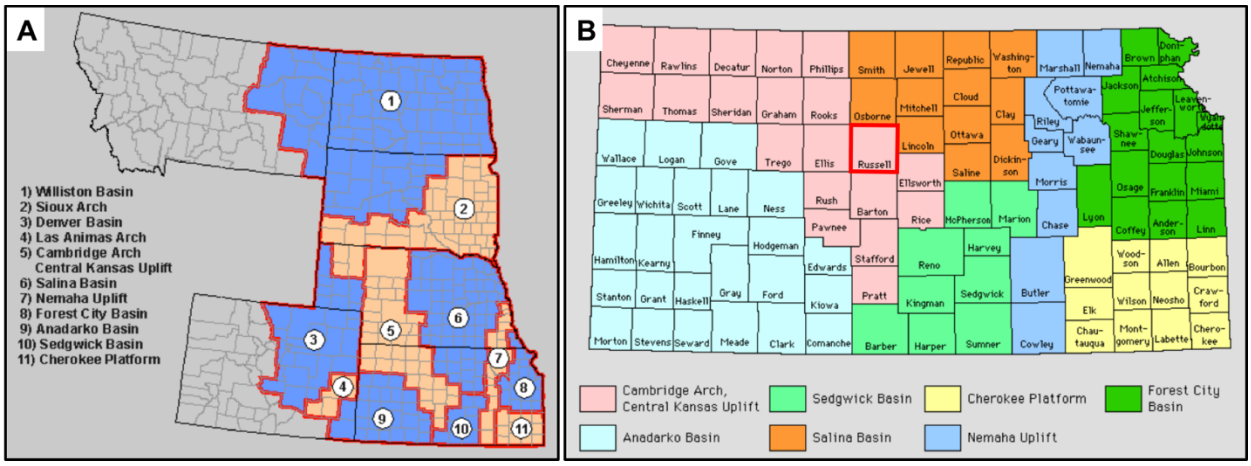

Figure 2.2: Geologic provinces mapped (A) through the Northern Mid-Continent, and (B) by Kansas counties, with Russell County outlined in red. (A) and (B) modified after KGS (1996b) and KGS (1996a), respectively.

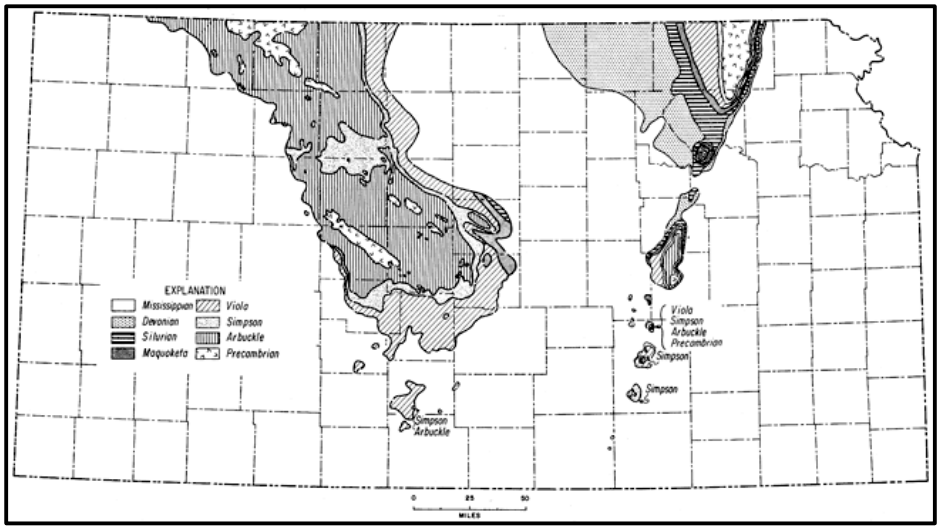

Figure 2.3: Geologic map of Kansas showing age of rocks underlying Pennsylvanian strata. A post-Mississippian, pre-Pennsylvanian unconformity outlines major tectonic structures which likely developed between mid-Mississippian and mid-Pennsylvanian. Mississippian rocks are absent beneath Pennsylvanian strata on the Cambridge Arch, Central Kansas Uplift, Pratt Anticline, and Nemaha Anticline. After Figure 95 in: Merriam (1963).

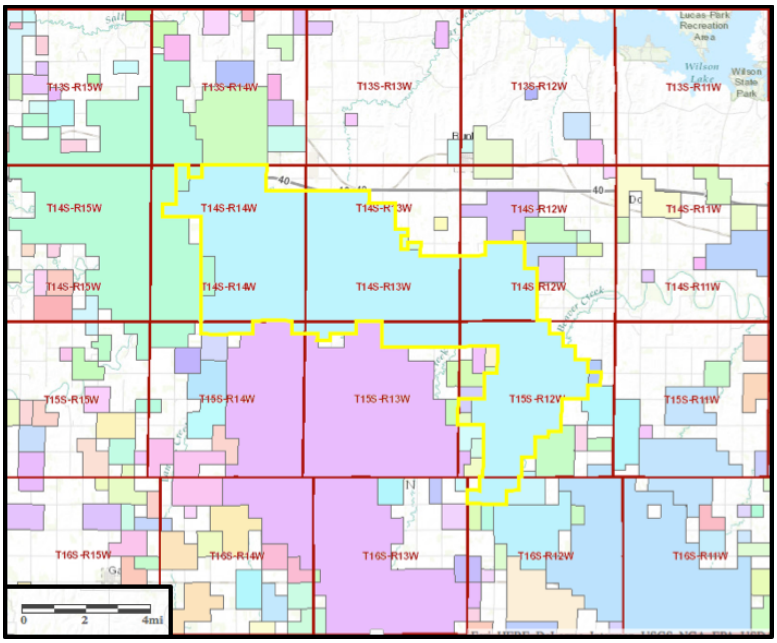

Figure 2.4: Township-range map of Hall-Gurney Field within Russell and Barton Counties, Kansas, outlined in yellow. Modified after KGS (2011).

Petroleum System

Higley (1995) categorizes six conventional petroleum plays primarily by age within the Central Kansas Uplift, which include the Permian, Mississippian-Devonian, Pennsylvanian Cyclical Carbonates and Sandstones, Ordovician, and Early Ordovician-Cambrian Arbuckle (Higley, 1995). Carbonates dominate production from the Pennsylvanian Cyclical play, which produces from the following units: Wabaunsee, Shawnee, Douglas, Lansing, Kansas City, Marmaton, Cherokee, and the informal Pennsylvanian conglomerate and basal Pennsylvanian sandstone (Higley, 1995). As seen in Figure 2.5A, petroleum production within the Central Kansas Uplift is dominated by oil, with a minor gas component. Russell County oil, gas, and oil and gas fields surrounding the prolific Hall-Gurney oilfield are presented in Figure 2.5B. Within Hall-Gurney, seven producing formations (with approximate depth in feet) identified by KGS (2016) include the Wabaunsee (2,400), Shawnee (2,675), Douglas (2,828), Pennsylvanian Sand (2,813), LKC (2,985), Cambrian (3,156), and Arbuckle (3,192). The remainder of discussion will

focus on the LKC petroleum system within the Hall-Gurney Field – the only LKC giant oil field (Newell et al., 1987).

The multi-pay zone LKC is characterized by thin, cyclical, carbonate-shale successions. The subject of LKC source rocks, and subsequent hydrocarbon generation and migration, has conflicting standpoints since Pennsylvanian shales are considered thermally immature within the Central Kansas Uplift. One model suggests oil migrated northward from the Anadarko Basin at some point between the Pennsylvanian-Permian (Higley, 1995). Another model proposes the role of radioactivity to onset hydrocarbon generation above the conventional oil window, which only considers thermogenic maturation (Kelly, 2014). Potential source rocks containing exceptionally high gamma radiation include black marine shales, which commonly overlay a lower transgressive limestone within the four-component LKC cyclothem (Newell et al., 1987). Pennsylvanian LKC carbonate reservoirs were deposited across the Central Kansas Uplift, over structurally deformed, pre-Mississippian strata (Baars et al., 1993) following the erosion of Mississippian strata seen in Figure 2.3. Typical reservoirs are regressive limestone members within the cyclothem sequences which comprise the LKC. As regional subsidence commenced, basins proximal to the Central Kansas Uplift subsided at significantly faster rates than the uplift, creating a depositional environment along the uplift which formed complex structural and structural-stratigraphic combination traps (Baars et al., 1993), of which oil accumulates predominately in anticlines (Higley, 1995). Depositional complexity was exacerbated by tectonic activity from the Early Pennsylvanian to Early Permian due to collision between North American and South American-African plates, and glacioeustatic control on sea level fluctuation (Baars et al., 1993). LKC interbedded shales likely serve as seals for these stacked reservoirs.

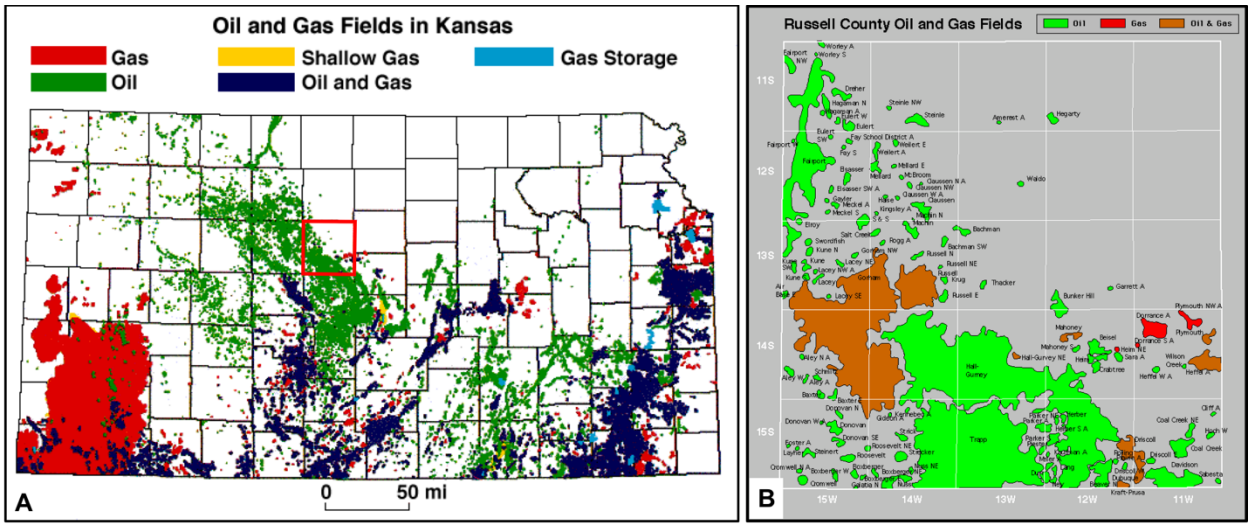

Figure 2.5: Distribution of oil and gas (A) throughout Kansas (Russell County outlined in red), and (B) by field within Russell County. (A) and (B) modified after KGS (1997) and KGS (2000), respectively.

Production History

The Hall-Gurney Field discovery well – the J.J. Hall and Russell Oil Corporation No. 1 Miller – was drilled in SW1/4SE1/4SE1/4 section 30, T14S-R13W in May 1931 (Riggs et al., 1963). The field was extensively developed in 1941, saw declining production during World War II with subsequent field development following the war, and significant decline in oil production by 1960 (Riggs et al., 1963). Hall-Gurney LKC reservoirs underwent primary production via solution gas drive until approximately 1958 (Willhite et al., 2012). Waterflooding was introduced to the field during the 1950s-1960s, and largely reached its economic limit through the 1970s-1980s (Dubois et al., 2001), with the majority of Hall-Gurney LKC zones shut-in by 1984 (Willhite et al., 2012) – leaving significant potential of bypassed oil for tertiary recovery. LKC reservoirs in Northern and Central Kansas are typically characteristic of solution gas drive, with typical primary recovery less than 20% OOIP, and secondary recovery less than 19% OOIP (Watney, 1994). The Hall-Gurney Field's poor waterflood performance is associated with

reservoir heterogeneity, weak driving mechanism, and commingled production from stacked reservoirs (Watney, 1994).

In 2001, the LKC accounted for approximately 59% of the Hall-Gurney Field's cumulative production, and a total 1,200 MMbbl from 3,500 Kansas oilfields (Dubois et al., 2001). As of March 2016, 1,285 of 3,173 total wells remain oil-productive within the Hall-Gurney Field, which has yielded 163.34 MMbbl since the 1931 discovery (KGS, 2016). As of July 1994, the field contained 7 gas-productive wells and a cumulative 710.86 MMCF produced (KGS, 2016).

Lansing-Kansas City Reservoir Characterization

Depositional Setting and Regional Stratigraphy

The Lansing Group and Kansas City Group commonly amalgamate in the subsurface, which gives rise to their common supergroup reference as the Lansing-Kansas City (LKC) (Newell et al., 1987). As shown in Figure 2.6, the LKC was deposited throughout the U.S. Midcontinent during the Missourian Stage of the Upper Pennsylvanian – roughly concomitant with the global Kasimovian Stage. The LKC top-structure of Kansas is mapped in Figure 2.7, along with a green overlay of oil production. Between the Middle Pennsylvanian and Early Permian, North America's Midcontinent region underwent a series of sea-level fluctuations dominated by glacioeustatic control (Algeo and Heckel, 2008). A visualization of these sea-level changes is depicted in North American paleogeographic reconstructions from the Early Mississippian to Early Permian, displayed in Figure 2.8.

The development of an epicontinental sea with sea level fluctuation is apparent between Figure 2.8C-E, with Kansas' current geographic position outlined for context. In response to these recurrent marine transgressions and regressions, LKC stratigraphy is dominated by

cyclothemic successions of interbedded limestones and shales. Midcontinent Middle-Late Pennsylvanian cyclothems of all scales (major, intermediate, minor) are greatest in number near the shelf-basin margin (present day Kansas-Oklahoma border), and reduce northward with pinching out of minor cycles (Heckel, 2008). These LKC cyclothems are characterized by four-component stratigraphically-upward sequences of a transgressive carbonate, marine shale, regressive carbonate, and a regressive shale (Watney, 1980). A detailed geologic characterization of these Midcontinent cyclothems' formation and characteristics is modeled in Figure 2.9 and further described in Table 2.1.

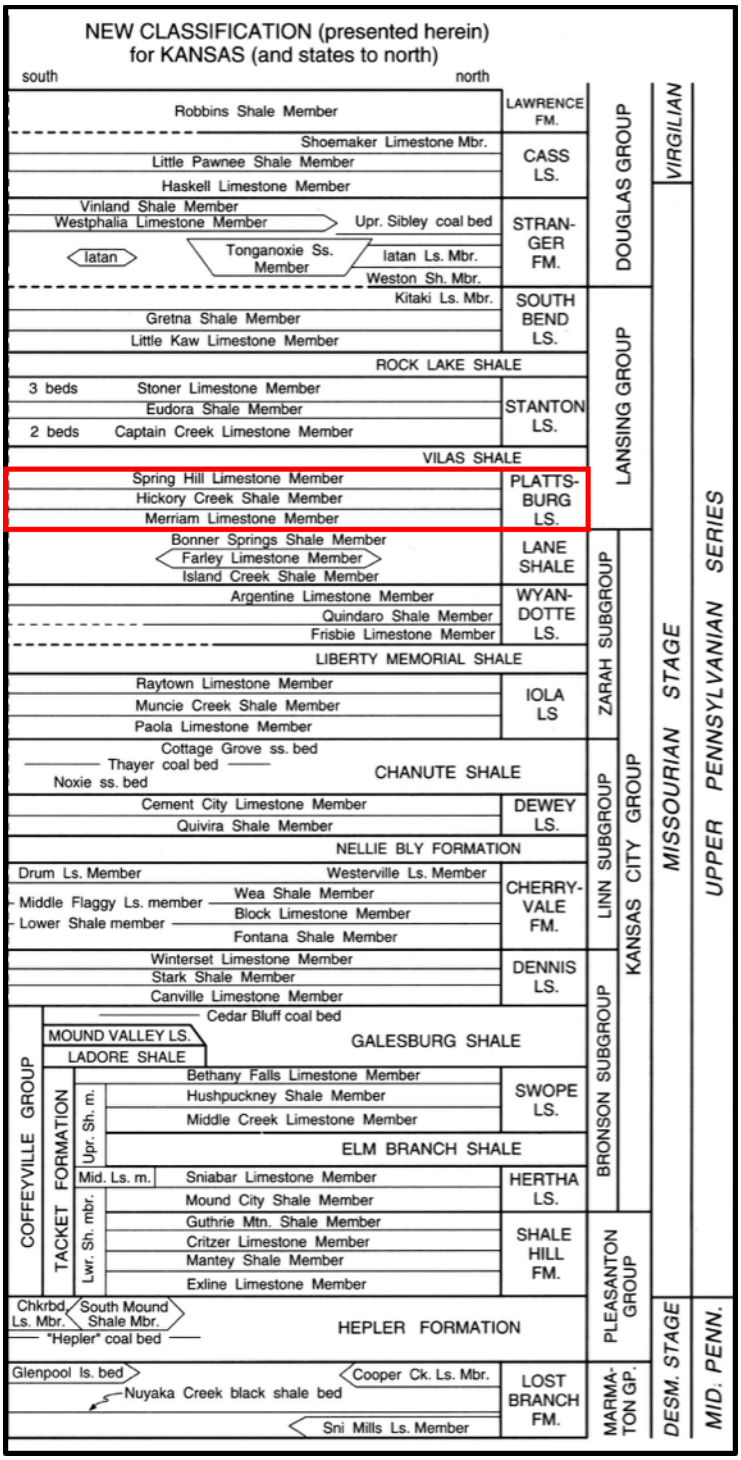

Figure 2.6: Stratigraphic nomenclature of Upper Pennsylvanian strata in Kansas, as of 2002. The LKCC (Plattsburg Limestone), outlined in red, is present at the base of the Lansing Group, deposited during the Missourian Stage – Upper Pennsylvanian. Modified after Figure 1 in: Heckel and Watney (2002).

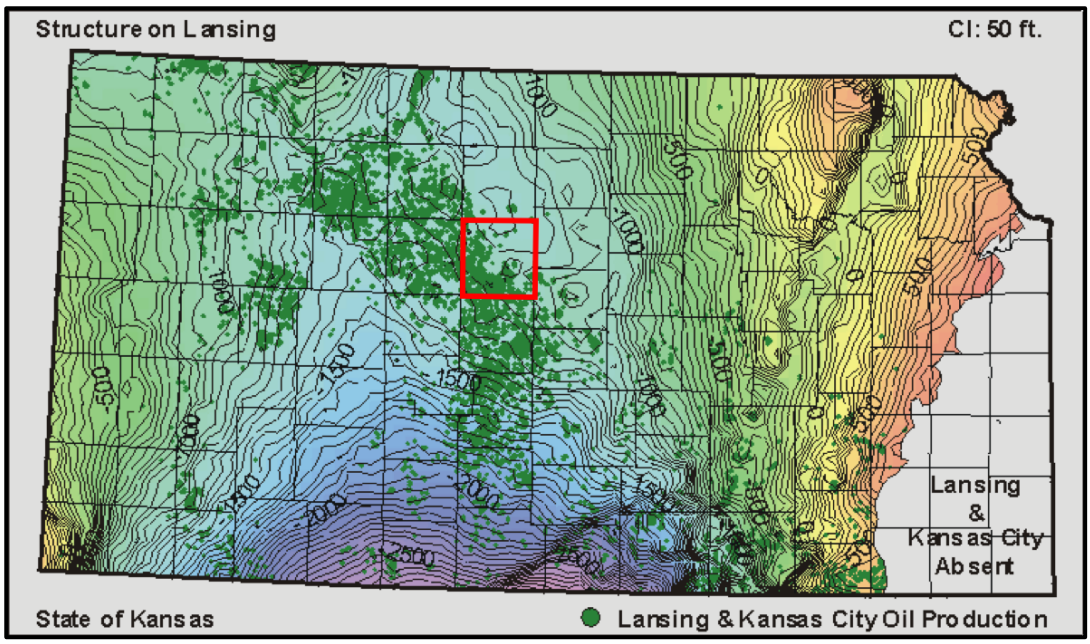

Figure 2.7: Kansas LKC top-structure referenced to sea-level (contour interval: 50 feet), with LKC oil production displayed in green. The study area (Russell County) is outlined in red. Modified after KGS (1998).

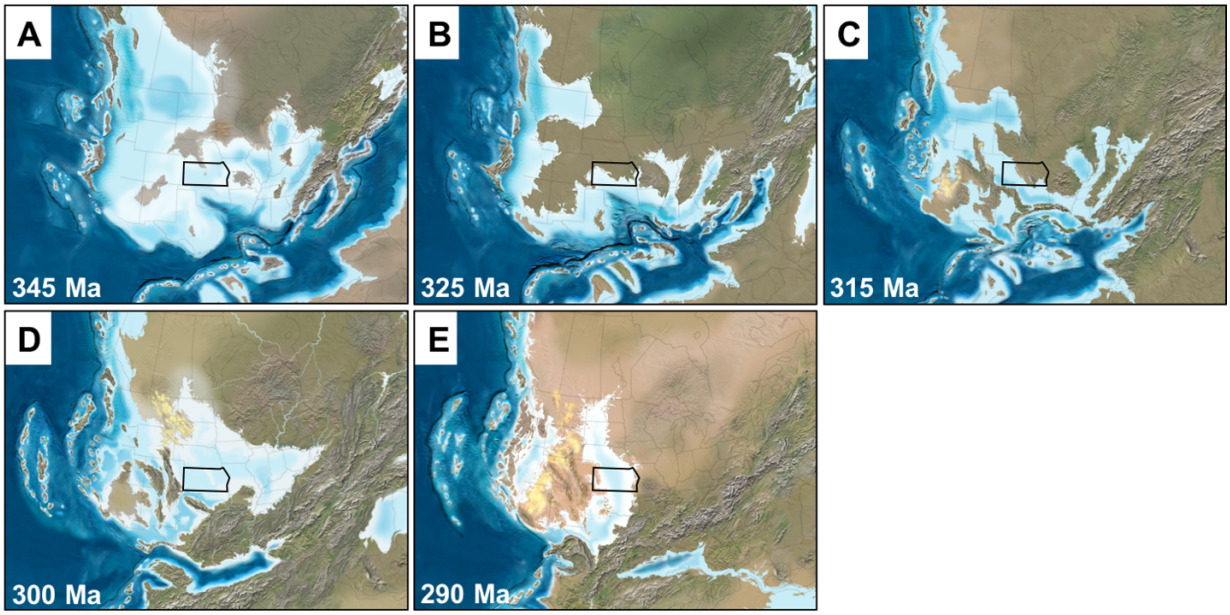

Figure 2.8: Paleogeographic evolution of North America from approximately 345 Ma to 290 Ma: (A) Early Mississippian, (B) Late Mississippian, (C) Early Pennsylvanian, (D) Late Pennsylvanian, and (E) Early Permian. The relative position of Kansas is outlined in black for each time frame. (A), (B), (C), (D), and (E) modified after Blakey (2005b), (2005a), (2005e), (2005d) and (2005c), respectively.

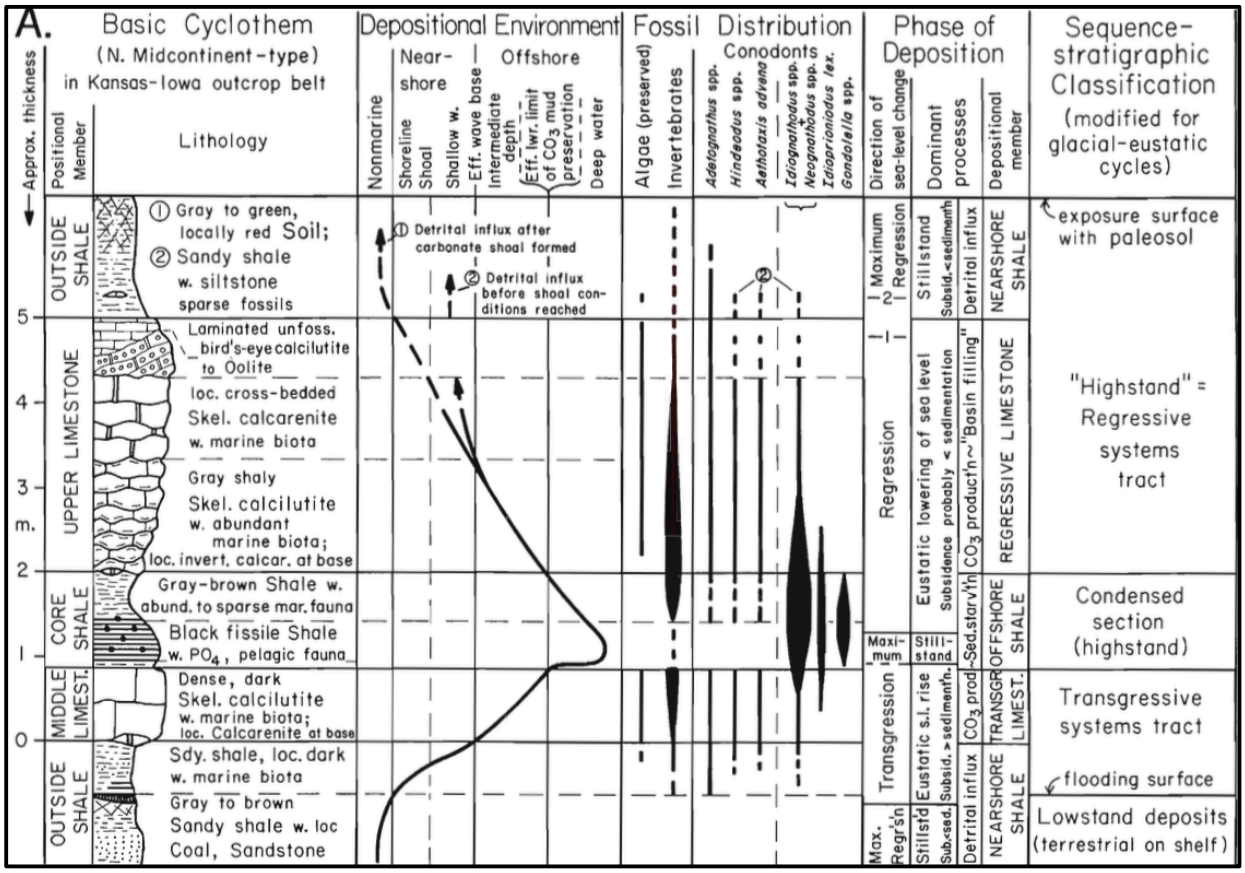

Figure 2.9: Kansas cyclothem model with lithology, depositional environment, fossil distribution, and phase of deposition. After Figure 2A in: Heckel (1994).

Descriptive Facies	Thickness (Ft.)	Lithology	Diagenetic Alternation	Facies Contacts	Equiv. # in Fig. 36	Genetic Facies	Depositional Environment
Upper Shale	<5-30	Red-brown, unbedded silty shale	intense		7	Regressive Shale	oxidized, continental clastics
				S			
Upper (upper)	<1-15	Lime-mudstone to grainstone common; occ. dolomitic; sparse to very fossiliferous	moderate to intense		3,3a,4 5,6	Regressive Carbonate	shallow, clear-water carbonate; tidal flat, lagoon, and open marine; high and low energy
Carbonate (lower)	5-25	Lime-mudstone or wackestone, argillaceous at bottom; fossiliferous			2		Subtidal, low-energy, clear-water, open-marine carbonate grading downward to mixed turbid argillaceous carbonate
				G			
Lower Shale	2-20	Fossiliferous, gray-green; occ. black	minimal		1	Marine Shale	Subtidal, low energy, marine; restricted, anoxic conditions prevalent to south and to north locally shallow water
				G			
Lower (upper)	0-15	Lime-mudstone to wackestone, fossiliferous	minimal to locally moderate		2	Transgressive Carbonate	Subtidal, low energy, open marine; clear to turbid water conditions
Carbonate (lower)	0-8	Silty grainstone to packstone; occasionally, base rich in quartz sand or silt			unique combination of 2,3,4,5		Sandy or silty reworked shoal water, intermittent restricted to open marine
				S			

S = Sharp Contact
G = Gradational Contact

Table 2.1: Properties and interpretation of four-component Midcontinent LKC cyclothems. After Table 2 in: Watney (1980).

LKC Plattsburg Limestone 'C Zone'

Within the Central Kansas Uplift, the LKC Plattsburg Limestone is identified as the 'C Zone' (LKCC) – one of approximately a dozen limestones separated by shale units. Geologic descriptions, approximate depths, relative thicknesses, and typical gamma ray (GR)-neutron log response of these zones are shown in Figure 2.10. The LKCC is the reservoir target for the Hall-Gurney Field CO_2-EOR project, and is characterized as a regressive limestone – the dominant reservoir within LKC cyclothems (Watney, 1994) which contains as a grain-rich top interval deposited in a high-energy, shallow shelf marine environment (Newell et al., 1987). Optimal reservoir properties (thickness, porosity, permeability, low clay content, better sorting) of these grain-rich ooid shoal facies are associated with deposition on the flanks and crests of paleostructural highs (Byrnes et al., 2003).

Subaerial exposure and meteoric water percolation of these shoals shortly following deposition led to extensive diagenetic overprinting, resulting in the development of oomoldic porosity – a reversal in original pore and solid space (Byrnes et al., 2003). Permeability of the LKCC is controlled by porosity, oomold connectivity, matrix crushing, fracturing, oomold diameter, oomold packing, and matrix properties (Byrnes et al., 2003). LKCC lateral heterogeneity may be affected by the occurrence and variance of shingling, weathering, and diagenetic processes (Willhite et al., 2010). LKCC rock, fluid, and environmental reservoir properties obtained from wells within the pilot pattern and adjacent leases are listed in Table 2.2. As seen in Figure 2.11, the LKCC contains up to six layers characterized as 2-3 shallowing-upward 5^{th} order parasequences (Watney et al., 2006).

Interpretation of LKCC shoals by Watney et al. (2006, 2007) reveal geometric features (sinuous, lobate, parabolic, linear) analogous to modern, active Bahamian shoal systems as seen in Figure 2.12. Interplay between global glacioeustatic sea-level and local geologic changes

resulted in deposition, re-working, and re-deposition of ooid shoals (Byrnes et al., 2000). These phenomena produced complex LKCC reservoir architecture, containing stacked, cross-cutting, and shingled ooid shoals (Byrnes et al., 2000). Watney (2015) and Watney et al. (2006, 2007) suggest the deposition of three multiple, stacked, high-frequency shoal complexes in the Hall-Gurney CO_2-EOR pilot region. The cross-sectional and spatial interpretation of these complexes are outlined in Figure 2.13 and Figure 2.14, respectively, based on their elevation in reference to the Spring Hill Limestone Member base, uniformity in lithofacies identified through petrophysical data, and data from cores and cuttings (Watney, 2015).

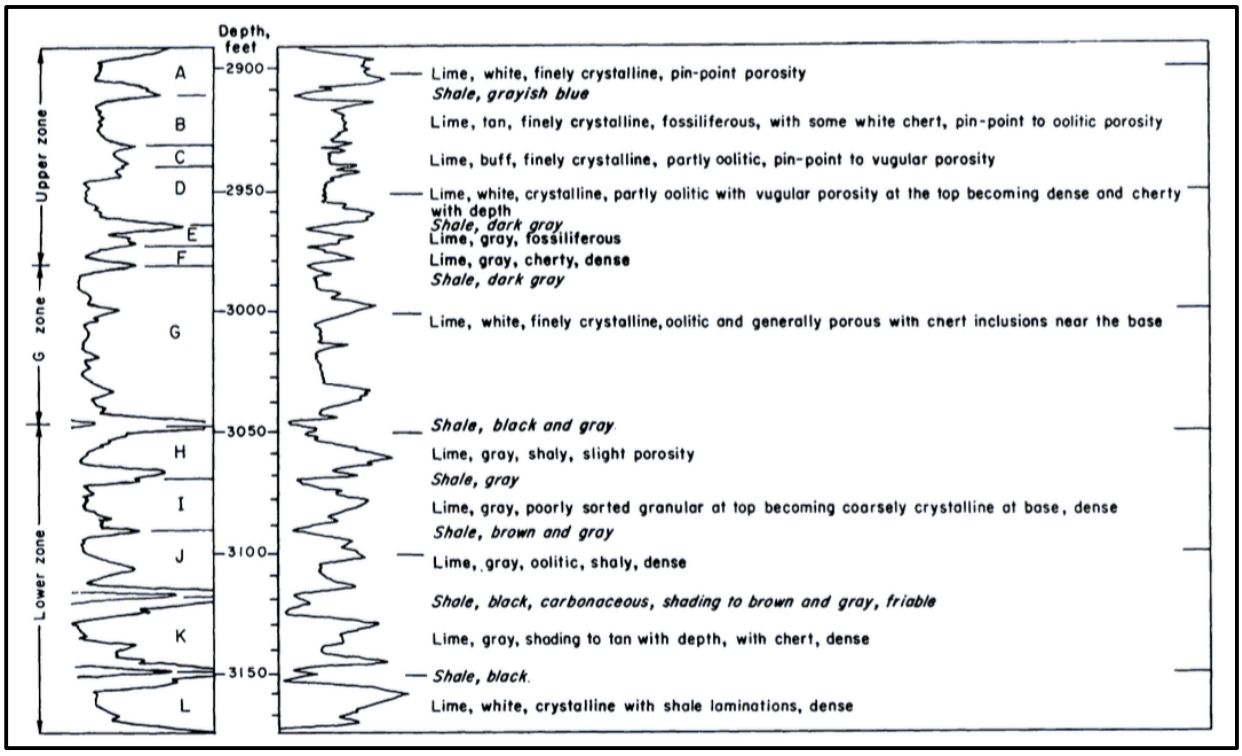

Figure 2.10: GR-neutron type log response and description of LKC strata within the Central Kansas Uplift. Twelve zones (A-L) are assigned to limestone members, which are commonly separated by shale members. After Figure 19 in: Riggs et al. (1963).

LKCC Reservoir Properties		Source
Approximate Depth	2900 ft (880 m)	
Thickness	10-20 ft (3.6 - 6.0 m)	
Lithology	Limestone	
Texture	Oomoldic	
LKCC Layer#1: Average (thickness, ϕ, k)	1 ft, 18.8%, 8 mD	Willhite et al. (2012)
LKCC Layer#2: Average (thickness, ϕ, k)	4 ft, 150 mD, 25.8%	Willhite et al. (2012)
LKCC Layer#3: Average (thickness, ϕ, k)	3 ft, 40 mD, 22.0%	Willhite et al. (2012)
LKCC Layer#4: Average (thickness, ϕ, k)	2 ft, 6 mD, 19.4%	Willhite et al. (2012)
LKCC Layer#5: Average (thickness, ϕ, k)	5 ft, 2 mD, 14.7%	Willhite et al. (2012)
LKCC Layer#6: Average (thickness, ϕ, k)	4 ft, 0.3 mD, 12.0%	Willhite et al. (2012)
Salinity	4900 mg/L	Byrnes et al. (2002)
Oil API	36	Willhite et al. (2012)
Sorw	27.4%	Willhite et al. (2010)
(pCO2):(pOil)	0.6-0.8	Willhite et al. (2010)
Reservoir Temperature	98ºF (36.67ºC)	Willhite et al. (2012)
Pressure Prior to CO2-EOR	800 psi (5.52 MPa)	Willhite et al. (2010)
Pressure During CO2-EOR	>1400 psi (9.65 MPa)	Willhite et al. (2010)
LKC Crude at 98ºF	3 cP	Willhite et al. (2012)
MMP for LKC Crude at 98ºF	1120 psi (7.72 Mpa)	Willhite et al. (2012)

Table 2.2: LKCC reservoir properties from data acquired in pilot pattern and surrounding leases.

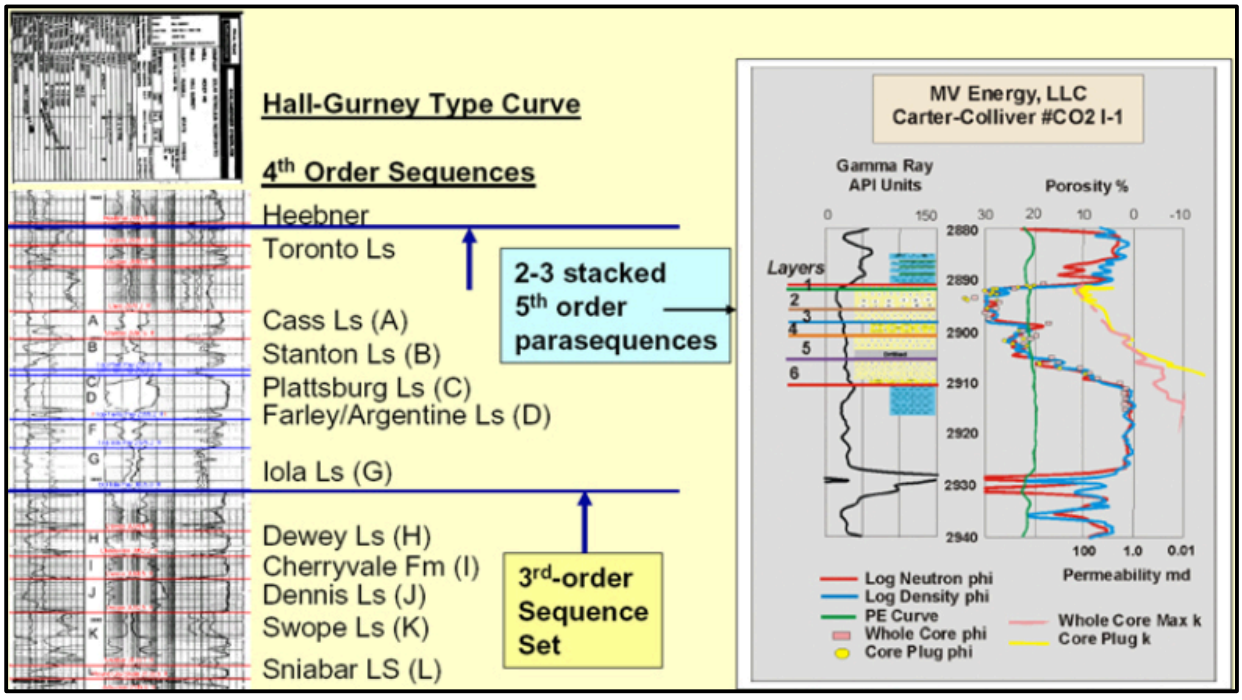

Figure 2.11: Hall-Gurney type log with 4th order parasequences (left), and LKCC Plattsburg 5th order sequence classification of Well CO2-I #1 (right) with six identified LKCC layers. Modified after Watney et al. (2006).

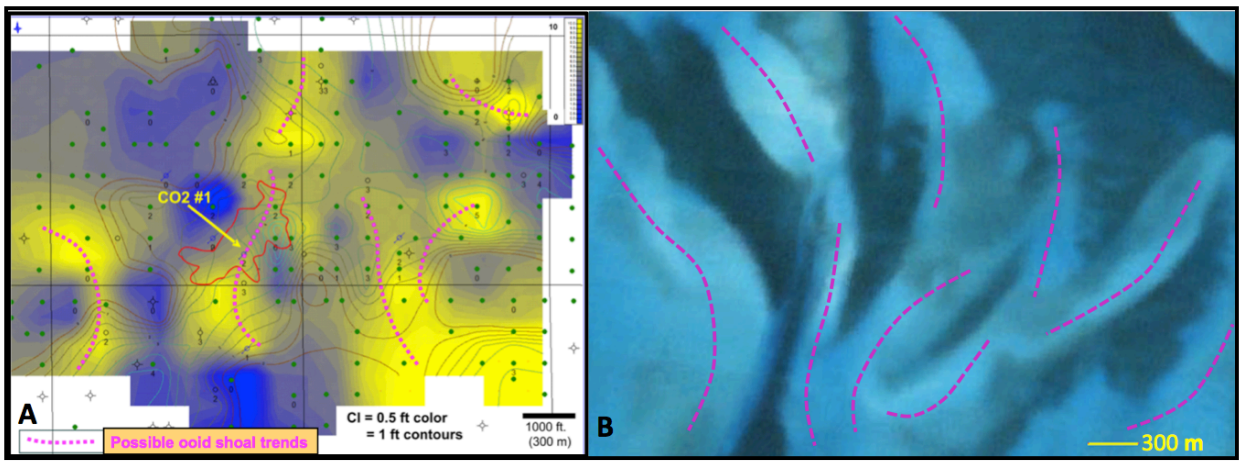

Figure 2.12: Interpretation of (A) potential LKCC ooid shoal trends (Watney et al., 2006), and (B) comparison with modern ooid shoal systems (Google Earth, 2015). Images are adjusted to approximately the same scale.

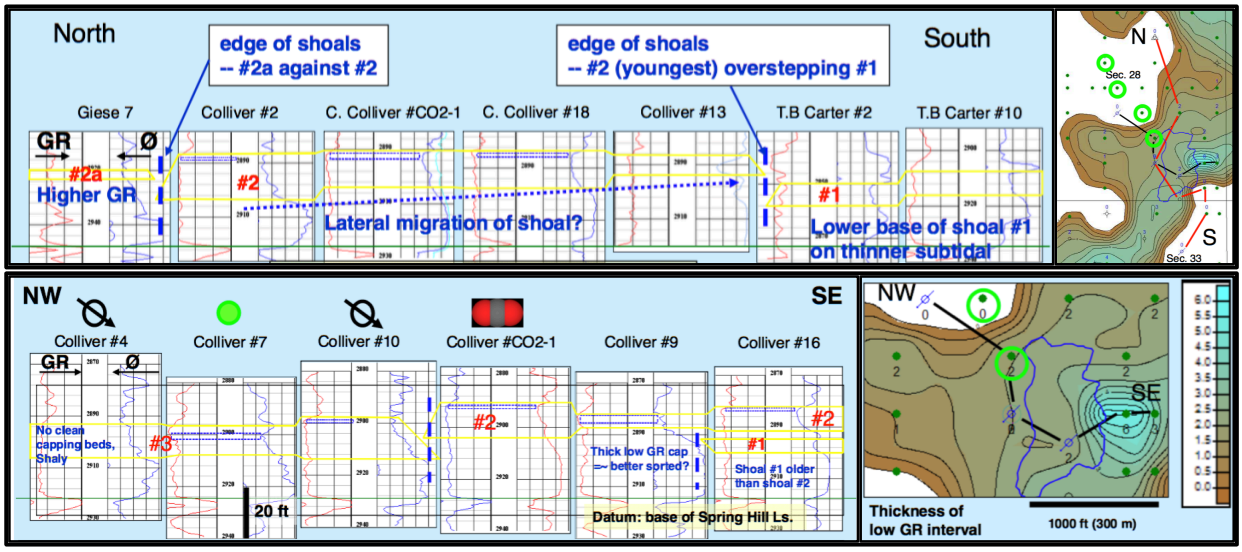

Figure 2.13: Cross-section of stacked LKC shoal complexes across the Hall-Gurney CO_2 pilot region. After Watney et al. (2007).

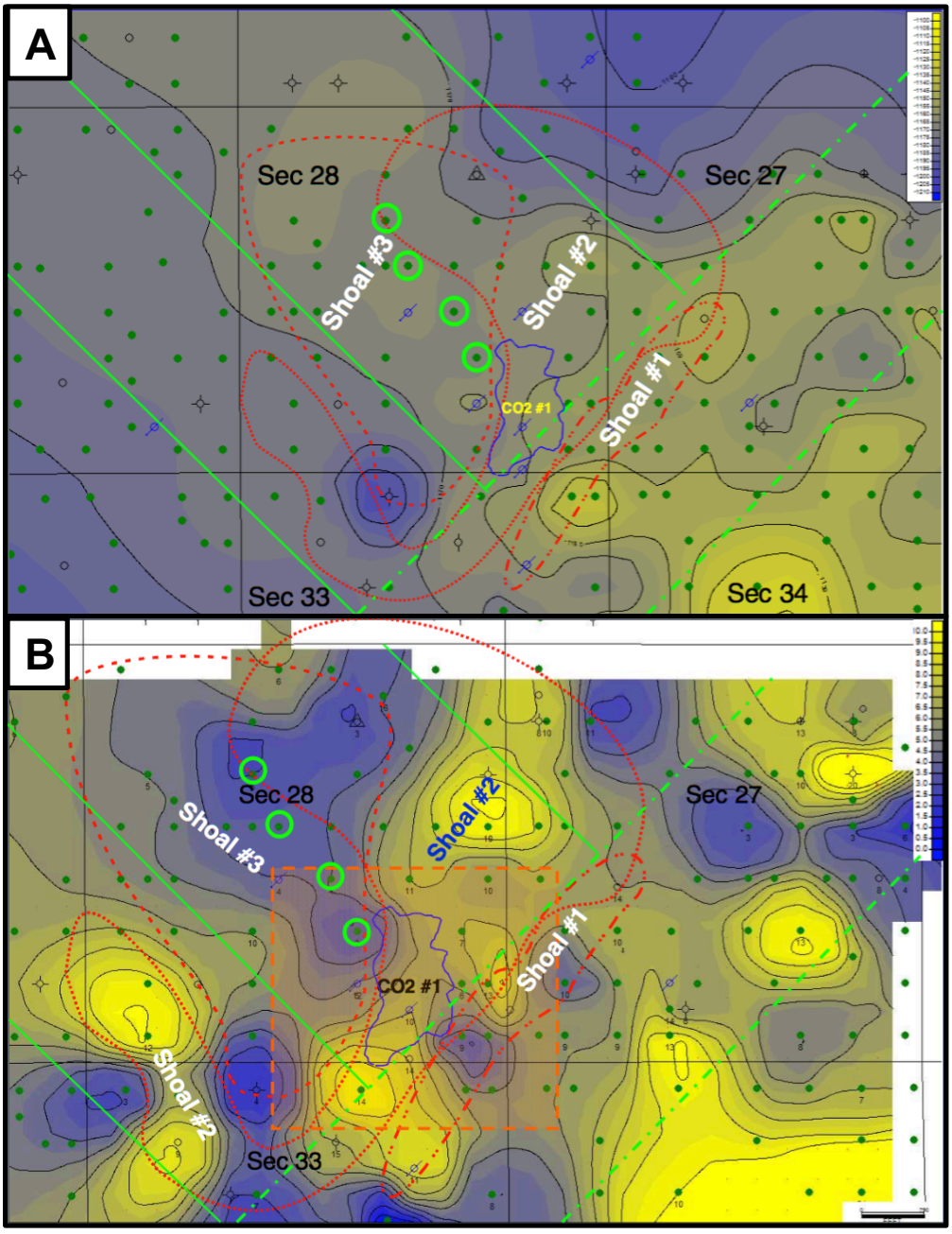

Figure 2.14: Interpretation of stacked, high-frequency shoal deposits (red polygons) with reference to (A) LKCC top-structure, and (B) LKCC layer #2 isopach with bounds of seismic survey coverage (orange square). Interpretation of CO_2 plume migration (blue polygon) and wells outside the pilot pattern lease which responded to CO_2-EOR (circled in green) are plotted with local structural lineaments (solid green lines) and regional structural lineaments (dashed green lines). Modified after Watney et al. (2007).

Hall-Gurney CO_2-EOR Pilot Demonstration

Well Pattern and Injection

A ten-acre, inverted half five-spot pattern was designed for the CO_2-EOR pilot project. This pattern included one CO_2 injector (Well CO2-I #1), two water injectors (Well #10, Well #18) for pressure containment, two producers (Well #12, Well #13), and one monitoring well (Well #16). Well CO2-I #1 also served as a water injection well to follow the WAG injection cycle applied for this CO_2-EOR project. This pilot pattern configuration is displayed in Figure 2.15.

Water injection into Well CO2-I #1 began on 23 April 2003 to test absolute average permeability in the pilot pattern, and this injection rate was increased to pressurize the injection zone up to the MMP on 5 September 2003 (Willhite et al., 2010). Water injection for pressure maintenance in the pilot pattern began on 15 and 16 September 2003 on Well #10 and Well #18, respectively (Willhite et al., 2010). Well CO2-I #1 had CO_2 injected between 23 November 2003 and 17 June 2005, and water injected between 21 June 2005 and the project's termination (Willhite et al., 2010). A total of 16.19 million pounds (138.05 MMCF) was injected in Well CO2-I #1 over seventeen months (Willhite et al., 2010). Due to a low response of Well #13 to CO_2 injection from Well CO2-I #1, CO_2 (86,260 pounds) was injected into Well #13 on 9 December 2004 in order to increase the permeability of CO_2 around the well (Willhite et al., 2010). BHP pressure for injection wells was controlled to avoid fracturing of the reservoir, which contains calculated breakdown pressure, fracture propagation pressure, and closure pressure of 2200, 2114, and 1965 psi respectively (Willhite et al., 2010).

The transition from CO_2 to water for WAG injection in Well CO2-I #1 is shown in Figure 6.1. Well CO2-I #1 BHP was controlled at approximately 1900 psi during CO_2 injection to

maintain MMP, control CO_2 loss to the north, and avoid fracturing the reservoir (Willhite et al., 2010). BHP was maintained at approximately 2150 psi in Well CO2-I #1 following the switch to water injection (Willhite et al., 2010). Water injection for pressure containment in Well #10 and Well #18 is plotted on different scales in Figure 6.2 and Figure 6.3, respectively. To avoid fracturing the reservoir, water injection rates into Well #10 and Well #18 were controlled and maintained at approximately 1900 psi during CO_2 injection to prevent CO_2 loss to the north and south, respectively (Willhite et al., 2010). Following the switch of CO_2 to water injection in Well CO2-I #1, BHP in Well #10 was maintained at approximately 1550 psi between January 2006 until the project's completion in March 2010 (Willhite et al., 2010). A significant pressure drop between Well CO2-I #1 and Well #10 suggests a significant loss of fluid to the north occurred by December 2005 – January 2006 (Willhite et al., 2010). Water and oil production, and CO_2-GOR are plotted for Well #12 and Well #13 on different scales in Figure 6.4 and Figure 6.5, respectively. Notable deviation of production scales reveals the poor response of Well #13 in comparison to Well #12 for oil production and CO_2 response from Well CO2-I #1. The initial CO_2-GOR spike in Well #13 was quickly followed by a rapid decline, and no additional response seen until after CO_2 was injected directly into Well #13 with the intent to increase CO_2 permeability.

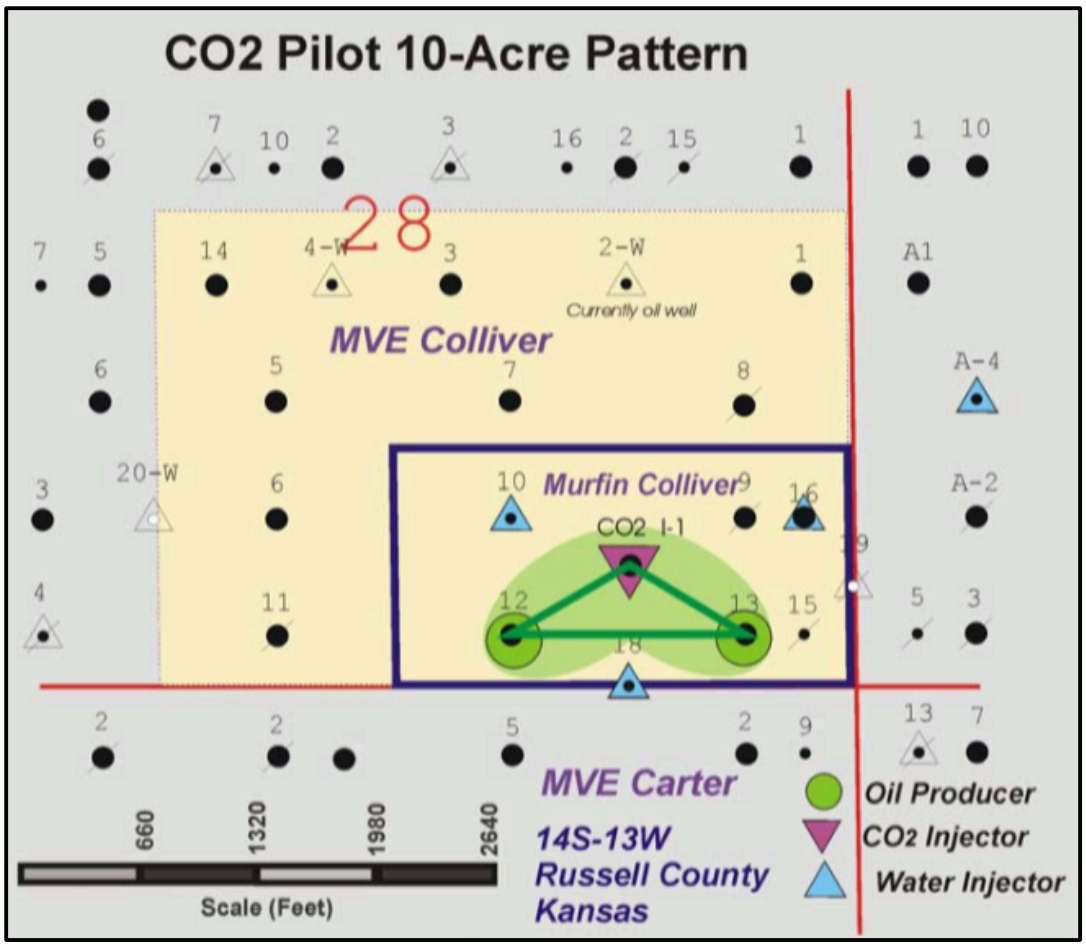

Figure 2.15: Hall-Gurney CO_2-EOR Well Pattern, after Figure 3.1.20 in: Willhite et al. (2010).

4D Seismic Monitoring Program

The Class Revisit project's monitoring component – '4-D High-Resolution Seismic Reflection Monitoring of Miscible CO_2 Injected into a Carbonate Reservoir' – was initiated to monitor CO_2 injection into the LKCC. This monitoring component was designed to transpire between 2003 and 2009, with the first and second halves of the project primarily focused on acquisition and processing, and interpretation and analysis, respectively (Miller et al., 2007). Early termination after the monitoring program's third year resulted in discontinuation of additional acquisition of monitor surveys (#9, #10, and #11), further interpretation, and secondary processing of the 4D dataset's seismic volumes (Miller et al., 2007).

Survey Design and Data Acquisition

The pilot-scale Hall-Gurney 4D seismic survey was designed to image CO_2 injected in smaller volumes, and into thinner layers, than conventional 4D seismic monitoring projects operating at considerably larger scales. Considerations in survey design for acquiring these seismic data included optimization of repeatability, azimuthal and fold coverage, subsurface resolution, and minimization of footprint (Raef et al., 2005c). A modified brick, single-patch survey (Figure 2.16) was designed to meet these criteria with 810 source shot points and 240 receiver stations, the locations of which were positioned using differential GPS to maximize repeatability (Raef et al., 2004). Source positions were oriented along nineteen 100-meter spaced north-south trending lines 1.5 km long, with 20-meter station spacing (Raef et al., 2004). Five 10-second linear upsweeps spanning 25-250 Hz were generated from an IVI Minivib II - the first used to couple the pad and the latter four to stack (Miller et al., 2007). It is important to note the source vibrator was not phase locked, and therefore wavelet phase variations should be expected between shots within the same survey, as well as between data across surveys (Raef et al., 2005c). Receivers were configured in five 200-meter spaced east-west trending lines 1.0 km long, with 20-meter station spacing (Raef et al., 2004). These parameters provided 10- x 10-meter bin size with 20- to 24-fold coverage over the injection well and approximately 12-fold coverage over the water injectors (Miller et al., 2007). As seen in Figure 2.17, a 112-degree grid rotation was applied to the survey data in order to improve fold distribution (Miller et al., 2007).

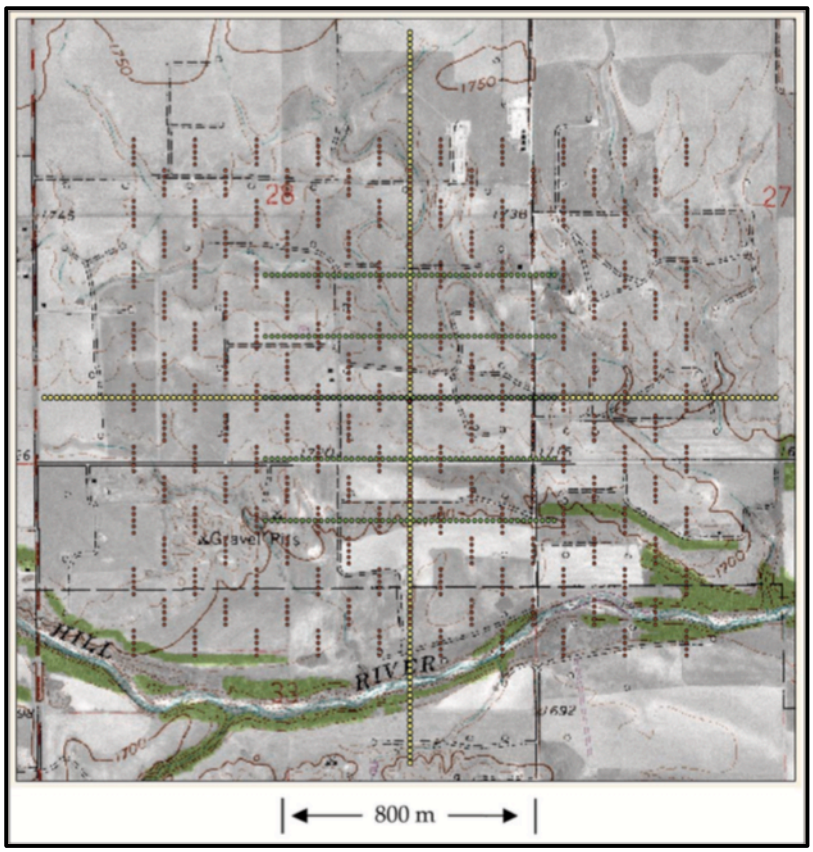

Figure 2.16: Design of 3D seismic survey using a modified brick pattern, with N-S trending source lines (red) and E-W trending receiver lines (green). After Figure 1 in: Raef et al. (2004).

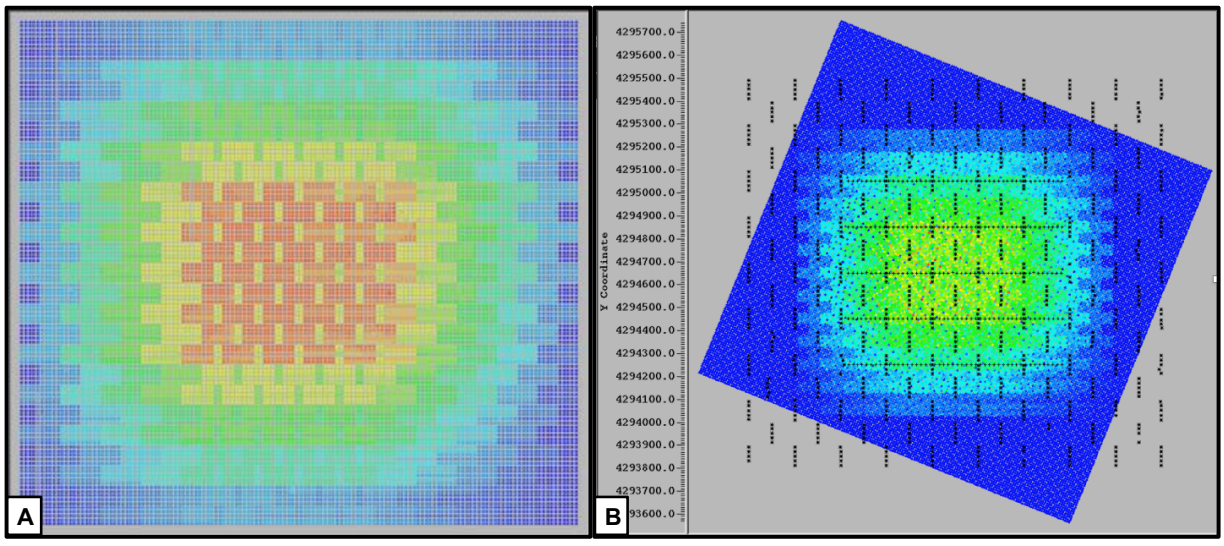

Figure 2.17: Fold of coverage (A) prior to grid rotation, after Figure 57 in Miller et al. (2007), and (B) with 112-degree rotation and improved fold distribution. Red = 24-fold, yellow = 20-fold.

Seismic Data Processing

Processing of these high-resolution data was consistent across all 3D seismic volumes, using an up-tuned, multi-path workflow (Raef et al., 2005c). Emphasis was placed on reflection-specific enhancement, amplitude analysis, and signal enhancement including noise removal and improvement of spectral richness (Raef et al., 2005c). The approach taken to process these data was to compromise structural imaging and event continuity quality in order to maintain pre-stack data character and preserve subtle 4D seismic signatures across surveys (Raef et al., 2006b). An example of one of 800+, 240-channel four-shot vertical shot gathers with velocity to reflectors is shown in Figure 2.18. Raising the seismic dominant frequency from 55 Hz to 90 Hz after the high-resolution tuned processing flow resulted in approximate improvements of 15% and 8% in seismic resolution and SNR, respectively (Raef et al., 2006a). Moderate cross-equalization was applied to avoid diluting the subtle 4D anomalies expected, while managing to still minimize non-repeatable differences between surveys (Raef et al., 2004). Near-surface inter-survey velocity perturbations introduced significant obstacles with statics' time shifts, as seen in the example between the Baseline and M2 survey in Figure 2.19. This problem was unavoidable with the acquisition of seismic monitor surveys in fine time steps over all seasons. Early termination of this project's monitoring component led to cancellation of the originally planned secondary processing, and as a result the 4D seismic data were only subjected to preliminary processing. At the time, secondary processing of these data was expected to yield data resolution

surpassing any documented study for thin beds at these depths (Miller et al., 2007).

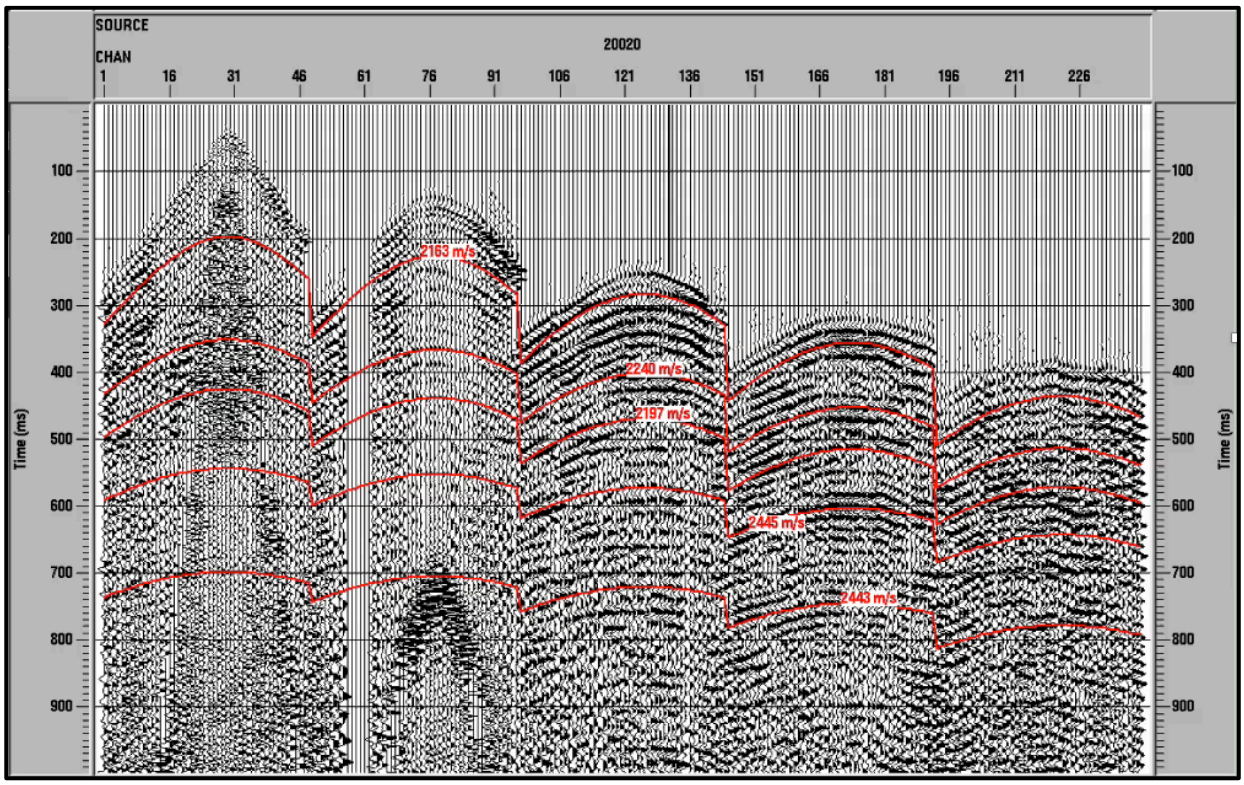

Figure 2.18: Example of 240-channel four-shot vertical stack shot gathers with velocity to reflectors.

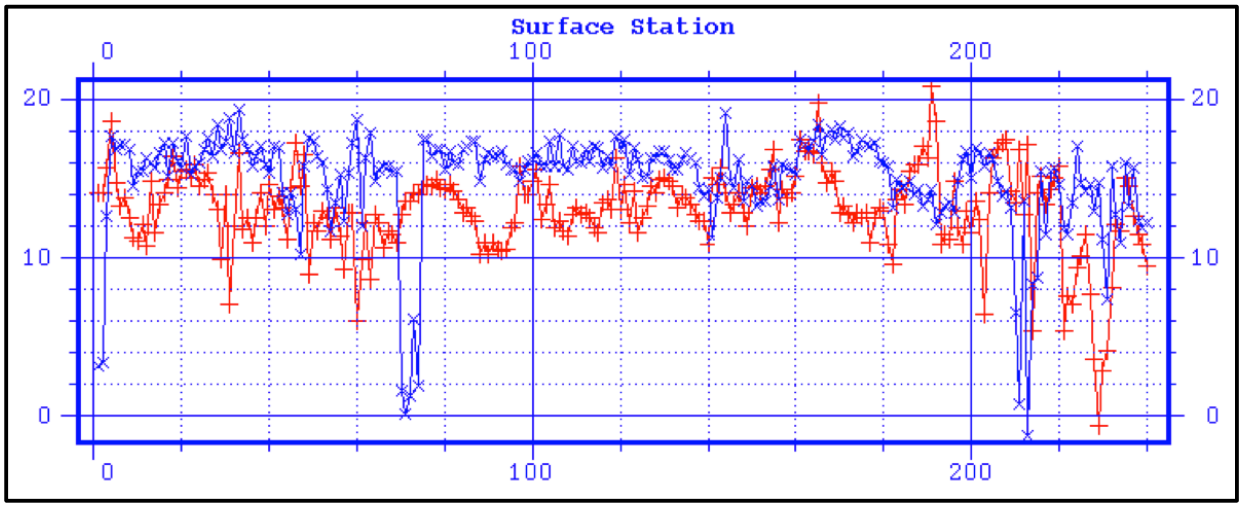

Figure 2.19: Effect of near-surface perturbations on statics (y-axis = ms) between the Baseline (red) and M2 (blue) Surveys.

Interpretation

An unconventional approach toward interpretation of the high-resolution 4D seismic data set proved successful in imaging and monitoring CO_2, forecasting CO_2 and oil breakthroughs at wells, and overall improving reservoir characterization. Interpretation of the 4D seismic data, in combination with production data, highlighted lineaments within the injection zone which appeared to strongly influence reservoir fluid flow (Miller et al., 2007). VSP data were acquired for well #16 to establish T-D relationships and identify the LKCC reflection. Sonic log data were combined with these T-D conversions to generate synthetic seismograms, which placed the LKCC top at approximately 548 ms (Raef et al., 2005c).

Selection of attributes capable of revealing subtle, meaningful differences between surveys' data representative of CO_2 fluid replacement required careful understanding of high-resolution data's inter-survey sensitivity to time and phase shifts, the trade-off of data bandwidth and event continuity, and the expected response from 4D seismic modeling of fluid replacement (Raef et al., 2006b). Seismic attributes which demonstrated value in enhancing the LKCC geologic interpretation of reservoir architecture and lithology include time-structure, amplitude, frequency, and similarity (Raef et al., 2005c). An expected change in amplitude from CO_2 fluid replacement was observed in the vicinity of the injection point within the reservoir interval (Figure 2.20), and migration of CO_2 from the well largely complied with seismic lineaments identified on the Baseline Survey, as well as changes in containment pressures (Miller et al., 2007). Away from Well CO2-I #1, conventional differencing of seismic data between the Baseline and Monitor Surveys did not yield sufficient results for interpretation above noise.

Parallel progressive blanking (PPB), a non-differencing approach to 4D seismic interpretation, was developed for this study and applied to amplitude envelope data (Raef et al., 2005a, 2005c, 2005d; Raef and Miller, 2006). The PPB method (Figure 2.21) revealed weak 4D

signatures in the data by focusing a high-resolution color bar on the interval of highly repeatable data to identify subtle anomalies and spatial textural changes in seismic data character (Raef and Miller, 2006). This high-resolution color bar was manually calibrated in attempt to achieve similarity in data character between data sets within the higher-fold region of coverage, but outside the immediate vicinity of CO_2 injection. PPB revealed weak anomalies suggestive of CO_2 fluid replacement, in which conventional differencing was insufficient to yield 4D anomalies above the noise threshold.

Rapid turnaround from acquisition to interpretation of seismic monitor surveys effectively imaged CO_2 movement in absence of reservoir simulation and production data. Interpretation of these seismic monitoring data following the second monitor survey predicted CO_2 breakthrough at Well #12, and identified a permeability barrier between Well CO2-I #1 and Well #13 with subsequent delay of CO_2 breakthrough at Well #13 (Miller et al., 2007). Incorporating the seismic monitoring data into reservoir models yielded greater simulation accuracy than what production history, rock measurements, water injectivity data, and interwell testing provided alone (Miller et al., 2007).

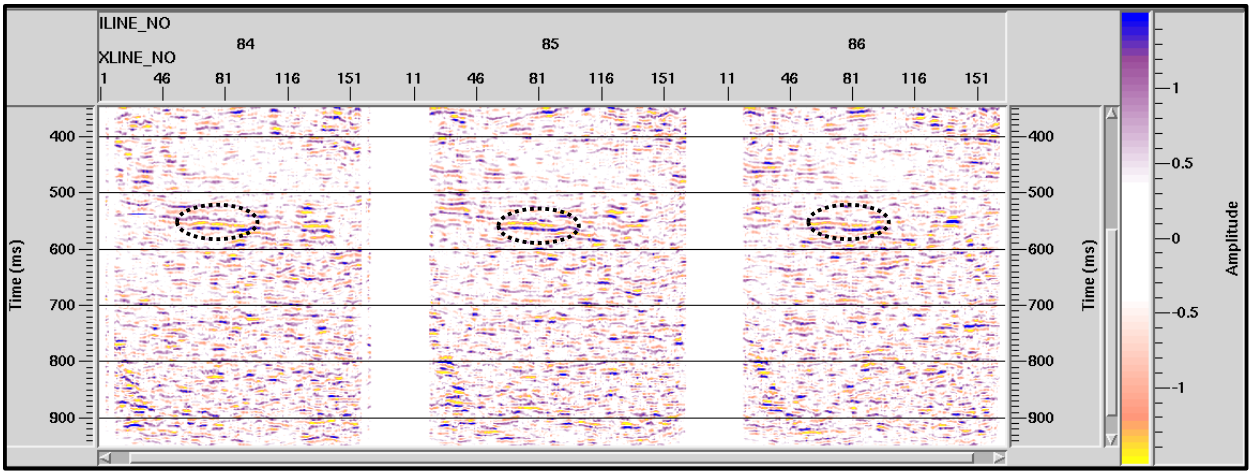

Figure 2.20: Vertical section of differenced amplitude between Baseline and Monitor Surveys within the immediate zone of CO_2 injection.

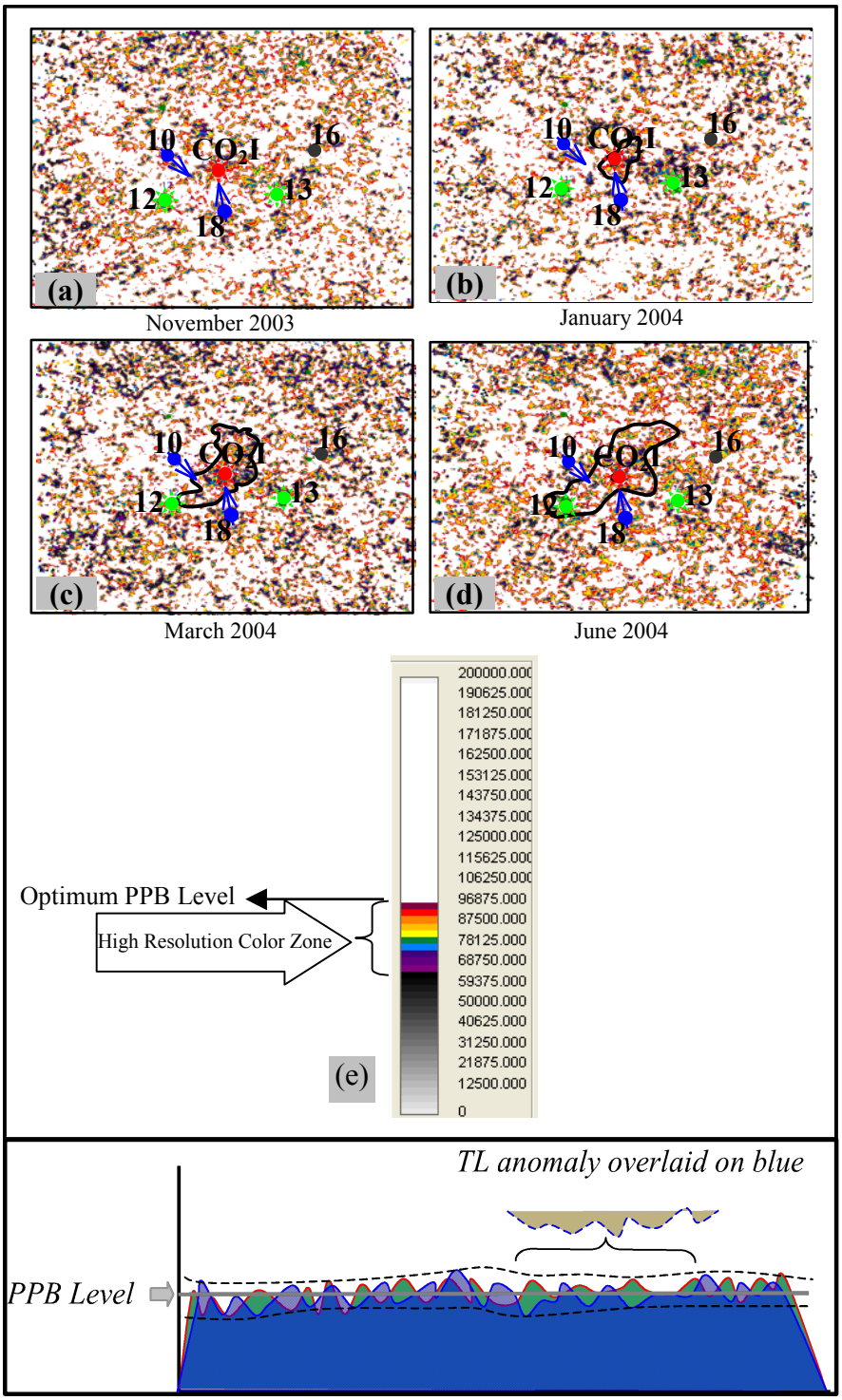

Figure 2.21: Parallel Progressive Blanking (PPB) – a non-differencing method applied to highlight weak 4D seismic textural anomalies of amplitude envelope data between the (A) Baseline and (B) M1, (C) M2, and (D) M3 Surveys with black polygon of interpreted CO_2 plume. Method discussed in Raef et al. (2004; 2005a; 2005c; 2005d), and Raef and Miller (2006).

Results

Due to an unexpected northwesterly loss of CO_2 outside the well pattern, the Hall-Gurney CO_2-EOR project was deemed uneconomic to continue and extend from pilot to commercial scale. Complex reservoir architecture and lateral heterogeneity are considered probably, primary causes of CO_2 loss. By March 2010, approximately 5-6% of injected CO_2 was produced (primarily from Well #12), resulting in a gross CO_2-gas-oil ratio (GOR) of 4.8 MCF/bbl (Willhite et al., 2010). Oil production attributed to the CO_2-EOR Hall-Gurney program was 27,902 bbl cumulative – 8,736 bbl (31.3%) of which was produced within the pilot pattern, with the remainder 19,166 bbl (68.7%) produced from adjacent Graham A (920 bbl) and Colliver A (18,246 bbl) leases to the northwest (Willhite et al., 2010). The significant boost in production from this CO_2-EOR project in the Colliver A lease (A3, A7, and A14 wells) is shown in Figure 2.22. Unconventional methods in 4D seismic data acquisition, processing, and interpretation were effective in tracking CO_2 movement. The CO_2-GOR of produced fluids from this CO_2-EOR demonstrate that although the pilot was not economic, CO_2 was successful in mobilizing residual oil.

Early termination of this multi-phase project left significant opportunities available for the advanced analysis and interpretation phase of this unique, data-rich case study. This MS thesis was designed to resume and fulfill interpretation of these 4D seismic data – specifically to investigate spectral implications of, and their sensitivity to, detecting seismic attributes' temporal anomalies in response to CO_2 fluid replacement.

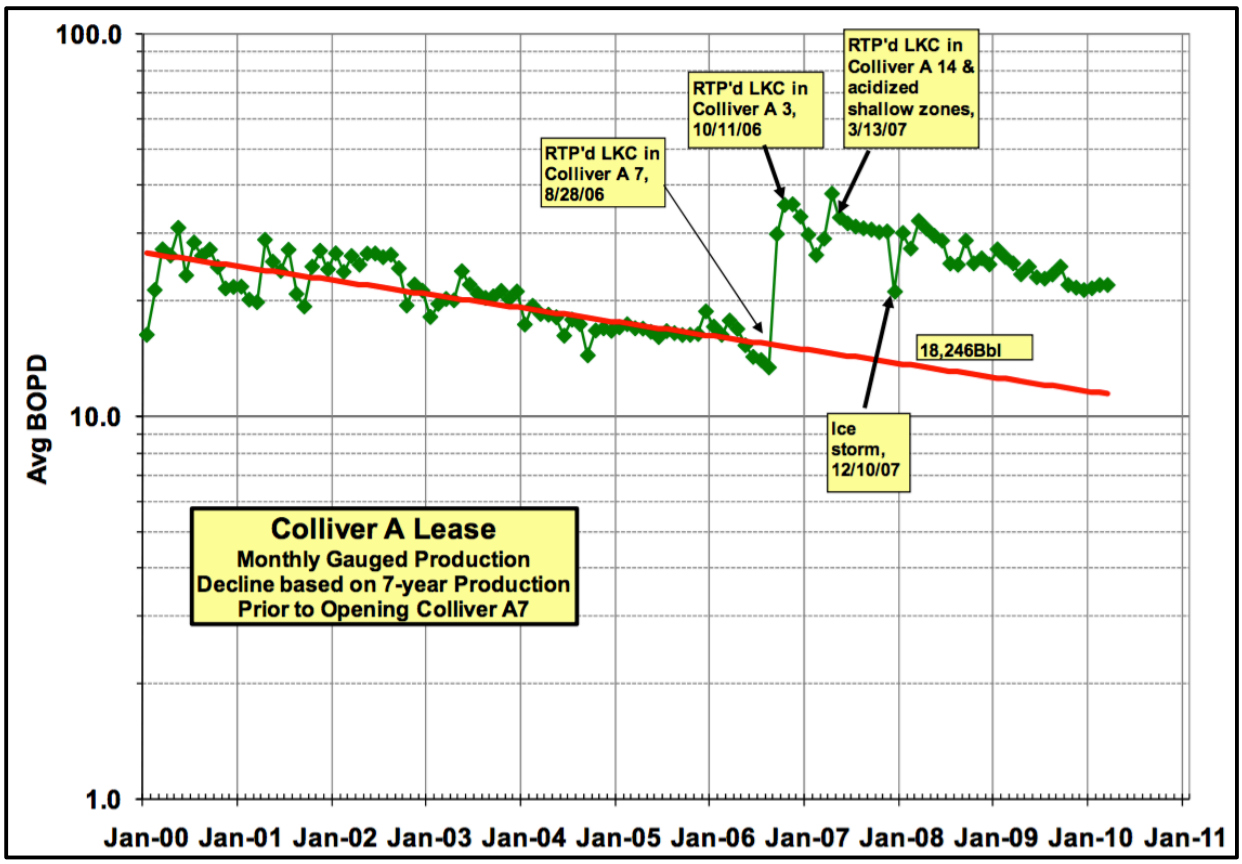

Figure 2.22: Boosted production in the Colliver A Lease (adjacent to the Hall-Gurney CO_2-EOR pilot pattern) as a result of opening the LKCC in Colliver A7, A3, and A14 wells. After Figure 5.4.27 in: Willhite et al. (2010).

Chapter 3 - Project Creation and Data Upload Parameters

Load Information, Grid Design, and 3D Seismic Data

Using IHS Kingdom software, the grid design and 3D seismic data upload were completed using the load data in Table 3.1. During the process of 3D seismic volume upload and grid design, the original coordinates in Table 3.2 were input and tested for orthogonality. As seen in Figure 3.1, these original coordinates were determined non-orthogonal, and the solution requiring the smallest change from the original coordinate data to achieve orthogonality was selected (Figure 3.2), resulting in a minor change in the Delta X value - the original X-coordinate for: Inline 1, Crossline 175. The new coordinates selected from this solution were used for each 3D seismic volume upload, and are displayed in Table 3.3. The Baseline and all available monitor (M1, M2, M3, M4, M5, M6) 3D seismic volumes were uploaded into a single project within IHS Kingdom software. Each 3D seismic volume was imported in time domain as a unique survey, and these seismic data were assigned to new data types as seen in Table 3.4. Except for the M1 seismic volume, which appeared to be a corrupt file and contained zero data, all seismic volumes were uploaded successfully with the same XY coordinates, inlines and crosslines, and bin spacing. Inlines and crosslines contain WNW-ESE and NNE-SSW orientations as seen in Figure 3.3, respectively. X, Y, and Z (depth) units for the project are set in meters, while Z (time) is set in seconds.

Load Data	
Inline Max	166
Inline Min	1
Crossline Max	175
Crossline Min	1
Inline Bin Spacing (m)	10
Crossline Bin Spacing (m)	10
Inline Bin Incrememnt	1
Crossline Bin Incrememt	1
Inline Number Starts in Byte	17
Inline Format	32-Bit
Crossline Number Starts in Byte	25
Crossline Format	32-Bit
Sample Interval (seconds)	0.001
Input Samples/Trace	800
Start Time Byte Location in Trace Header	105
Start Time of Imported Trace (seconds)	0
End Time of Imported Trace (seconds)	0.799
Output Data Format	32-Bit

Table 3.1: Load data for 3D seismic surveys.

Original Survey Coordinates			
Line	**Trace**	**X Coordinate**	**Y Coordinate**
1.00	175.00	52135943.000	429509450.000
1.00	1.00	51974612.000	429574650.000
166.00	175.00	52074134.000	429356450.000

Table 3.2: Original coordinates prior to testing for orthogonality.

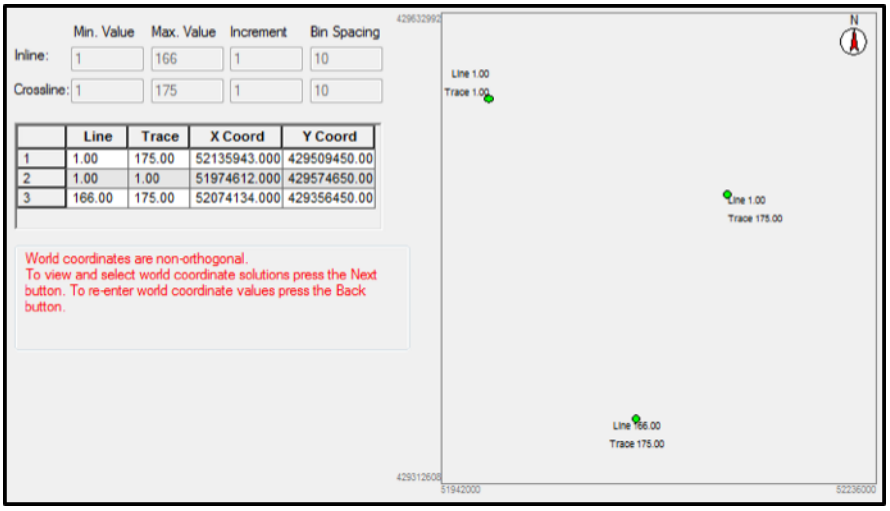

Figure 3.1: Test for orthogonality using original survey coordinates.

		Inline 1.0 Crossline 175.0		Inline 1.0 Crossline 1.0		Inline 166.0 Crossline 175.0						
		X	Y	X	Y	X	Y	Inline Bin	Crosslin	Delta X	Delta Y	RMS Err
Entered Values		52135943.	429509450	51974612.	429574650	52074134.	429356450	10	10	NA	NA	NA
Select Solution	◉	**52135960.**	42950945	51974612.	42957465	52074134.	42935645	1000.12	1000.14	17.4416	0.0000	7.8001
	○	**51912785.**	42950945	51974612.	42957465	52074134.	42935645	1347.61	516.396	-223157.	0.0000	99799.0
	○	52135943.	**42950949**	51974612.	42957465	52074134.	42935645	1000.33	999.95	0.0000	44.3080	19.8152
	○	52135943.	**42942160**	51974612.	42957465	52074134.	42935645	544.296	1278.01	0.0000	-87844.3	39285.1
	○	52135943.	42950945	**51974549.**	42957465	52074134.	42935645	1000.08	1000.38	-62.9716	0.0000	37.2545
	○	52135943.	42950945	51974612.	**42957462**	52074134.	42935645	1000.08	999.99	0.0000	-25.4393	15.0501
	○	52135943.	42950945	51974612.	42957465	**52074109.**	42935645	1000.13	1000.05	-24.1257	0.0000	14.2730
	○	52135943.	42950945	51974612.	42957465	52074134.	**42935650**	999.744	1000.05	0.0000	59.6962	35.3167
Delta		17.4416	0.0000	0.0000	0.0000	0.0000	0.0000	990.12	990.14	NA	NA	NA

Figure 3.2: Solution (outlined red box) selected to achieve orthogonality between 3D seismic surveys.

Corrected Survey Coordinates			
Line	**Trace**	**X Coordinate**	**Y Coordinate**
1.00	175.00	52135960.441	429509450.000
1.00	1.00	51974612.000	429574650.000
166.00	175.00	52074134.000	429356450.000

Table 3.3: Coordinates selected from solution in Figure 3.2 to achieve orthogonality.

Seismic Volume	Seismic Data Type
Baseline	Baseline Amplitude
Monitor 1 (M1)	M1 Amplitude
Monitor 2 (M2)	M2 Amplitude
Monitor 3 (M3)	M3 Amplitude
Monitor 4 (M4)	M4 Amplitude
Monitor 5 (M5)	M5 Amplitude
Monitor 6 (M6)	M6 Amplitude

Table 3.4: Seismic data types assigned to their respective seismic volumes.

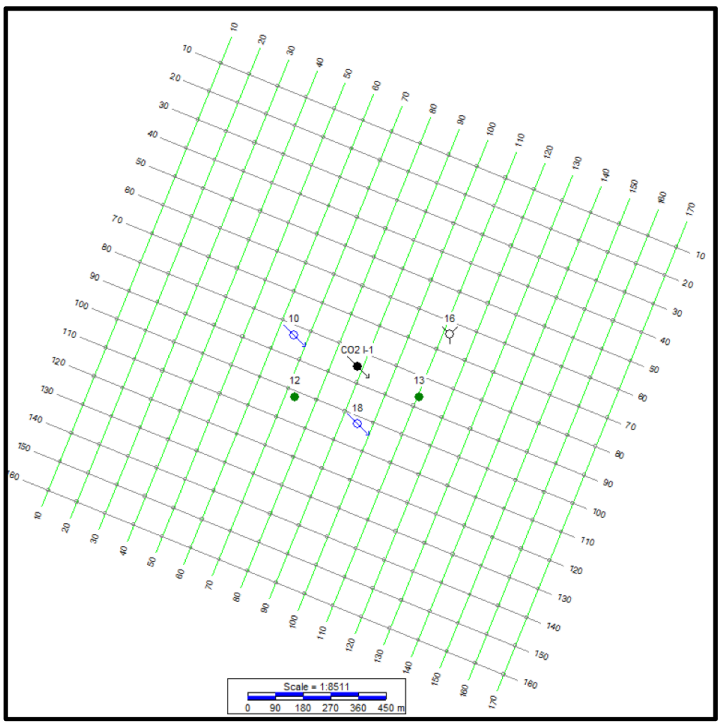

Figure 3.3: Seismic surveys' inlines (WNW-ESE) and crosslines (NNE-SSW) and CO_2-EOR pilot pattern wells.

Well and Formation Top Data

Following completion of grid design and upload of all seismic data, well data were input to the project for accessibility across all seismic surveys. UWI, type, surface coordinates, KB elevation, and total depth of wells used for this pilot demonstration project can be found in Table 3.5. Well tops for the Heebner Shale, LKC, LKCC, and LKC 'D Zone' (LKCD) are listed in Table 3.6. The surface X-Y position of wells outside the pattern from adjacent leases which showed a response to CO_2-EOR were plotted, which include Colliver A7, Colliver A3, Colliver A14, and Graham 4. No further data were acquired for these wells outside the injection pattern.

Well	UWI	Type	Surface X East (m)	Surface Y North (m)	KB Elevation (m)	Total Depth (m)
CO2-I #1	15-167-23179	CO2+Water Injector	520241.03	4294641.42	528.22	949.45
#10	15-167-02488	Water Injector	520034.51	4294744.01	530.05	911.96
#12	15-167-19056	Producer	520036.13	4294541.85	525.48	900.38
#13	15-167-02513	Producer	520442.62	4294542.73	524.26	900.68
#16	15-167-02515	Monitor	520540.96	4294745.26	528.52	905.56
#18	15-167-03816	Water Injector	520241.79	4294453.49	525.78	914.40

Table 3.5: Hall-Gurney CO_2-EOR pilot pattern well data.

Well #	CO2-I 1	10	12	13	16	18
Heebner Shale Top (m)	851.00	851.31	848.72	848.41	847.96	847.96
LKC Top (m)	868.93	871.73	869.29	869.90	873.02	868.68
LKCC Top (m)	881.03	883.31	879.81	879.81	878.43	878.74
LKCD Top (m)	886.97	887.88	885.14	885.14	883.92	883.31

Table 3.6: Formation top data for pilot pattern wells.

Chapter 4 - Methodology

Mistie Analysis

In attempt to cross-equalize Monitor Surveys (M2, M6) with the Baseline Survey and eliminate non-repeatable variance unrelated to subsurface fluid and pressure changes between surveys, mistie analyses were completed to equalize TWT arrival, phase, and amplitude scaling. For both M2 and M6 misties, an attempt was made to select the exact inlines and crosslines on the Baseline and Monitor Surveys, respectively. The trace data chosen for these analyses were selected across inlines and crosslines falling outside the immediate intersection of CO_2 injection zone and inside the higher-fold coverage zone (Figure 4.1A), and over a 0.15 second window selected below the shallow section of the data with low SNR and above CO_2 injection interval (0.35 – 0.50 seconds) (Figure 4.1B). Based on these results, minor time shifts, phase rotations, and amplitude scaling corrections were applied to the M2 and M6 surveys relative to the Baseline (Table 4.1).

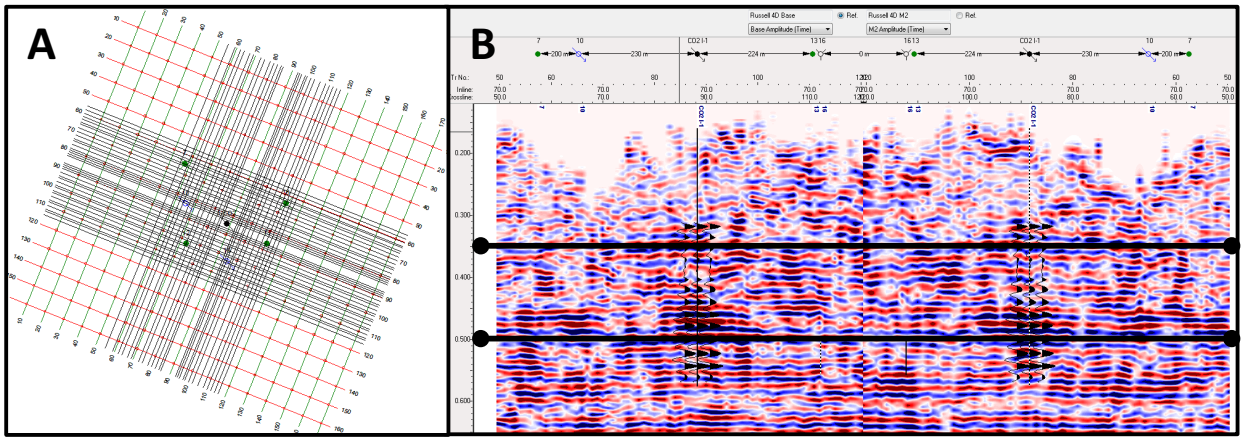

Figure 4.1: Example of mistie analysis conducted between M2 and Baseline Surveys with (A) inlines and crosslines selected, and (B) book view of surveys' vertical sections after recommended corrections (see Table 4.1) were made for time, phase, and amplitude.

Survey	Time Shift (seconds)	Phase Rotation (degrees)	Amplitude Scale
Baseline	0	0	1.0000
M2	0.0014	-50.18	0.9791
M6	0.0022	-106.5	0.9945

Table 4.1: Recommended time shift, phase rotation, and amplitude scaling corrections applied to the M2 and M6 surveys relative to the Baseline Survey.

Synthetic-to-Seismic Well Tie

Prior to creating the synthetic seismogram, conversions were applied to well data in order to standardize depth, velocity, and density units into meters, m/s, and g/cm^3, respectively. A synthetic seismogram was generated on the Baseline Survey for Well CO2-I #1 using a zero-phase wavelet (SEG Positive Standard polarity) extracted from the seismic data in reference to the well location, and a reflectivity series determined from velocity and density logs. A wavelet was extracted via frequency matching from a 150-meter radius extending outward from Well CO2-I #1 surface location, and over a 0.35-second time window (0.30 – 0.65 seconds) – an analysis covering 684 total traces (Figure 4.2). This wavelet was convolved with the reflectivity series to produce the synthetic seismogram. To tie the synthetic seismic with the Baseline Survey data, a trace was extracted by averaging data in a 150-meter radius extending outward from Well CO2-I #1 surface location. Bulk shifts were applied to achieve the most significant alignment of reflectors in the zone containing higher quality data near the LKC, which was constrained with a prior T-D relationship and known time to the LKC. No stretching or squeezing was applied to the synthetic following this bulk shift in order to preserve a practical T-D relationship, which resulted in a relatively low correlation coefficient (0.358) over the entire time window, but a sufficient correlation of reflector events around the reservoir interval. The resulting synthetic seismogram is displayed in Figure 4.3. This well tie on Well CO2-I #1 was used to track the horizon associated with the peak reflector between the LKC top and LKCC top (blue and green

tops in Figure 4.3, respectively) in the Baseline, M2, and M6 Surveys. To maintain consistency, the horizon tracked along this peak corresponding to the LKC and LKCC tops is referred to as the LKC horizon.

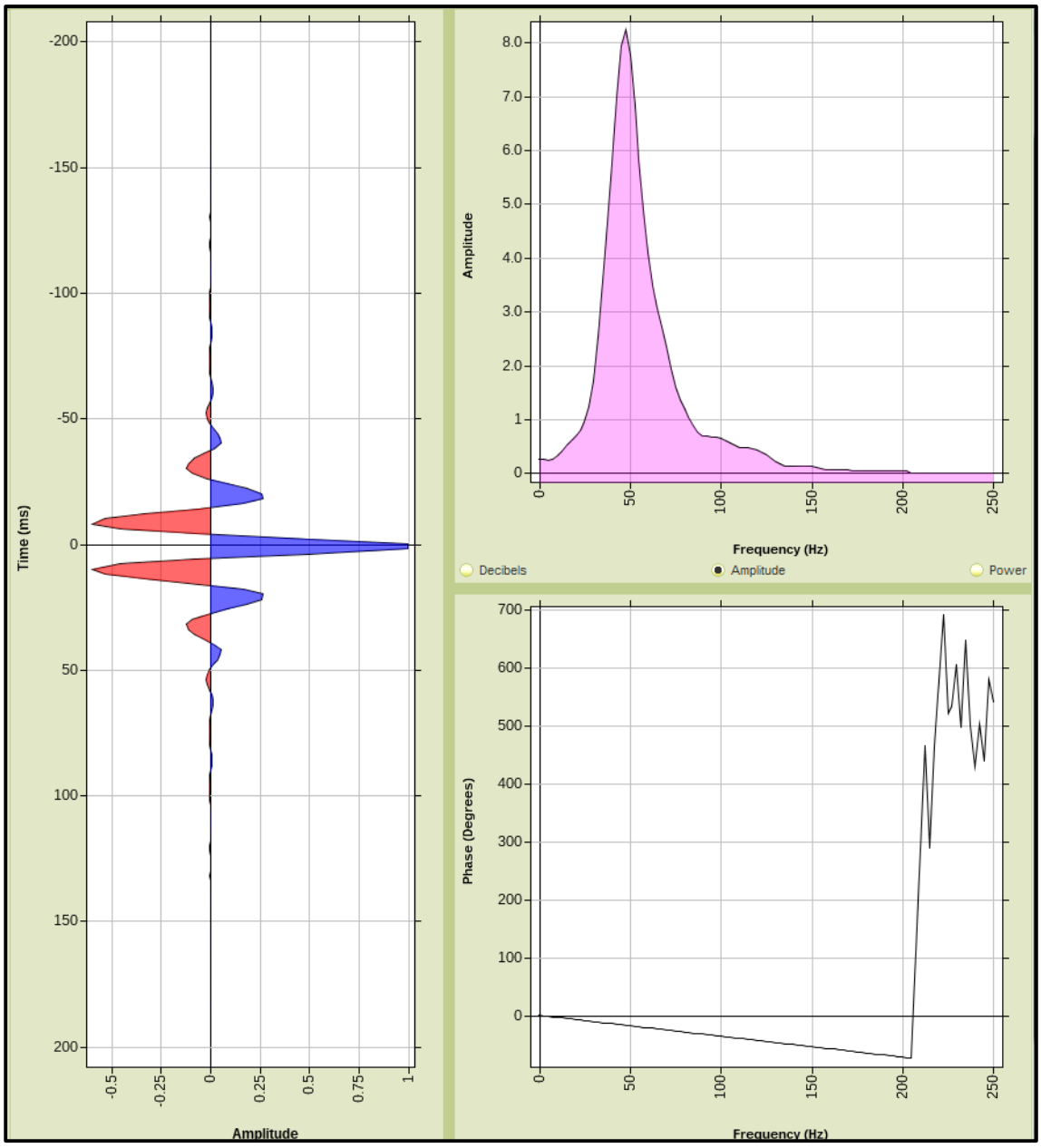

Figure 4.2: Amplitude, frequency, and phase character of the zero-phase wavelet extracted from the Baseline Survey via frequency matching.

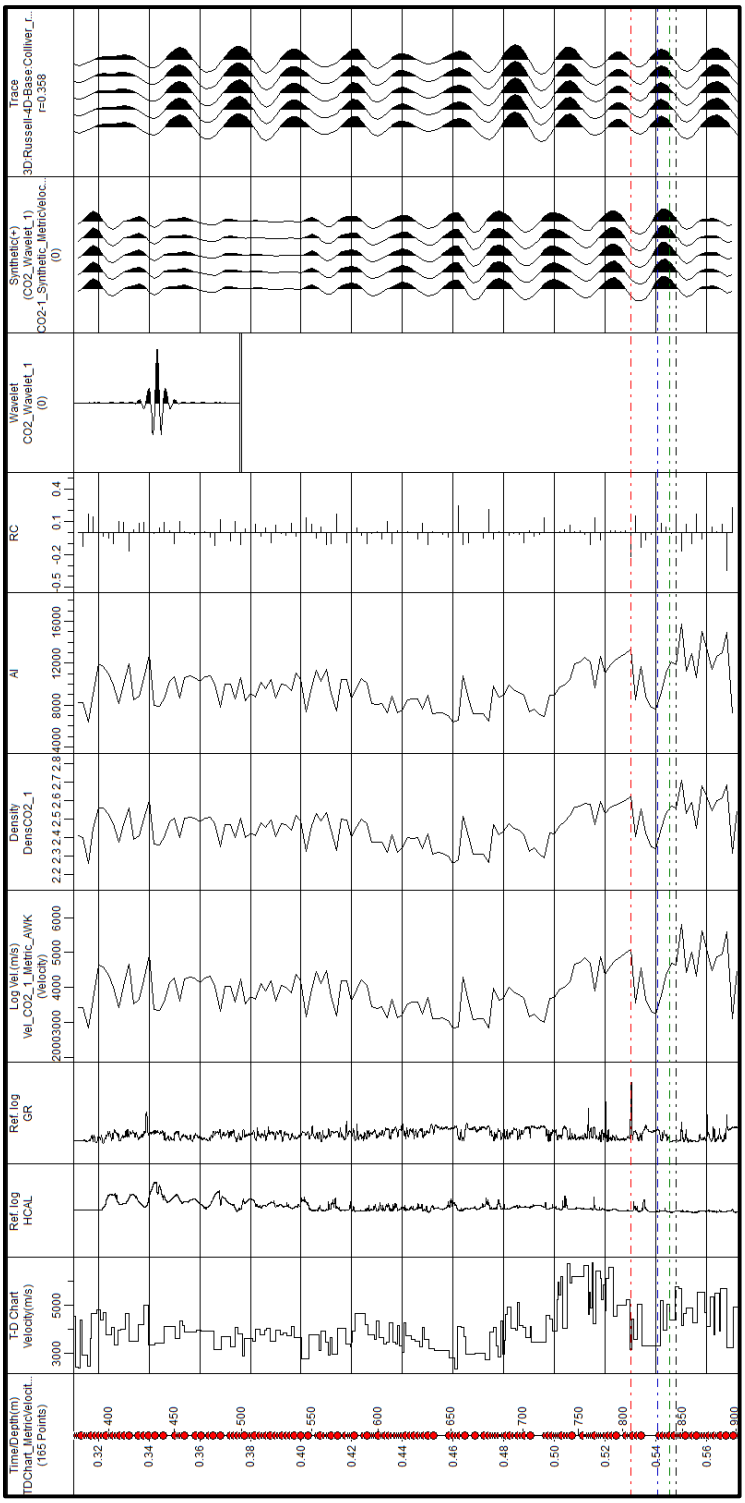

Figure 4.3: Synthetic-to-seismic well tie of Well CO2-I #1 to the Baseline Survey data. Panels from left to right include: T-D chart (seconds, meters), T-D chart velocity, caliper, GR, velocity, density, AI, reflection coefficient, extracted wavelet, synthetic seismogram, and extracted trace. Horizon tops, from top to bottom, include: Heebner Shale (red), LKC (blue), LKCC (green), and LKCD (black).

4D Seismic Horizon Tracking Workflow

A workflow was developed to track the LKC horizon over the Baseline, M2, and M6 Surveys to maximize certainty for qualitative and quantitative interpretation of horizon- and window-based seismic attributes between surveys. Due to the low SNR of these onshore data, conventional autotracking operations were not sufficient alone in yielding satisfactory results within each survey, let alone when attempting to track the same event over multiple surveys required by 4D seismic. The objective of this workflow was to determine which autonomous horizon tracking operations and parameters could be applied to a manually-tracked Baseline horizon interpretation to maximize duplication of these data, and if this approach could be employed to extend the Baseline horizon interpretation to monitor survey horizons. Major considerations and motivations within this process included the need to overcome low SNR and inter-survey non-repeatability, a quantitative approach to maximize accuracy in LKC horizon picking, avoiding biased manual picking in regions where CO_2 invasion was known or probable, and a need to reduce the degree of manual editing required over each survey. This workflow was completed in three stages, which included: 1) Baseline Horizon Manual Horizon Picking, 2) Duplication of Baseline Manual Horizon Picks Using Autonomous Snapping Operations, and 3) Extension of Baseline Horizon Data to Monitor Surveys Through Application of Autonomous Snapping Operations.

Following the completion of this systematic LKC horizon tracking across surveys, a suite of attributes was generated on these seismic volumes to aid in final edits of each Surveys' LKC horizon prior to interpretation. Instantaneous phase proved more effective than amplitude in tracking LKC continuity in low-fold zones, and relative acoustic impedance (RAI) was useful in validating the correct reflector to continue tracking when entering and exiting zones with significant tuning effects and/or low SNR character.

Baseline Horizon Manual Horizon Picking

The first step of this workflow required a solid interpretation of the Baseline Survey's LKC horizon. LKC time-structure (X-Y-Time) data of the Baseline Survey were available from prior interpretation, and these data were uploaded to guide initial interpretation of the Baseline Survey. Seed points for were placed using this guide in attempt to apply 3D horizon autotracking, but both standard and advanced autotracking operations failed to adequately track the LKC horizon. Instead, manual picking of every inline (n=166) and crossline (n=175) was performed using the guide horizon and synthetic-to-seismic well tie results – always starting with lines intersecting with Well CO2-I #1, and extending outward to the survey periphery. This process was first conducted on the Baseline Survey's inlines and crosslines, and then repeated for lines rotated 45° to the inlines' and crosslines' azimuth, followed by north-south and east-west lines, and finally again with inlines and crosslines. This approach was taken to reduce bias from acquisition footprint in picking inlines and crosslines alone, and is displayed in Figure 4.4. Extra emphasis was placed in horizon tracking within the coverage of higher-fold data, especially between inlines #60-110 and crosslines #60-115. Reflectors outside of these bounds in the lower-fold region were difficult to track, and less attention was placed on these data due to the uncertainty associated with the LKC reflector T-D position. Once these final manual edits were completed, the Baseline LKC horizon was finalized and duplicated for snapping operation trials in the next step.

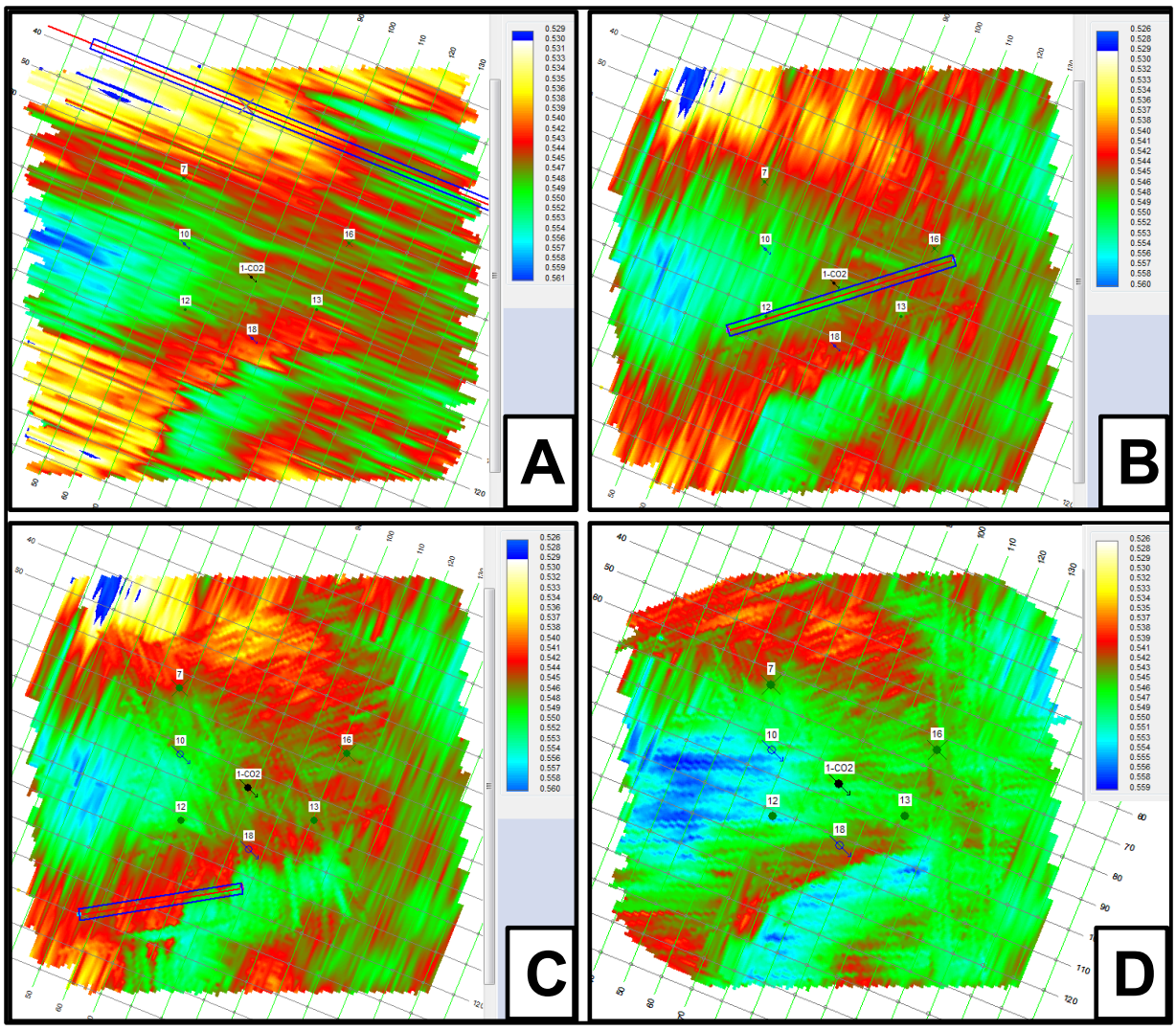

Figure 4.4: Manual LKC horizon tracking, covering results of picking from (A) inlines, (B) crosslines, (C) one set of lines approximately 45-degrees rotated from inline-crossline azimuths, and (D) final manual tracking result after inlines, crosslines, 45-degree rotated lines from inlines and crosslines, north-south and east-west trending lines, and inlines and crosslines picked once more.

Duplication of Baseline Manual Horizon Picks Using Autonomous Snapping Operations

Following completion of the manually-picked LKC horizon in the Baseline Survey, this horizon was duplicated and subjected to a multitude of horizon snapping methods and parameters in attempt to determine the combination of autonomous operations most effective in replicating the manually-derived result. The series of initial trials (B1-B12) applied to the

Baseline Survey 'input' horizon and their criteria are listed in Table 4.2 and displayed in Figure 4.5. Methods included a trace search shortcut (TSS) and guided window (GW). TSS allowed the first or nearest, absolute or relative event type (peak, trough, positive-to-negative zero crossing, negative-to-positive zero crossing) to be snapped above or below the input horizon. GW parameters included window length (seconds), guide window position, window offset direction, window offset distance, and event type. Snapping the manually-tracked horizon to an adjacent reflector of opposite polarity (first relative trough down – Trial B7, Figure 4.5G) stabilized and constrained the horizon's limits most effectively to be re-snapped to the subtle LKC reflector over a fine time window. Trial B7 horizon was duplicated and subjected to a series of additional methods and criteria for re-snapping – Trials B13-B16 (Figure 4.6). The resulting horizon which most closely reflected the initial manual interpretation was achieved through Trial B16 (Figure 4.6D) – snapping the input horizon to a relative peak, over a 0.018-second GW centered at the offset pick and shifted 0.006 seconds up. When comparing the autonomous picks of B7 and B16 to other trials in Figure 4.5 and Figure 4.6, respectively, it is clear why these trials were selected for further interpretation because of the significant mis-picks introduced from the other trials' methods and parameters – even within the vertical section displayed, which lies within the higher-fold zone of the surveys. To finalize the Baseline horizon's X-Y-Time data prior to its extension into the M2 and M6 Surveys, only significant mis-picks were corrected through manual editing, as demonstrated in Figure 4.7. Minor corrections were not applied to the Baseline LKC horizon for exportation in attempt to preserve repeatability of peak event location between data sets. The workflow, up until this point, is represented by an overlay of the horizons used in Figure 4.8. Minor corrections were applied to a copy of this Baseline LKC horizon to obtain a final LKC horizon for interpretation – the green horizon in Figure 4.8. The evolution of

LKC horizon tracking for this stage in map view is shown in Figure 4.9. A significant, regional LKC horizon mis-pick made south of Well #18 (Figure 4.9A-B) was corrected manually through validation of local LKCC top-structure trends (Figure 2.14A). This correction is shown in Figure 4.9C, and was only made for the extent of investigation for this study (Figure 4.9D).

Trial	Survey	Input Horizon	Snapped Horizon Result	Method	Snapping Criteria	Figure
B1	Baseline	LKC_C_Baseline_COPY_for_SAT	LKC_C_Baseline_snapped1	TSS	Nearest Absolute Peak	Figure 4.5A
B2	Baseline	LKC_C_Baseline_COPY_for_SAT	LKC_C_Baseline_snapped2	TSS	Nearest Relative Peak	Figure 4.5B
B3	Baseline	LKC_C_Baseline_COPY_for_SAT	LKC_C_Baseline_snapped3	GW	Snap to Largest Amplitude Peak, over a 0.004-second guide window centered at offset pick	Figure 4.5C
B4	Baseline	LKC_C_Baseline_COPY_for_SAT	LKC_C_Baseline_snapped4	GW	Snap to Absolute Peak, over a 0.004-second guide window centered at offset pick	Figure 4.5D
B5	Baseline	LKC_C_Baseline_COPY_for_SAT	LKC_C_Baseline_snapped5	GW	Snap to Relative Peak, over a 0.004-second guide window centered at offset pick	Figure 4.5E
B6	Baseline	LKC_C_Baseline_COPY_for_SAT	LKC_C_Baseline_snapped6	TSS	First Absolute Trough Down	Figure 4.5F
B7	Baseline	LKC_C_Baseline_COPY_for_SAT	**LKC_C_Baseline_snapped7**	TSS	First Relative Trough Down	Figure 4.5G
B8	Baseline	LKC_C_Baseline_COPY_for_SAT	LKC_C_Baseline_snapped8	GW	Snap to Relative Trough, over a 0.004-second guide window starting at pick and extending below	Figure 4.5H
B9	Baseline	LKC_C_Baseline_COPY_for_SAT	LKC_C_Baseline_snapped9	GW	Snap to Relative Trough, over a 0.006-second guide window starting at pick and extending below	Figure 4.5I
B10	Baseline	LKC_C_Baseline_COPY_for_SAT	LKC_C_Baseline_snapped10	GW	Snap to Positive-to-Negative, over a 0.010-second guide window centered at offset pick and shifted 0.002 seconds down	Figure 4.5J
B11	Baseline	LKC_C_Baseline_COPY_for_SAT	LKC_C_Baseline_snapped11	GW	Snap to Absolute Trough, over a 0.008-second guide window centered at offset pick and shifted 0.009 seconds down	Figure 4.5K
B12	Baseline	LKC_C_Baseline_COPY_for_SAT	LKC_C_Baseline_snapped12	TSS	Nearest Zero: Positive-to-Negative	Figure 4.5L
B13	Baseline	LKC_C_Baseline_snapped7	LKC_C_Baseline_RE_snapped7_2	TSS	First Absolute Peak Up	Figure 4.6A
B14	Baseline	LKC_C_Baseline_snapped7	LKC_C_Baseline_RE_snapped7_3	TSS	First Relative Peak Up	Figure 4.6B
B15	Baseline	LKC_C_Baseline_snapped7	LKC_C_Baseline_RE_snapped7_4	TSS	First Zero Up: Positive-to-Negative	Figure 4.6C
B16	Baseline	LKC_C_Baseline_snapped7	**LKC_C_Baseline_RE_snapped7_5**	GW	Snap to Relative Peak, over a 0.018-second guide window centered at offfest pick and shifted 0.006 seconds up	Figure 4.6D
M2-1	M2	LKC_C_M2_Import_BaseSAT1	LKC_C_M2_snapped1	TSS	Nearest Absolute Peak	Figure 4.10A
M2-2	M2	LKC_C_M2_Import_BaseSAT1	**LKC_C_M2_snapped2**	TSS	Nearest Relative Peak	Figure 4.10B
M6-1	M6	LKC_C_M6_Import_BaseSAT1	**LKC_C_M6_SAT1**	TSS	Nearest Relative Peak	Figure 4.12

Table 4.2: Trials of trace search shortcut (TSS) and guided window (GW) snapping methods, with a variety of snapping criteria applied to determine the approach most efficient in duplicating the Baseline manual horizon picks, as well as picking the M2 and M6 horizons from Baseline data. Snapped horizons in bold indicate the trial chosen to duplicate and re-snap, or to accept and begin manual editing.

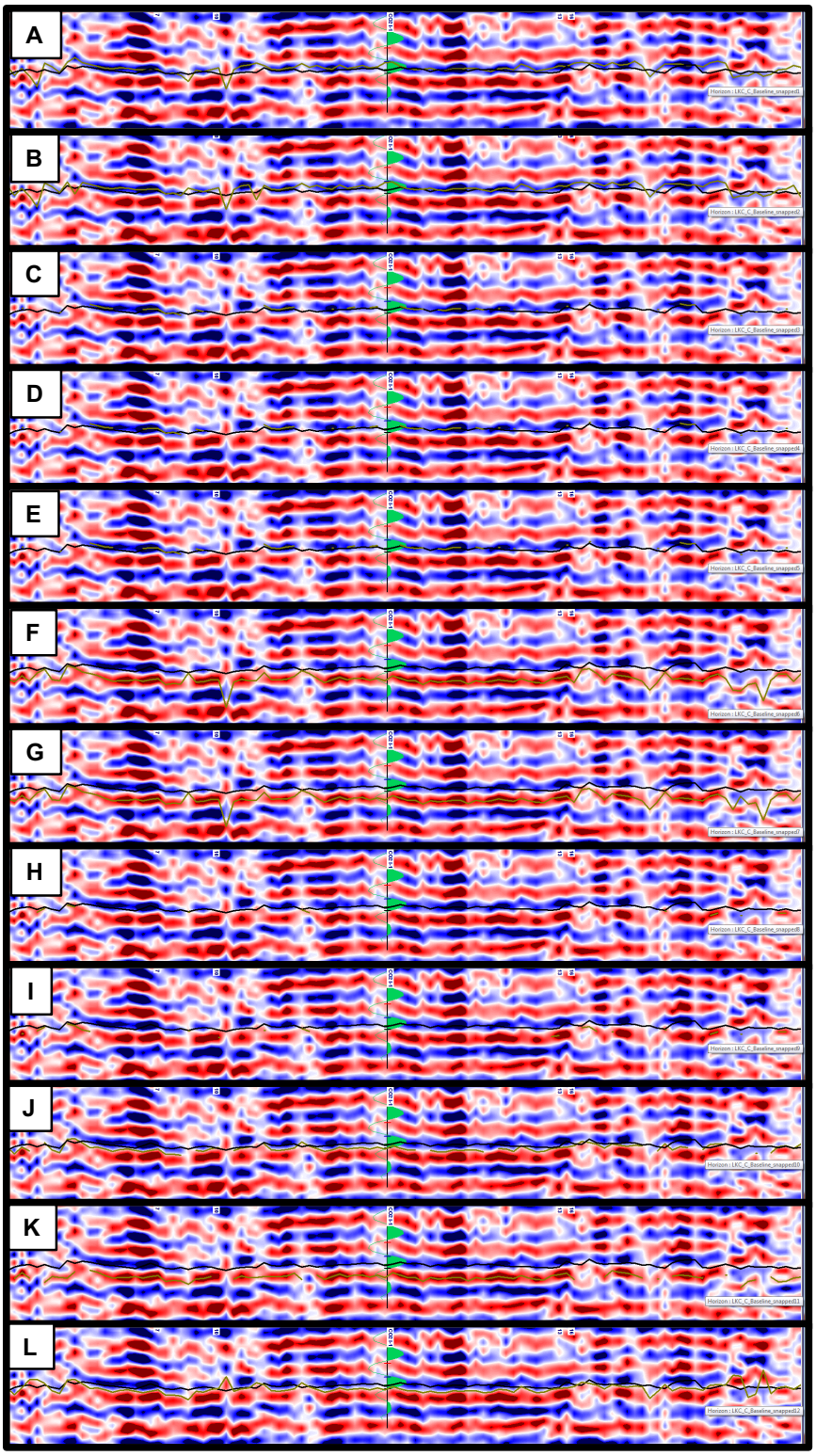

Figure 4.5: Trials B1-B12 (A-L, respectively) of snapping methods and parameters (Table 4.2) applied to a manually interpreted horizon in attempt to determine the method most efficient in duplicating the manual LKC horizon picks. Both the manually picked Baseline horizon (black) and the resulting snapped horizon (gold) are overlain for each trial.

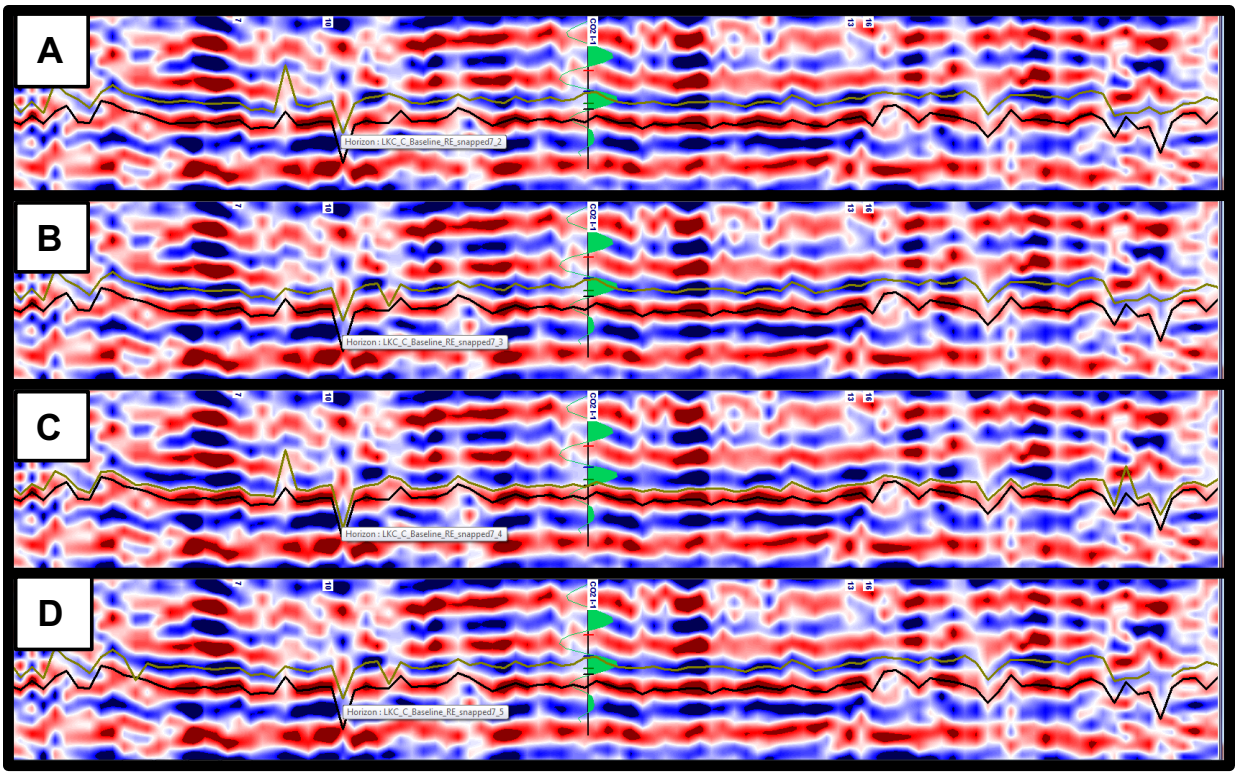

Figure 4.6: Trials B13-B16 (A-D, respectively) of snapping methods and parameters (Table 4.2) applied to trial result chosen ('LKC_C_Baseline_snapped7' horizon – Figure G). This prior horizon (black) and the resulting re-snapped horizon (gold) are overlain for each trial.

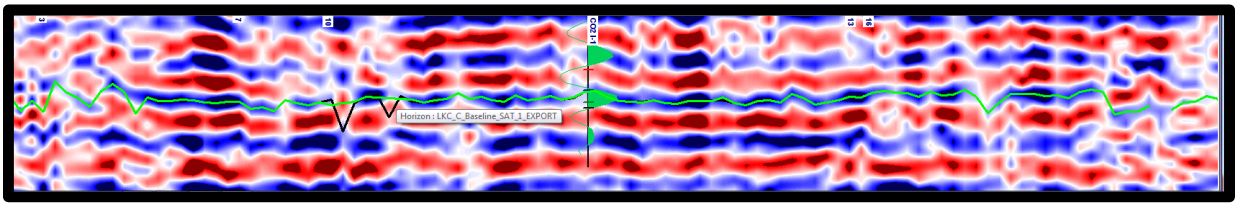

Figure 4.7: The result of Trial B16 (black) with an overlay of the final horizon for export (green) of which manual corrections were made in areas containing significant mis-picks.

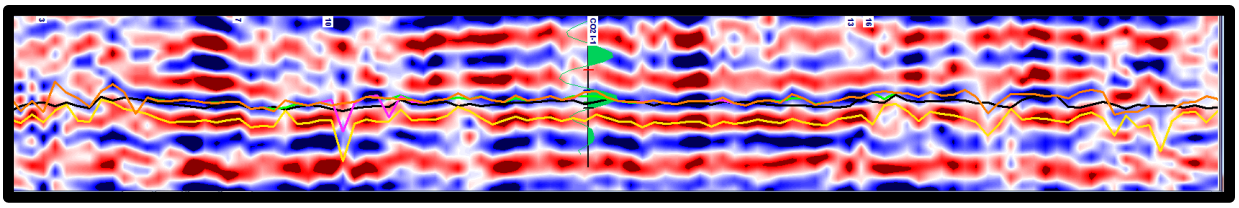

Figure 4.8: Workflow of LKC horizon interpretation for the Baseline Survey, including: imported reference horizon (black), Trial B7 (yellow), Trial B16 (pink), manual edits conducted on significant mis-picks (orange), and final interpretation with additional manual edits (neon green).

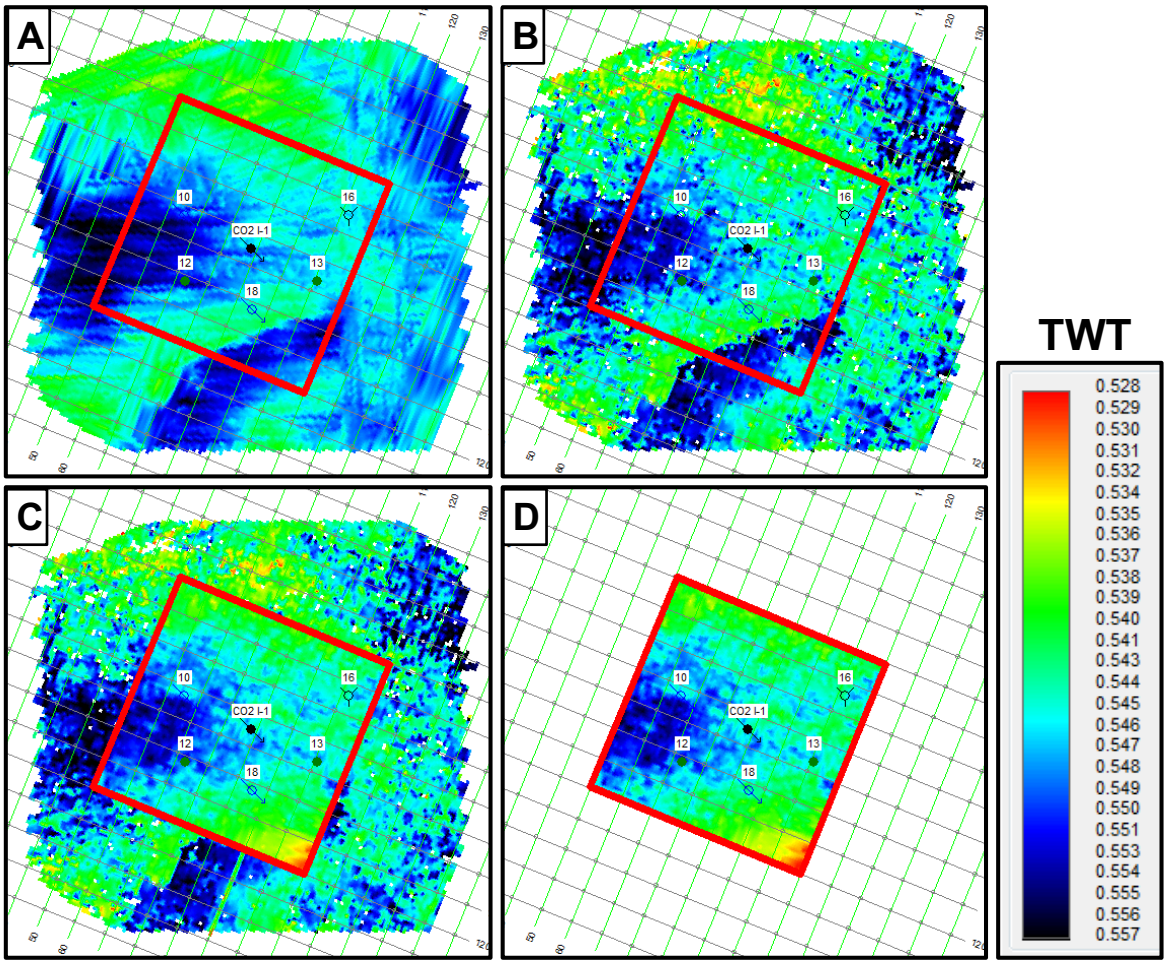

Figure 4.9: LKC horizon tracking after (A) input manually-tracked horizon was subjected to (B) snapping Trials B7 and B16, and (C) coarse manual edits over areas with significant mis-picks (this result exported for extension to M2 and M6). (D) Final horizon interpretation in the area of investigation (inlines #50-120, crosslines #50-120) after quality checking results obtained in (C) with use of non-amplitude attributes.

Extension of Baseline Horizon Data to Monitor Surveys Through Application of Autonomous Snapping Operations

The goal of this step was to systematically minimize the degree of manual editing required to translate data between the Baseline and Monitor Surveys, maintain a consistent and quantitative emphasis in horizon tracking to better capture relative and absolute changes between surveys, and to avoid bias in exaggerating manual picks of regions where CO_2 invasion was known and/or expected. To extend the LKC X-Y-Time horizon data from the Baseline to M2 and M6 Surveys, these Baseline Survey data were imported, assigned to each respective Monitor Surveys' data type, and subjected to a series of snapping methods and criteria listed in Table 4.2. Two snapping Trials, M2-1 and M2-2 (Figure 4.10), were conducted on the imported horizon within the M2 Survey data. Snapping the imported horizon to the nearest relative peak in Trial M2-2 resulted in an adequate fit to the LKC peak reflector, which required minimal manual corrections. The successful snapping criteria chosen to extend the Baseline data to M2 in Trial M2-2 – snapping Baseline input horizon to nearest relative peak – achieved sufficient results when applied to the M6 Survey, in Trial M6-1. The evolution of horizons through this workflow for the M2 and M6 Surveys are shown in Figure 4.11 and Figure 4.12, respectively. Final results of the LKC time-structure are shown in map view for the Baseline, M2, and M6 surveys in Figure 4.13.

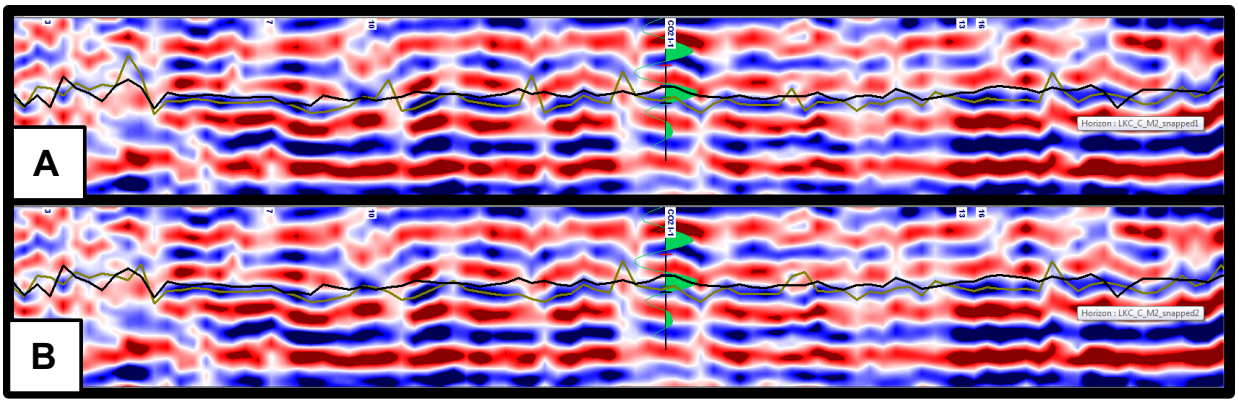

Figure 4.10: Trials M2-1 (A) and M2-2 (B) of snapping methods and parameters (Table 4.2) applied to the imported Baseline horizon (black), and the resulting snapped horizons (gold).

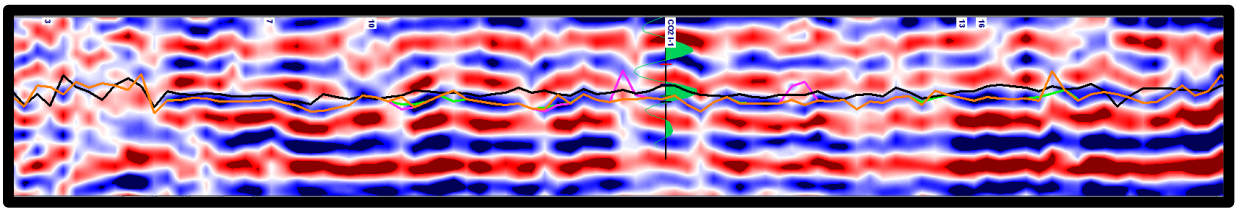

Figure 4.11: Workflow of LKC horizon interpretation for the M2 survey, including: imported Baseline horizon (black), Trial M2-2 (pink), manual editing conducted on significant mis-picks remaining (orange), and final interpretation with additional manual edits (neon green).

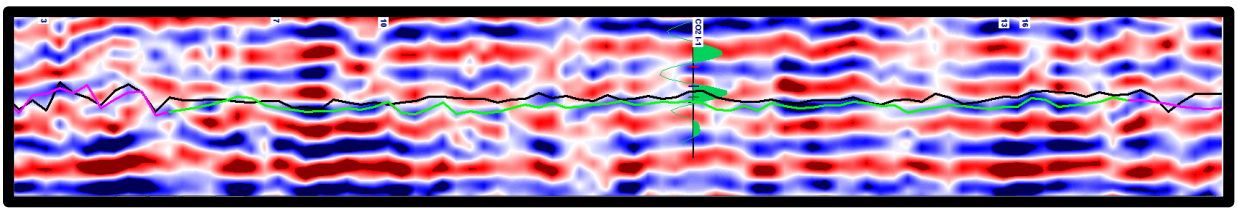

Figure 4.12: Workflow of LKC horizon interpretation for the M6 survey, including: imported Baseline horizon (black), manual editing conducted on significant mis-picks remaining on Trial M6-1 (pink), and final interpretation with additional manual edits (neon green).

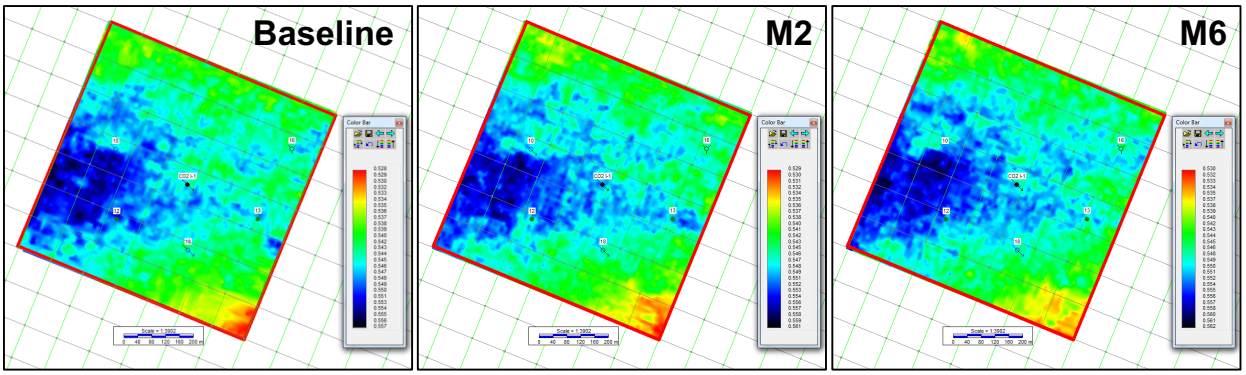

Figure 4.13: Final results of LKC horizon time-structure for the Baseline, M2, and M6 Surveys.

Conclusions

The application of single horizon autotracking and snapping methods alone was significantly less effective in tracking the LKC compared to the workflow developed for this study to maximize intra- and inter-survey horizon tracking accuracy. Applying a series of trials with varying horizon snapping methods and parameters to a manually-tracked horizon provided a better understanding of the sensitivity of these criteria – alone and in combination. The multi-step application of TSS and GW snapping methods was successful in constraining autonomous horizon picks within low SNR data, which closely duplicated the interpretation of a manually tracked horizon and maintained geological integrity. Unraveling effective horizon snapping methods and parameters from the Baseline Survey trials allowed rapid extension of accurate horizon tracking to the M2 and M6 Surveys. In addition to expedited horizon tracking, the snapping operations applied provided a quantitative and consistent means to track the reflection event corresponding to the LKC. By snapping to the same data type, relative and absolute comparison of these horizons between surveys is honored despite low SNR and non-repeatability present within the data. Additionally, this approach prevents any bias of exaggerating picks in zones where CO_2 is known to have invaded to intentionally create an anomaly. Avoiding biased manual picking allowed autonomous horizon tracking to be tested in its ability to consistently

track the LKC horizon, and reveal subtle changes in seismic data character across the Baseline and Monitor Surveys. This method provided powerful interpretation to highlight subtle anomalies associated with CO_2-EOR relative to the LKC horizon.

Spectral Decomposition

Analysis of frequency sub-bands across the Baseline, M2, and M6 Survey volumes was conducted using Rock Solid Images' Rock Solid Attributes (RSA) package in IHS Kingdom software. The spectral decomposition attribute 'SD Envelope Sub-band' was selected to partition the Surveys' amplitude envelope data into a series of sub-bands over a fixed bandwidth. The SD Envelope Sub-band attribute is generated using the Gabor-Morlet wavelet transform, which consists of applying Gabor-Morlet wavelets as filters to the full-band input seismic data to derive complex trace information from frequency sub-bands. These sub-bands contain the average amplitude and phase information for specific frequencies of the original input seismic data (Taner, 1983). In order to obtain amplitude data representative of a frequency, the sub-band's traces are divided by the original trace envelope for normalization and removal of individual reflection events (Taner, 1983). Comparison between a selection of sub-bands' amplitude envelope reveals the relative proportion of energy each sub-band contributes to the full-band data, which varies based on the selected low and high peak frequencies and number of output bands.

The bandwidth of data selected for spectral decomposition was determined through consideration of reservoir thickness range and amplitude-frequency content of the Surveys' effective bandwidth within a sub-volume encompassing the reservoir interval (time window) over the spatial extent of higher-fold coverage (Figure 5.2). This was completed in two trials – initially with a first-run trial with a coarse sampling interval (20 bands, octave scale) applied to a

broad bandwidth (20.0-85.0 Hz), which was completed to determine the effective range of amplitude-frequency over the Baseline Survey. After validating the effective bandwidth, a second trial using a finer sampling interval (25 bands, linear scale) was applied to the selected, narrower bandwidth (30.0-80.0 Hz) on the Baseline Survey (parameters displayed in Figure 4.14, results displayed in Figure 5.4). The spectral decomposition data from the second trial was analyzed on the Baseline Survey to enhance reservoir characterization by improving the understanding of LKC thickness variation and boundary (shoal, facies) identification. Following establishment of the Baseline Survey's spectral decomposition interpretation, the same data (30-80 Hz, 25 bands, linear scale) were generated for the M2 and M6 Surveys to investigate 4D seismic spectral and tuning anomalies at frequency sub-bands related to injection and production activity. Amplitude envelope color bars were standardized to range from zero to the maximum value observed across all frequency sub-bands within each trial and survey. These data were extracted to each Surveys' LKC horizon for display in map view for the Baseline (Figure 5.4, Figure 5.6) and Monitor Surveys (Figure 6.10).

Display and interpretation in spectral decomposition of amplitude envelope data are described here, and should be acknowledged prior to analyzing these data for the Baseline (Figure 5.4, Figure 5.6) and Monitor Surveys (Figure 6.10). Comparison of amplitude response across frequency sub-bands in the spectral decomposition data was made to identify anomalous zones within the area of investigation, which were outlined with polygons and overlain on the Baseline (Figure 5.4, Figure 5.6) and Monitor Survey data (Figure 6.10). Anomalies included low- and high-frequency responses, and spatial trends in tuning frequency shifts. These trends suggest lateral facies change and thickness variation, in addition to pressure and fluid content when analyzed from Baseline to Monitor Surveys. When describing amplitude response from a

frequency or bandwidth to a trend observed in the spectral decomposition data, this does not suggest the anomaly is completely limited to the frequency or bandwidth described, but rather the observed feature is strongly associated with this frequency or bandwidth. In this application, spectral decomposition of amplitude envelope data reveal amplitude response for a number of frequency bands over a determined bandwidth, so amplitude data within the interval between frequency bands may be more representative of an identified anomaly. Considerations of data scaling criteria include minimum and maximum values selected to standardize the color bar to each frequency sub-band within one survey, and the effect of scale range with variation in the bandwidth interpreted. Selection of color bar minimum and maximum values to standardize the scale between frequencies within a survey always assigned zero for the minimum and used the maximum value observed across all frequencies analyzed within the survey. Since all spectral decomposition analyses extended above and below the dominant frequency of the data (approximately 50 Hz, Figure 5.7) containing the highest reflection strengths, qualitative comparison between the Baseline, M2, and M6 Surveys' data with this scaling method was sufficient. The maximum amplitude response around the dominant frequency served as a calibration to the value used as the maximum in standardizing the color bar across frequencies for a given survey's data – reducing the degree to which false anomalies are created at the same XY-location between surveys.

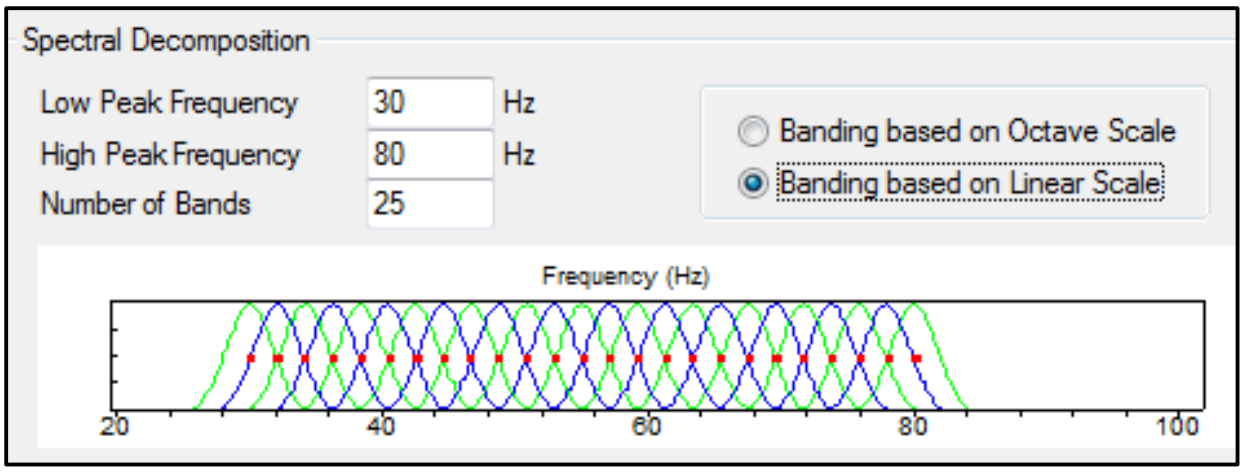

Figure 4.14: Parameters to generate spectral decomposition data. This trial includes 25 linearly distributed sub-bands of amplitude envelope calculated between low- and high-peak frequencies of 30 and 80 Hz, respectively.

Chapter 5 - Baseline Seismic Reservoir Characterization

Interpretation of the Baseline, M2, and M6 Surveys was completed following mistie corrections, synthetic-to-seismic well tie, and horizon tracking. These three surveys were selected for analysis based on data quality and potential to correlate 4D seismic anomalies to known changes in injection and production at well locations. Cross-equalization results (Figure 5.1) were used to determine the spatial extent of inter-survey trace similarity, which served as an interpretation guide for horizon tracking and 4D seismic anomalies. As discussed in 4D Seismic Horizon Tracking, the peak event associated with both the LKC and LKCC top was tracked, and is referred to as the LKC. Based on these results, qualitative and quantitative interpretation methods were applied to a selected zone of higher-fold coverage between inlines #50-120 and crosslines #50-120 (Figure 5.2) – the bounds delineated for investigation of this study. The data outside this coverage were not considered due to the uncertainty associated with low-fold and low SNR character. Due to inconsistencies expected between Surveys' phase and amplitude, interpretation of these seismic data placed emphasis on post-stack windowed attributes in reference to the LKC horizon. This included amplitude envelope (30-80 Hz, 20ms window), displayed with amplitude and dominant frequency extracted from the LKC horizon in Figure 5.3. These data provided some insight into potential boundaries and thickness trends of LKC shoals. Spectral decomposition of the amplitude envelope was generated to analyze changes in reflection strength across frequency sub-bands, and provide more detailed insight into facies boundary positions and thickness variation.

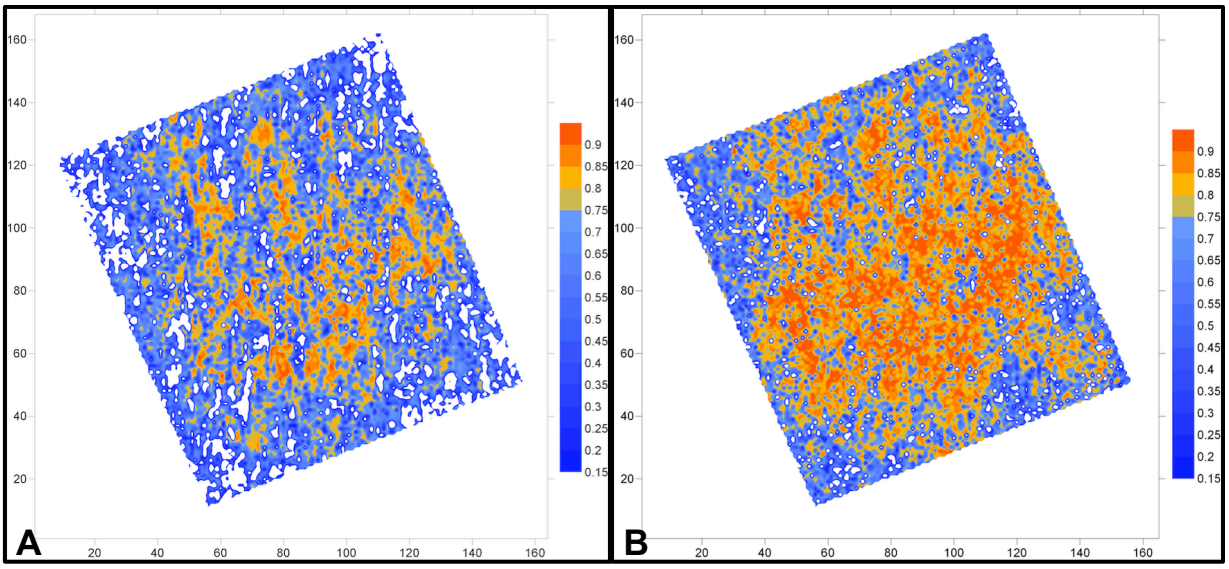

Figure 5.1: Correlation coefficient between the Baseline and M2 Surveys (A) before and (B) after cross-equalization. These results aided in placing confidence in 4D seismic anomalies.

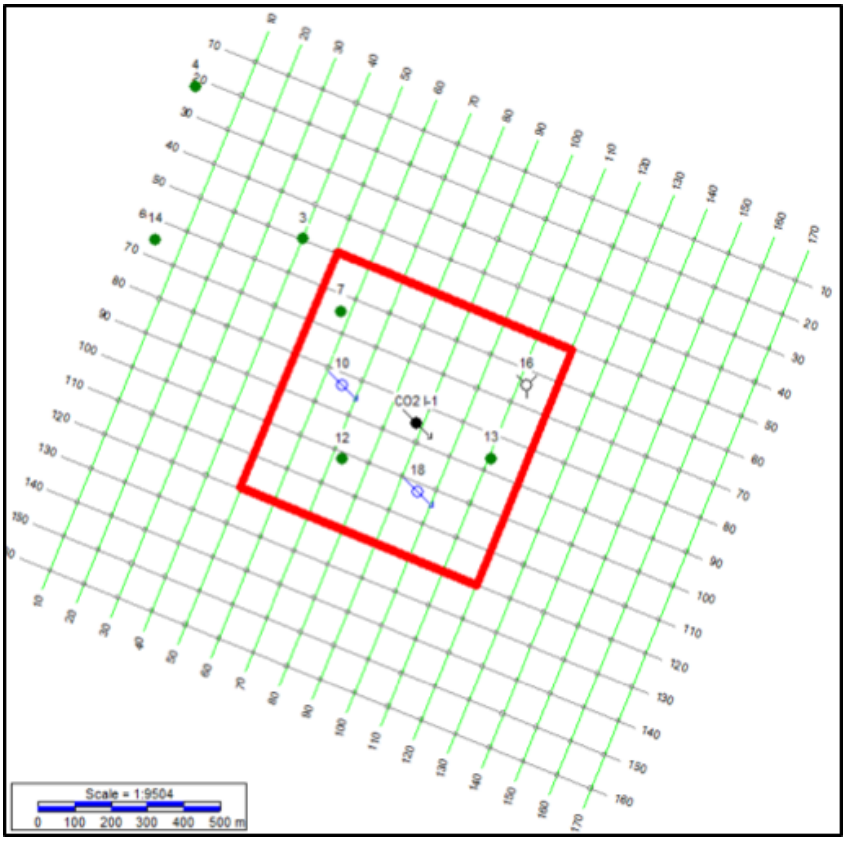

Figure 5.2: Extent of seismic surveys, with red perimeter encompassing the higher-fold zone used for seismic interpretation (Inlines #50-120, Crosslines #50-120).

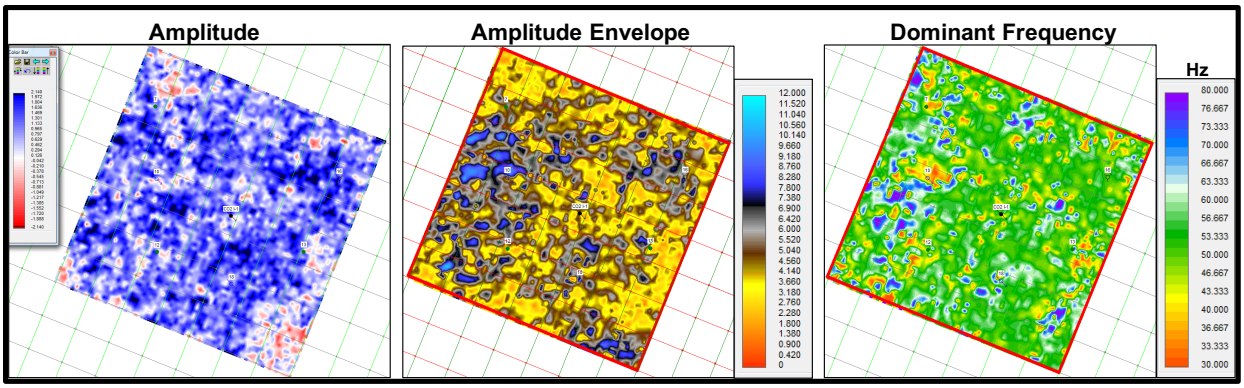

Figure 5.3: Amplitude, amplitude envelope, and dominant frequency of the Baseline Survey LKC horizon. Amplitude envelope calculated with 30 Hz low peak and 80 Hz high peak frequencies over a 20-ms window centered on the LKC.

Spectral Decomposition of Amplitude Envelope

Spectral decomposition was applied to the Baseline Survey data to improve characterization of LKC reservoir architecture in detail beyond the capacity offered from full-band conventional seismic data. This included analysis of amplitude envelope across frequency sub-bands (Figure 5.4: 30-80 Hz, 25 bands, linear scale) for relative and absolute thickness estimation, and delineation of major lateral facies changes – including porosity and permeability – which may highlight boundaries of fluid pathways or baffles. Characterizing these criteria in the Baseline Survey was essential prior to investigating 4D seismic spectral and tuning anomalies, and assigning these to potential saturation and/or pressure changes in response to injection and production.

Interpretation of LKC stacked ooid shoal complexes through spectral decomposition of the Baseline Survey was guided by, and corroborated with, geological findings by Watney et al. (2006, 2007) and Watney (2015) (Figure 5.5A-B) to improve reservoir characterization away from well control. Potential shoal boundaries and bodies (polygons #1-5) delineated from amplitude anomalies across frequencies are displayed in Figure 5.5C, listed in Table 5.1, and overlain on the same spectral decomposition data in Figure 5.6. Polygons were identified as

spatially sustained anomalies with relative band-to-band trends in reflection strength (amplitude envelope) suggestive of facies boundaries, relative thickness variation, and zones of overlap in stacked shoals. Although these polygon boundaries are by no means definitive, they contain trends and positions corresponding to those suggested by geological interpretation (Figure 5.5).

Polygon #1 is a sinuous, low-frequency anomaly located near Well #10 and Well #12. This anomaly stands out significantly above the majority of data between frequencies 34.2-42.5 Hz. Higher frequency amplitude reflection strength occurs near the polygon's periphery between frequencies 46.7-57.1 Hz. The low-frequency nature of this anomaly suggests it is either a thicker zone of Shoal #3, a zone varying from its surroundings in facies type or porosity, or both.

Polygon #2 is a curved boundary which trends with Polygon #5 and is indicative of the western boundary of Shoal #2. A defined amplitude response emerges at 55.0 Hz on the polygon edge, with a tuning response migrating eastward at progressively lower frequencies – indicating relative thickening toward the center of interpreted Shoal #2 until 44.6 Hz.

Polygon #3 is a sinuous line representing the suggested eastern boundary of Shoal #2 and/or a point of overlap between Shoal #2 and Shoal #1. This line follows a low-frequency trend from 34.2-40.4 Hz, and a higher amplitude envelope response trending away from both sides of this line at progressively higher frequencies is indicative of thinning in both directions. If this thinning response only trended easterly away from polygon #3, then this would suggest the east boundary of Shoal #2. In combination with thinning from both sides of this line, further evidence of the low-frequency response reinforces the scenario of this polygon outlining the overlap between Shoal #2 and Shoal #1.

Polygon #4 is a sub-sinuous line placed as a marker for the boundary separating a low reflection strength anomaly on the eastern portion of the line across nearly all frequencies, and a

less extreme, similar anomaly in some portions west of the line and between polygon #3. This line is associated with a subtle, low-frequency trend which persists between 34.2-38.3 Hz, and erratic and inconsistent amplitude response at higher frequencies. Polygon #4 potentially represents either the thickest part of Shoal #1 within the area of study or the western edge of Shoal #1. For the case of the former, the western edge of Shoal #1 may fall between, or extent to, polygon #3 – in support of the scenario for overlap between Shoal #2 and Shoal #1.

Polygon #5 is suggestive of the eastern edge of Shoal #3. Amplitude response is apparent at low frequencies in the polygon's center around 36.2-38.3 Hz and extends toward the polygon periphery at progressively higher frequencies until 57.1 Hz. Reflectivity strengths within this polygon are highly similar to those of the suggested boundaries of Shoal #2 (polygons #2 and #3) in terms of both magnitude and tuning response across the range of 44.6-57.1 Hz.

Shoal #2 – bounded by polygons #2 and #3 – contains a notably strong amplitude response starting at 44.6 Hz, which extends outward to the suggested boundaries' periphery until 57.1 Hz. The interpreted edge of Shoal #3 through spectral decomposition (polygon #5) follows the geologic interpretation, and encompasses the low-frequency anomaly of polygon #1, which may be a thicker portion of the shoal, a change in facies, or potentially contain anomalously high pressure relative to other regions of the pilot with similar LKC thickness. Re-pressurization from Well #10 and saturation changes could contribute to tuning of lower frequencies for the LKC. Effects of potential overlap between Shoal #3 and Shoal #2 are observed in the region between polygon #5 and polygon #2. A significant low-frequency amplitude response (38.3-40.4 Hz) occurs in the northern portion of this zone, whereas an intermediate amplitude response (46.7-50.8 Hz) occurs in the southern portion of this region. This region appears as an anomaly with

weak reflection strength at, and above, 55.0 Hz, suggesting this is a zone of overlap between Shoal #3 and Shoal #2, with greatest thickness in the northern portion.

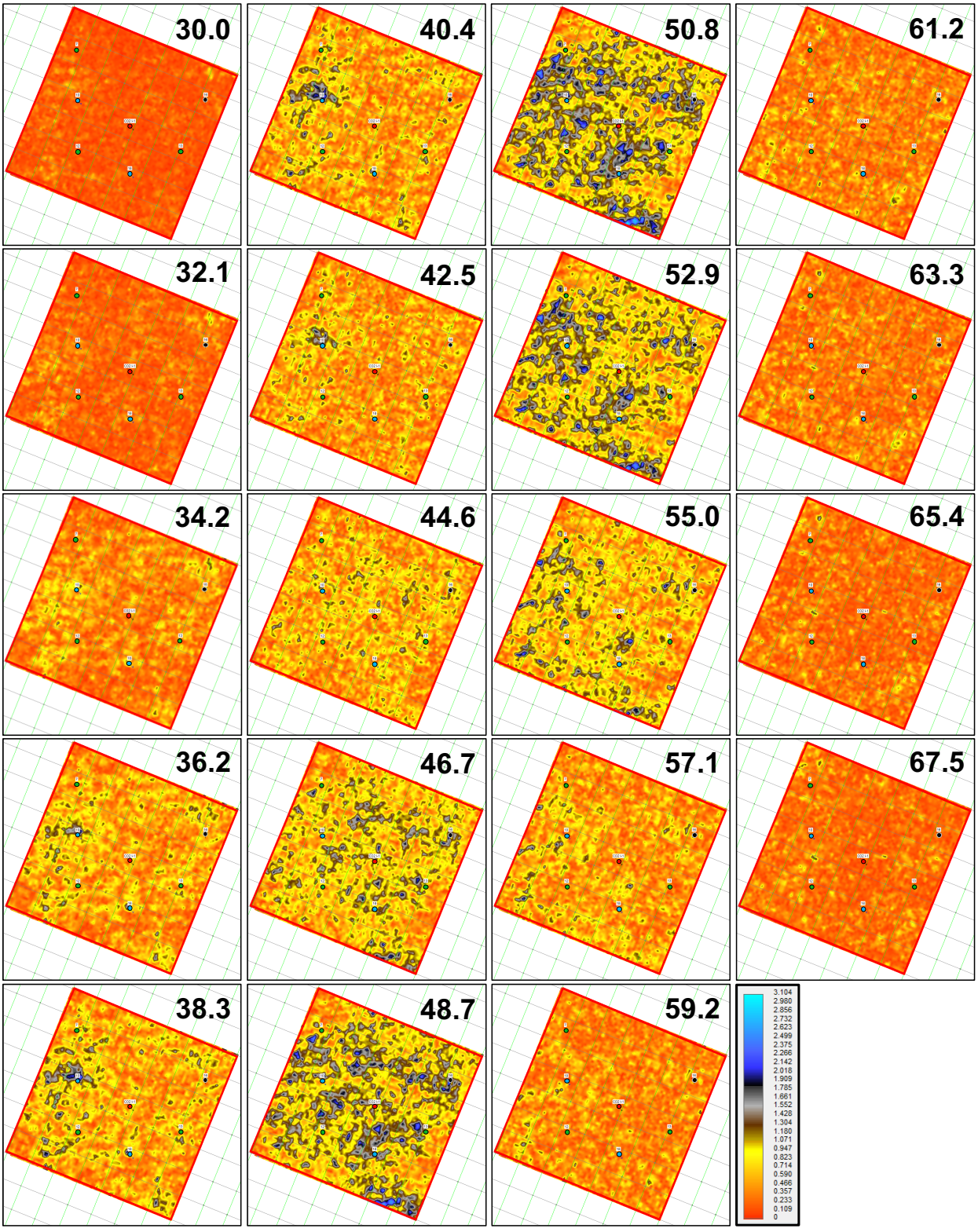

Figure 5.4: Spectral decomposition results (30.0-80.0 Hz tested, 30.0-67.5 Hz shown) of the Baseline amplitude envelope extracted to the LKC horizon.

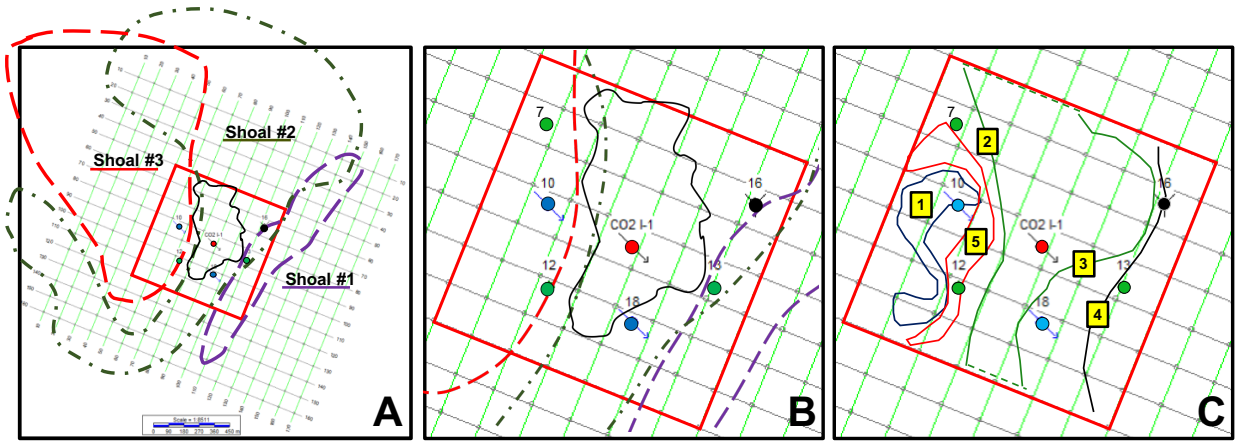

Figure 5.5: Polygon outlines of CO_2 plume from PPB interpretation and LKC shoal complexes' geologic interpretations by Watney et al. (2006, 2007) and Watney (2015) in reference to (A) the entire seismic survey, and (B) the bounds of this study's investigation. These findings were used to guide interpretation of the Baseline Survey's amplitude variation across frequency sub-bands, which identified (C) potential shoal boundaries and bodies beyond detail available with well data. Descriptions of the polygons (#1-5) representing these seismically-identified boundaries and bodies are outlined in Table 5.1.

Polygon	Interpretation
1	Thicker zone and/or unique facies within Shoal #3
2	Western boundary of Shoal #2
3	Eastern boundary of Shoal #2 and/or point of stacked overlap between Shoal #2 and #1
4	Thickest part of Shoal #1, or western edge of Shoal #1
5	Eastern edge of Shoal #3

Table 5.1: Interpretation of polygons #1-5 (Figure 5.5C) identified through spectral decomposition of the Baseline Survey and their corroboration with LKC Shoals (#1, #2, #3) identified through geological interpretation (Figure 5.5A-B).

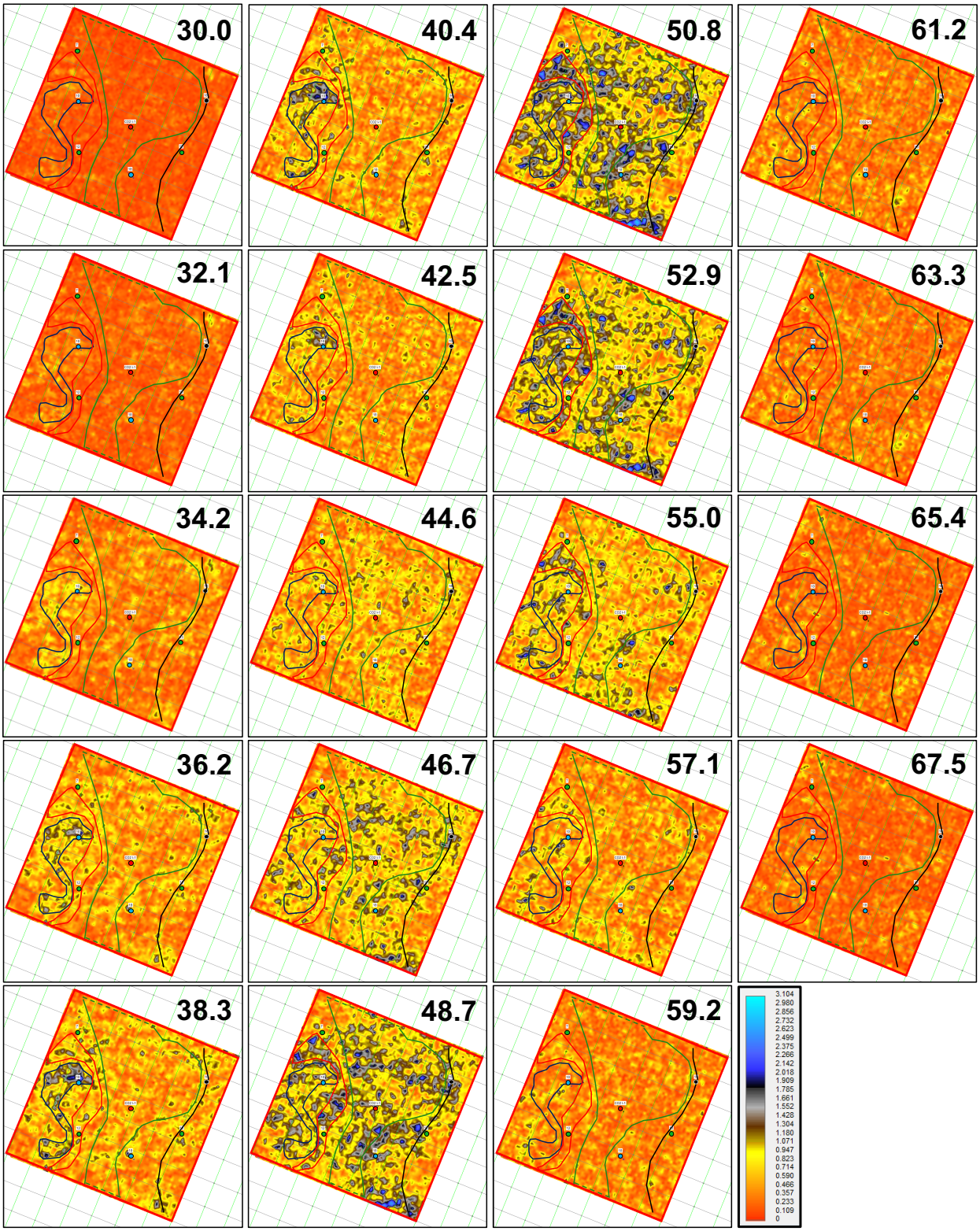

Figure 5.6: Spectral decomposition results (30.0-80.0 Hz tested, 30.0-67.5 Hz shown) of the Baseline amplitude envelope extracted to the LKC horizon and polygons of boundaries and seismic bodies displayed in Figure 5.5C and described in Table 5.1.

Tuning Modeling and Analysis

Using interval velocity and thickness of the LKC (calculated here as the LKC top to LKCD top) and LKCC, a model was developed to understand tuning thickness-frequency relationships of the data. Theoretical tuning bounds relative to the signal wavelength were calculated to determine if the data from formation thickness and observed tuning frequency through spectral decomposition at well locations are likely to be susceptible to tuning effects. These bounds include the upper limit of tuning ($\lambda/2$), tuning thickness ($\lambda/4$), and lower limit of tuning (threshold of resolution) ($\lambda/8$).

Based on the amplitude-frequency character of the seismic data for the Baseline, M2, and M6 Surveys within the reservoir interval (500-600 ms) and over the spatial extent of investigation (inlines #50-120, crosslines #50-120), low- and high-peak frequencies (30 and 80 Hz, respectively) were selected at approximately 0.5 amplitude (Figure 5.7) for analysis. Theoretical tuning curves ($\lambda/2$; $\lambda/4$; $\lambda/8$) were calculated using average interval velocity (4490 m/s) of the LKC to reveal the bandwidth of data required to resolve and capture tuning effects from both the LKC and LKCC based on thicknesses observed within the pilot region (Figure 5.8). Although the LKCC was the target reservoir interval for CO_2 injection, its thickness (3.6 – 6.0m) across the pilot region is considered incapable of observing tuning effects within the Surveys' amplitude-frequency content, as its maximum thickness would require at least 95 Hz to reach the theoretical threshold of resolution. Therefore, the focus of this investigation was tuning effects of the LKC due to its sufficient thickness (+15m) observed within the pilot region, with consideration that physical changes onset from CO_2 fluid substitution – even if these effects were limited completely to the LKCC interval within the LKC – would contribute to net changes in

the LKC. The limited extents of effective bandwidth (30-80 Hz) and thickness (5-30 m) range determined in Figure 5.8 are plotted in Figure 5.9.

Through analysis of spectral decomposition results, the observed frequency containing maximum reflection strength at well locations was plotted with known LKC thickness (Figure 5.10) in attempt to calibrate apparent tuning frequency with actual thickness. LKC thickness plotted for wells represent the thickness between the LKC top and the LKCD top. These data – plotted with observed tuning frequency from spectral decomposition data and known LKC thickness data at well locations – fail to plot on the theoretical tuning thickness curve ($\lambda/4$), but fall within the bounds of tuning investigated ($\lambda/8$ to $\lambda/4$) based on LKC average interval velocity. Potential explanations for this phenomenon include an overestimation of LKC interval velocity, underestimation of LKC thickness representing variations in amplitude envelope, and/or scaling bias from the dominant frequency. LKC interval velocity for theoretical tuning calculations was determined by averaging velocity obtained through well log data acquired from the Well CO2-I #1. As seen in Figure 5.10, the tuning thickness-frequency response of Well CO2-I #1 is positioned considerably closer to the theoretical tuning frequency curve compared to the other wells for its given thickness. Velocity perturbations in the LKC between Well CO2-I #1 and other wells may explain their deviation if average LKC interval velocities were lower in these wells. Additionally, thickness values may be underestimated for all wells, and especially for wells besides Well CO2-I #1, in terms of the representative thickness contributing to tuning responses observed in amplitude envelope data across frequencies. Thickness between the LKC top and LKCD top represented the higher-velocity interval in Well CO2-I #1 corresponding to a peak when matching the synthetic to seismic trace data, as seen between their respective blue and black tops in Figure 4.3. Stratigraphy beyond the LKC top to LKCD top interval may contribute

to this peak event, and therefore a thicker interval may be contributing to the amplitude response at tuning frequencies observed. Increasing the thickness for each well in Figure 5.10 for the observed tuning frequency drives data toward the theoretical point of maximum tuning. Increasing interval thickness would onset tuning at lower frequencies, and a combination of these effects would drive the observed values toward the theoretical point of maximum tuning. Additionally, implementing a standardized scale for amplitude envelope across all frequencies analyzed via spectral decomposition based on the maximum amplitude envelope value observed naturally introduces bias in scaling due to the dominant frequency. Due to attenuation and other factors in signal propagation, the frequencies returning to the receiver may be underestimating the theoretical tuning frequency response of the LKC. It is important to note observed tuning frequency values were based on an approximately 2 Hz sampling interval between bands, and therefore each tuning frequency contains potential error of approximately +/- 1 Hz. Nonetheless, an optimistic case of adding 1 Hz to each data point in Figure 5.10 would still not place the observed values on the theoretical point of maximum tuning.

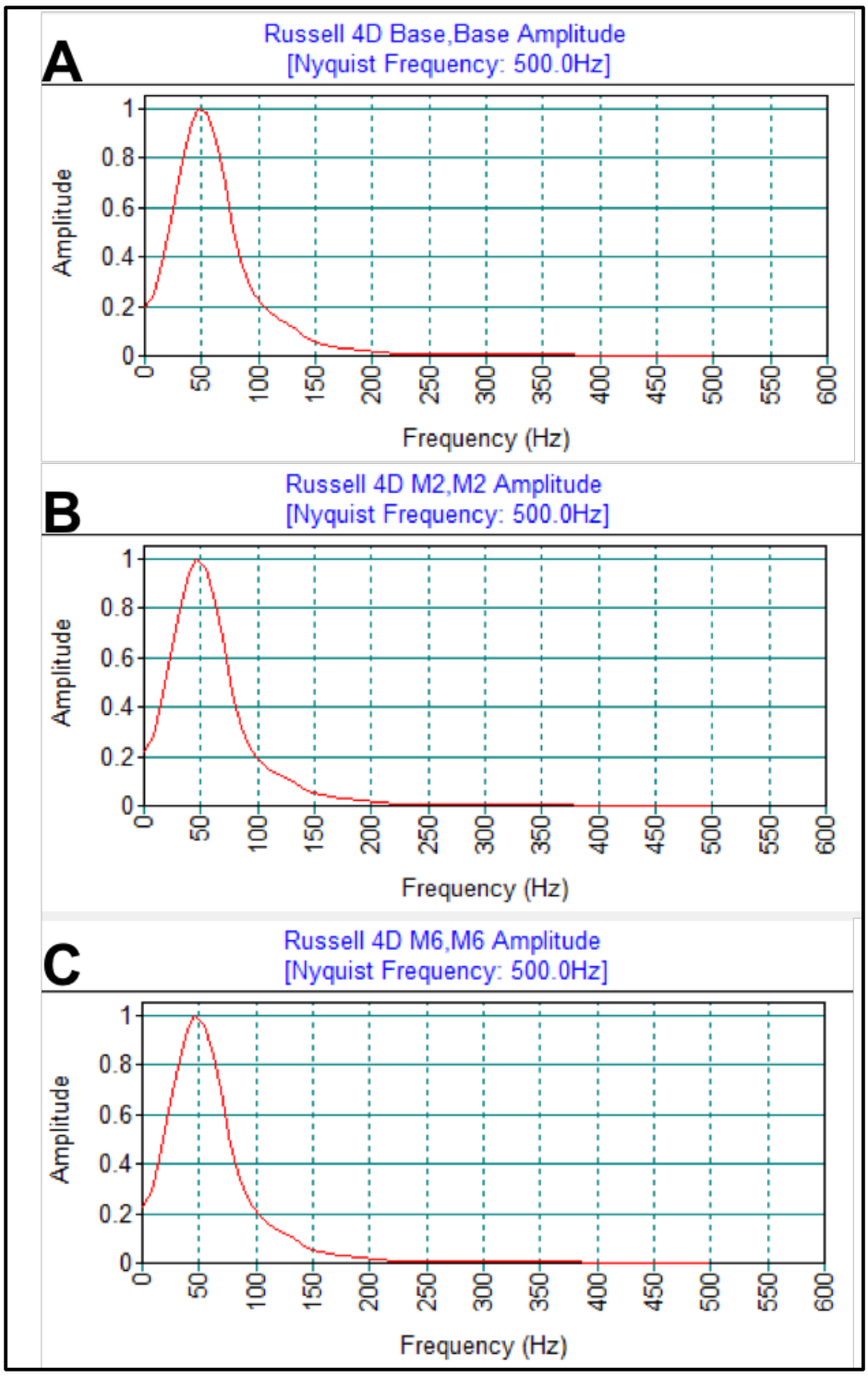

Figure 5.7: Amplitude-frequency character within the sub-volume of interpreted data (inlines #50-120, crosslines #50-120, time window 0.500 – 0.600 seconds) for the (A) Baseline, (B) M2, and (C) M6 Surveys.

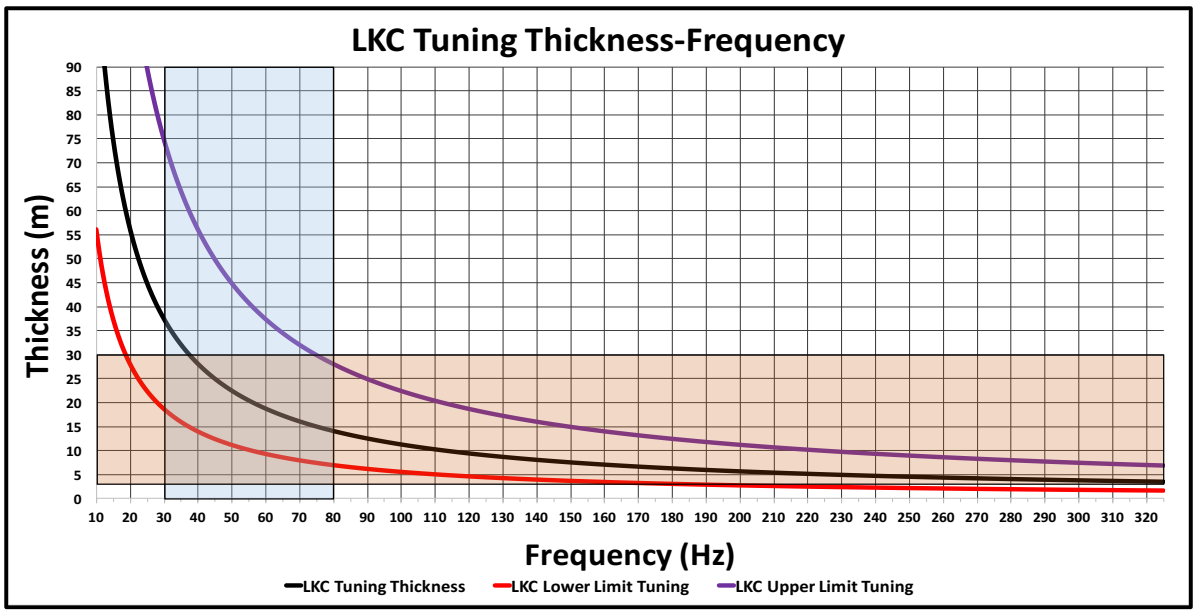

Figure 5.8: Theoretical measures of lower limit tuning thickness (λ/8), tuning thickness (λ/4), and upper limit tuning thickness (λ/2) plotted based on average LKC interval velocity from Well CO2-I #1 (4490 m/s). Orange zone indicates thickness range observed between the LKC (+15m) and LKCC (3.6 - 6.0m) in the pilot region. Blue zone covers usable bandwidth at the reservoir interval from Figure 5.7. For a fixed thickness, increasing frequency transitions from below resolution to the threshold of resolution (red line), to increasing amplitude (red to black line) until the point of maximum amplitude (black line), to decreased amplitude (black line to purple line), and above the upper limit of thickness without tuning effects (purple line).

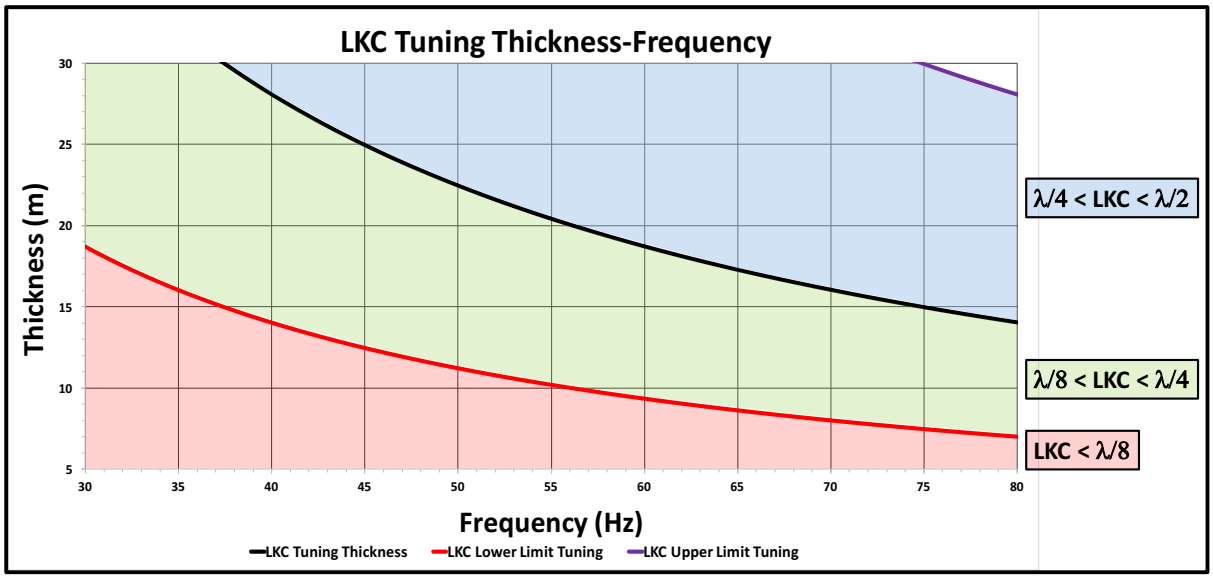

Figure 5.9: Theoretical bounds for the LKC below resolution (red), between the lower limit of tuning and tuning thickness (green), and above tuning thickness (blue) over the extent of usable bandwidth and observed LKC thickness range over the pilot region.

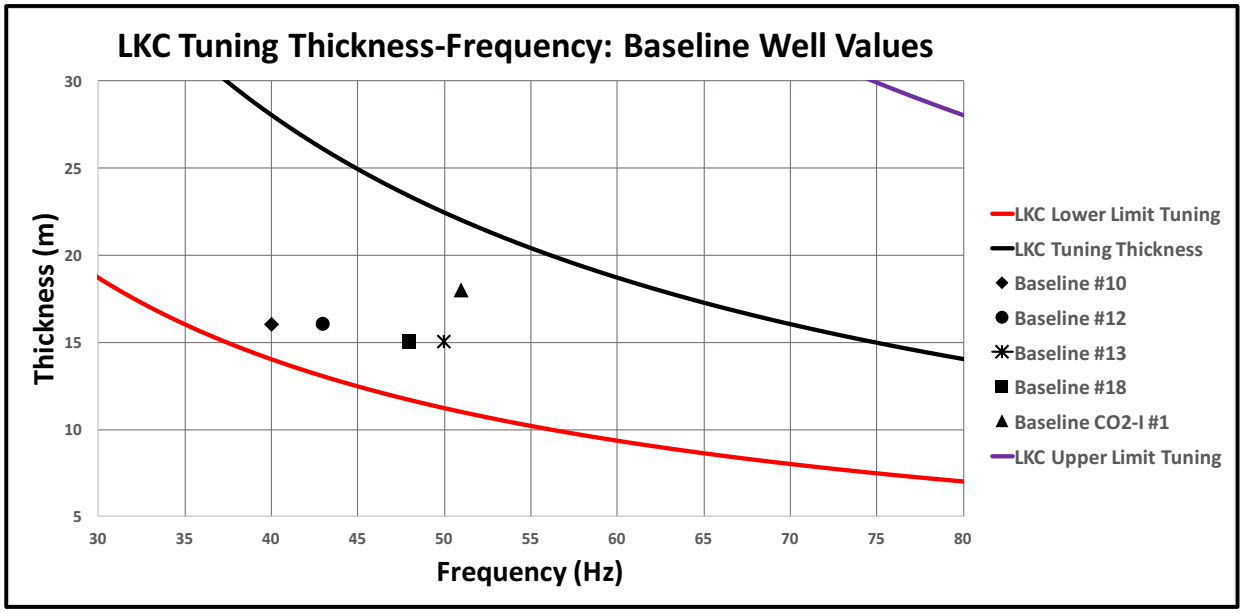

Figure 5.10: Observed tuning frequency from spectral decomposition at well locations plotted with LKC-LKCD thickness within theoretical tuning bounds displayed in Figure 5.9.

Conclusions

Analysis of amplitude envelope across frequency sub-bands through spectral decomposition was successful in revealing additional detail of distinct LKC shoal geometries, which are not resolved through interpretation of full-band data using conventional amplitude. Comparison of amplitude envelope data between surveys accounted for minor time shift misties expected between the Baseline and Monitor Surveys, and enabled effects of CO_2 to be captured in a window relative to the LKC horizon. Partitioning the full-band data into isolated frequency components allowed variation in reflection strength to be attributed to LKC thickness variation and boundaries characteristic of abrupt lateral facies changes.

Although the observed tuning frequencies at well locations did not match those of theoretical tuning calculations based on LKC thickness, interpretation of amplitude envelope at frequency sub-bands across the effective bandwidth (30-80 Hz) based on LKC thickness range in the pilot region and usable bandwidth at the reservoir interval (500-600ms; inlines #50-120,

crosslines #50-120) yielded powerful interpretation beyond the capacity of both full-band data and conventional amplitude. Spectral decomposition of the amplitude envelope data revealed low- and high-frequency anomalies suggestive of distinct shoal boundaries and potential areas of stacked shoal overlap verified by prior geological interpretation using well log data. Seismic interpretation confirmed these general shoal boundaries and revealed detail beyond the capacity of 1D well log data in terms of spatial extent and geometric trends of shoal complexes. Although absolute thickness was unable to be extrapolated from tuning observed at frequency sub-bands, relative LKC thickening and thinning from band-to-band analysis is observed and delineates additional reservoir architecture detail away from well control – which provides insight into thickness and facies of regions containing similar amplitude-frequency response. Delineating LKC shoal bodies and boundaries in the Baseline Survey seismic data corresponding to those made through geological interpretation provided a detailed interpretation of LKC reservoir characterization within the pilot region, which allowed subtle changes to be highlighted through further comparison of M2 and M6 Surveys**.** Despite the deviation of observed tuning frequency from theoretical tuning frequency based on thickness and interval velocity data, these data fall within the bounds of tuning – between $\lambda/8$ and $\lambda/4$ – deeming amplitude brightening as a potential phenomenon from CO_2 fluid replacement, an effect described below in: Ambiguity of Tuning Phenomena from CO2 Fluid Replacement.

Chapter 6 - CO_2 Impact on Spectral Components

Major obstacles in seismic data repeatability included inter-survey inconsistencies in receiver coupling, and high variance of seasonal, near-surface effects of Monitor Surveys acquired in fine time steps. Due to these factors of non-repeatability in seismic data acquisition, conventional differencing between Baseline and Monitor Surveys' seismic attributes was largely ineffective in revealing anomalies suggestive of CO_2 fluid replacement.

Injection (CO_2, water) and production (oil, water, CO_2-GOR) data were plotted by pilot pattern well over the project's duration with seismic surveys' approximate dates of acquisition to aid in corroboration of temporal changes between surveys' data character with potential saturation and pressure changes. A chronological listing of these significant events is outlined in Table 6.1. Seismic attributes were analyzed between the Baseline and Monitor Surveys in attempt to track spatiotemporal changes of dynamic (fluid, pressure) LKC reservoir properties in response to injection and production activity over the course of the Hall-Gurney CO_2-EOR pilot project. By corroborating observations across seismic surveys with CO_2 and water injection (Figure 6.1, Figure 6.2, Figure 6.3), and water and oil production with CO_2-GOR data (Figure 6.4**,** Figure 6.5) at well locations, observed 4D seismic anomalies gained validation in terms of their likely contributing factor(s). Changes in amplitude-frequency response of the data were analyzed from the Baseline to Monitor Surveys using spectral decomposition of the amplitude envelope (Figure 6.10), which were cross-validated with additional attributes including amplitude envelope filtered to a low- and high-cut frequency range of 30-80 Hz and over a 20-ms window centered on the LKC horizon (Figure 6.6), and dominant frequency (Figure 6.7).

Year	Month	Day	Event
1999	October		DOE Class Revisit Award Announced
2000	September-October		Well CO2-I #1 Drilled
2003	April	23	Start of Water Injection into Well CO2-I #1
2003	September	5	Water Injection Rate Increased on Well CO2-I #1
2003	September	15	Start of Water Injection into Well #10
2003	September	16	Start of Water Injection into Well #18
2003	November	5	Baseline Survey Acquired
2003	November	23	Start of CO2 Injection into Well CO2-I #1
2004	January		Monitor Survey #1 Acquired
2004	April		Monitor Survey #2 Acquired
2004	June		Monitor Survey #3 Acquired
2004	October		Monitor Survey #4 Acquired
2004	December	9	Start of CO2 Injection into Well #13, Well Shut-In for 26 Days
2005	January		Monitor Survey #5 Acquired
2005	June	17	End of CO2 Injection into Well CO2-I #1
2005	June	21	Start of Water Injection into Well CO2-I #1
2005	July		Monitor Survey #6 Acquired
2006	January		Monitor Survey #7 Acquired
2010	March	7	End of Hall-Gurney CO2-EOR Pilot Project

Table 6.1: Timeline of significant events over the Hall-Gurney CO_2-EOR project, including injection activity and 4D seismic data acquisition.

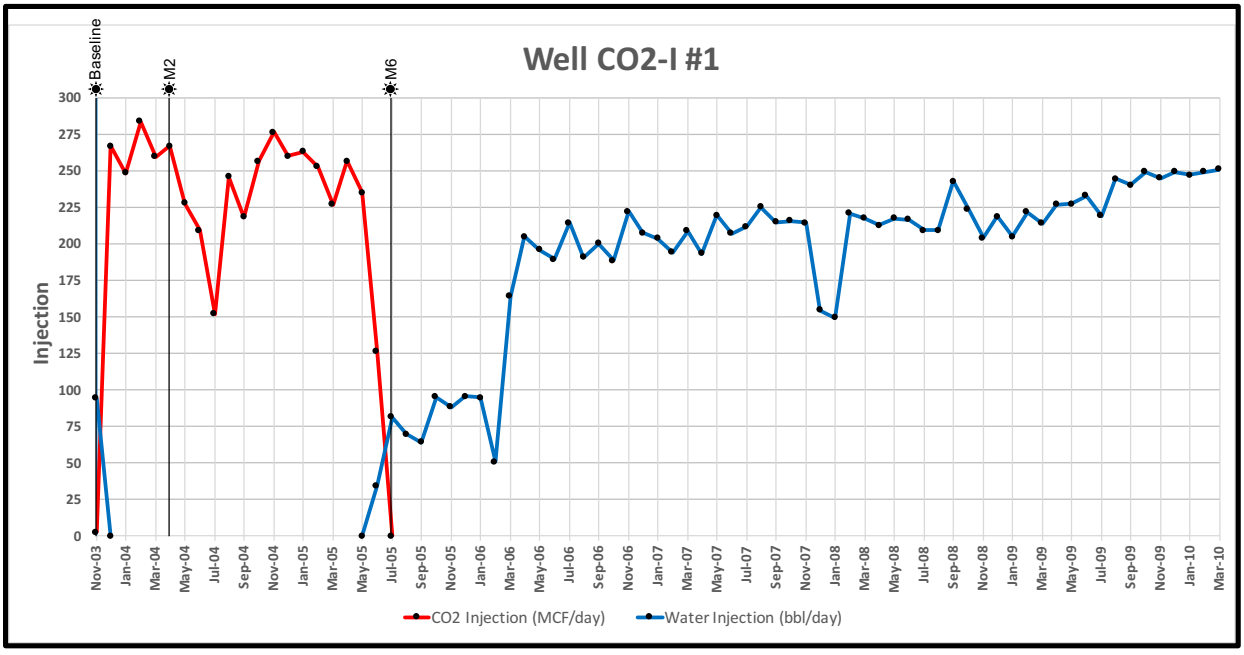

Figure 6.1: Monthly-averaged daily injection rate of CO_2 (MCF/day, red) and water (bbl/day, blue) into Well CO2-I #1, with references of seismic data acquisition for Baseline and Monitor Surveys.

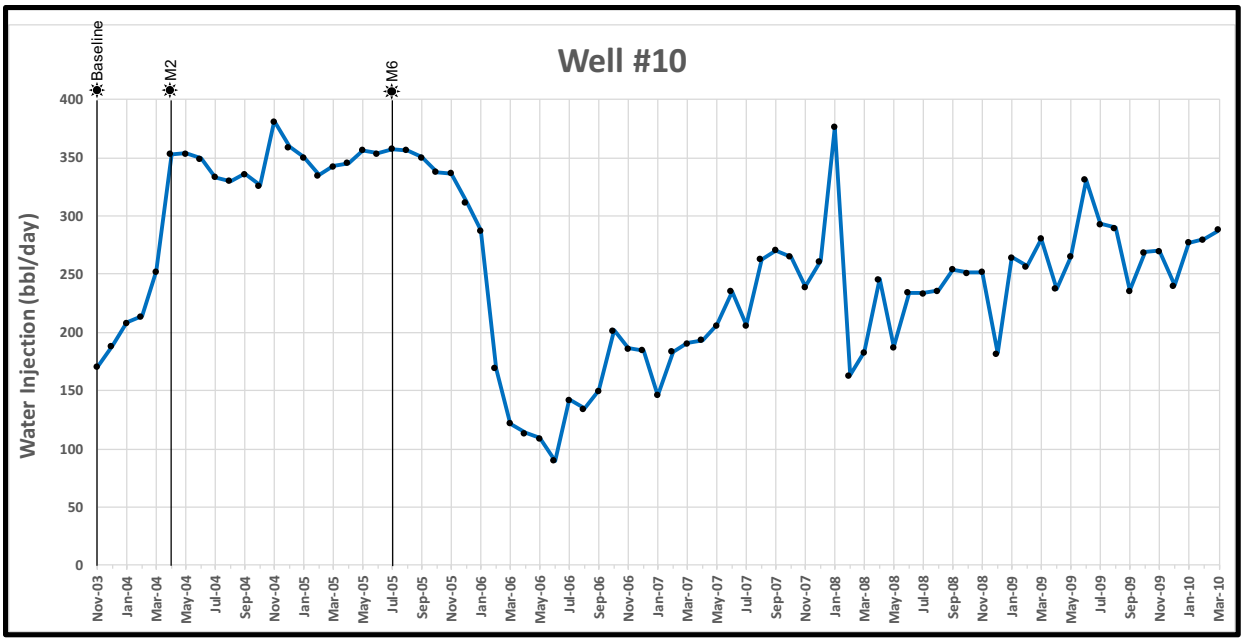

Figure 6.2: Monthly-averaged daily injection rate of water (bbl/day) into Well #10, with references of seismic data acquisition for Baseline and Monitor Surveys.

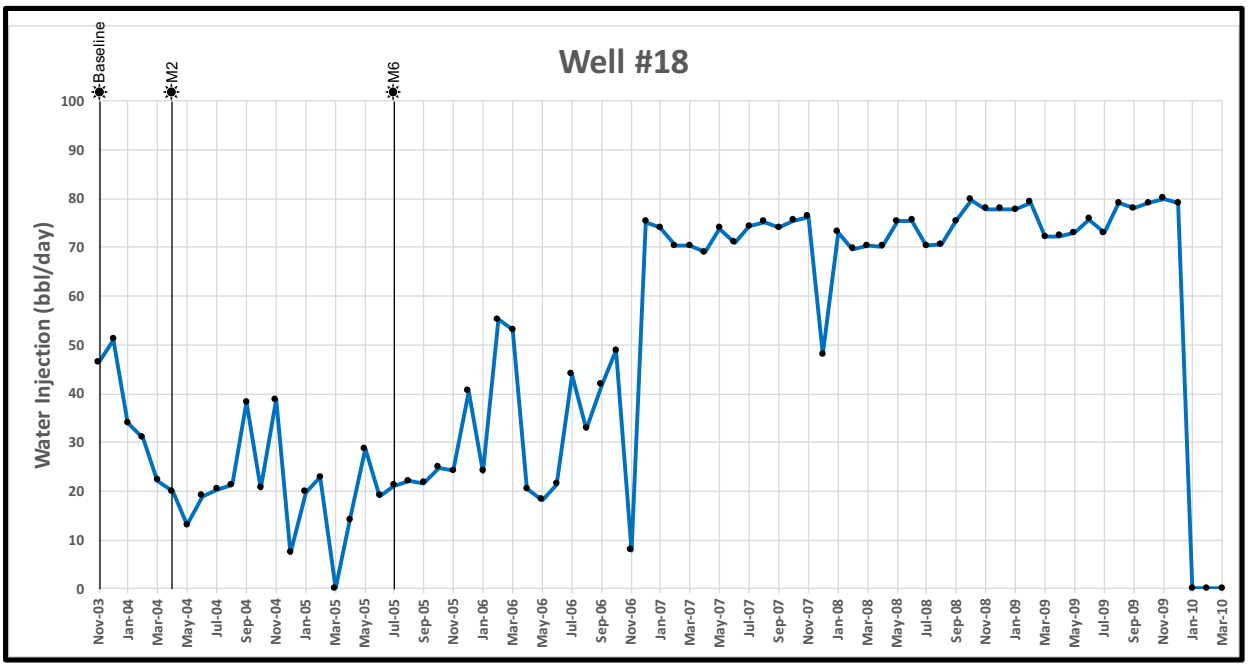

Figure 6.3: Monthly-averaged daily injection rate of water (bbl/day) into Well #18, with references of seismic data acquisition for Baseline and Monitor Surveys.

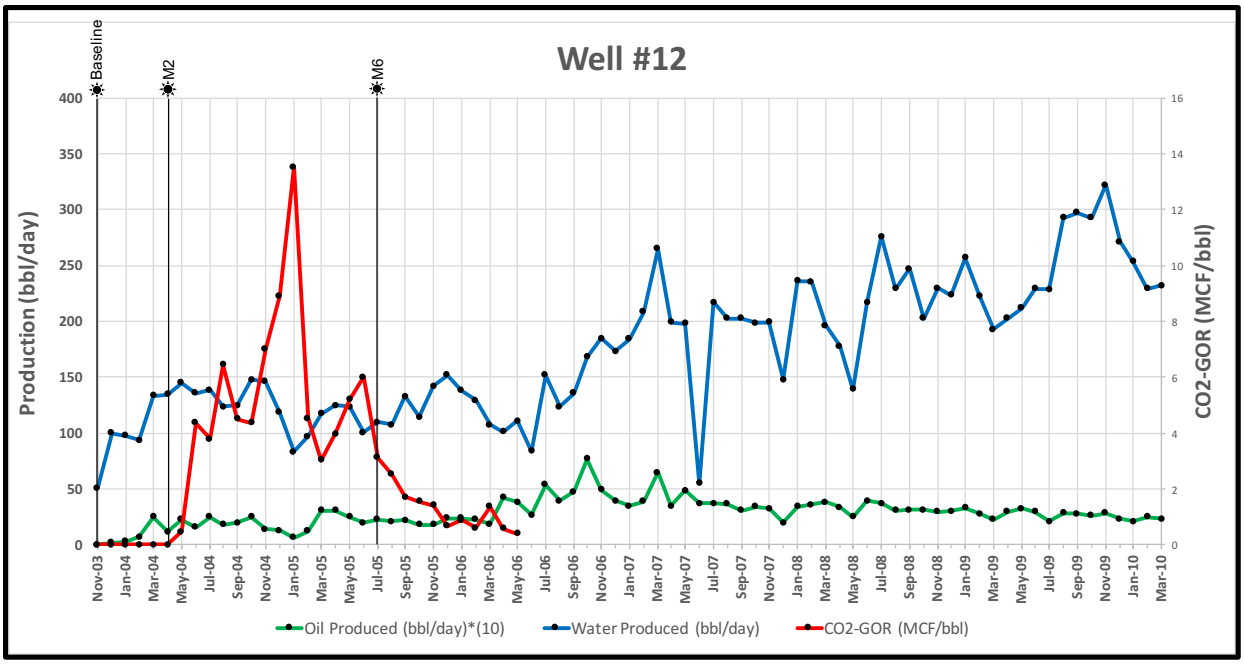

Figure 6.4: Monthly-averaged daily production for water (bbl/day, blue), oil ([10*(bbl/day)], green), and CO_2-GOR (MCF/bbl, red) from Well #12, with references of seismic data acquisition for Baseline and Monitor Surveys.

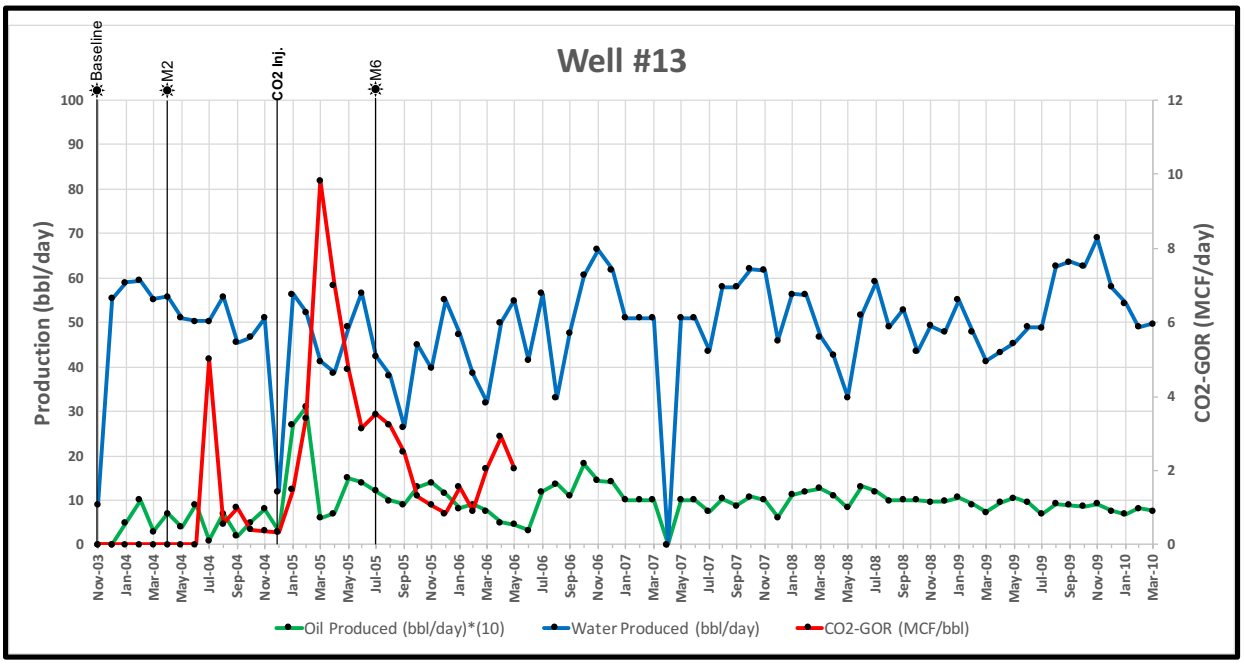

Figure 6.5: Monthly-averaged daily production for water (bbl/day, blue), oil ([10*(bbl/day)], green), and CO_2-GOR (MCF/bbl, red) from Well #13, with references of seismic acquisition for Baseline and Monitor Surveys and the December 2004 CO_2 injection.

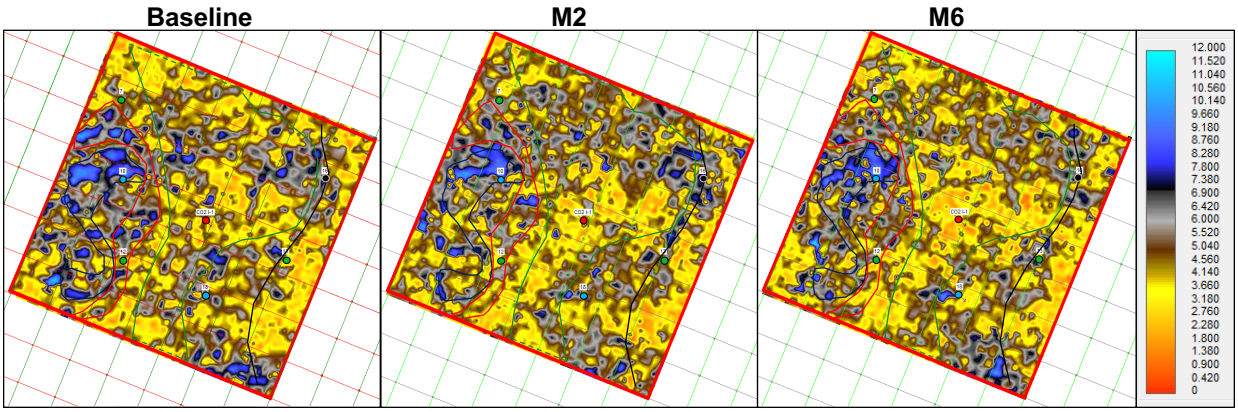

Figure 6.6: Amplitude envelope of the Baseline, M2, and M6 Surveys with polygons overlain from Baseline Survey interpretation via spectral decomposition. These data were calculated with a 30 Hz low cut frequency and 80 Hz high cut frequency over a 20-ms time window centered on the LKC horizon.

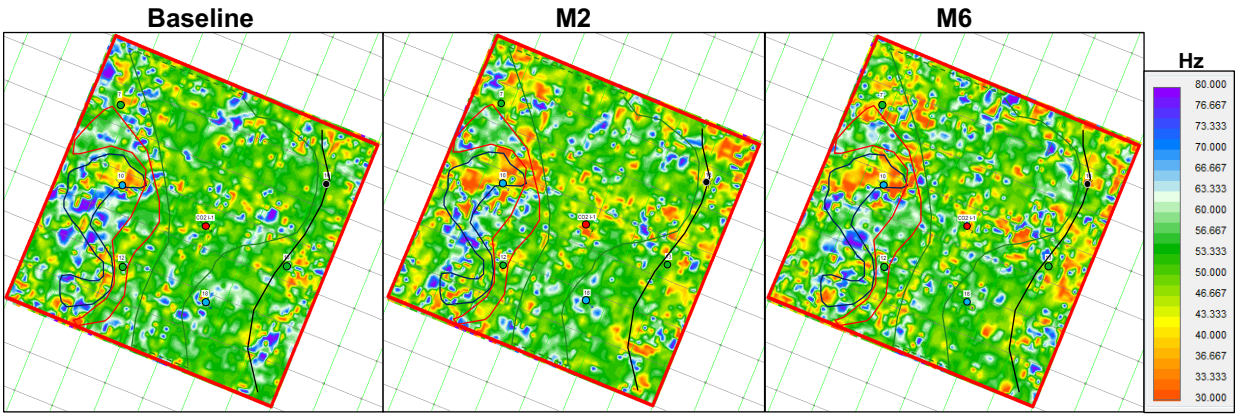

Figure 6.7: Dominant frequency of Baseline, M2, and M6 Surveys with polygons overlain from Baseline Survey interpretation via spectral decomposition.

Preliminary Analysis of 4D Seismic Anomalies

Injection (Figure 6.1, Figure 6.2, Figure 6.3) and production (Figure 6.4, Figure 6.5) data were analyzed with 4D seismic data to develop a spatiotemporal understanding of reservoir fluid and pressure changes over the Hall-Gurney CO_2-EOR pilot demonstration project. Corroborating physical changes at discrete well locations with changes observed in the seismic character added credibility to 4D seismic anomalies in the M2 and M6 Surveys relative to the Baseline Survey. These preliminary outlines are displayed between the Baseline Survey, and M2 and M6 Surveys in Figure 6.8A and Figure 6.8B, respectively.

An obvious anomaly likely to be observed is an amplitude and frequency change within the vicinity of Well CO2-I #1 between the Baseline and M2 Surveys, which if present, should grow outward from M2 to M6. As M6 was acquired shortly after the WAG transition from CO_2 to water injection, a minor change in the immediate vicinity of Well CO2-I #1 is possible from water displacing CO_2. No response from CO_2 is expected at Well #12 and Well #13 between the Baseline and M2 Surveys, but anomalies may occur at these well locations between the Baseline and M6 surveys due to the presence of CO_2 at these points since CO_2-GOR response was observed from produced fluids between acquisition of the M2 and M6 surveys (Figure 6.4, Figure 6.5).

An anomaly may be present between the Baseline and M6 surveys highlighting the pathway of CO_2 between Well CO2-I #1 and Well #12. A pathway suggesting CO_2 movement is unlikely to be present between Well CO2-I #1 and Well #13 due to the poor connectivity and breakthrough response of CO_2 at Well #13. CO_2-GOR was still observed at Well #13 between M2 and M6 from a minor, abrupt breakthrough from Well CO2-I #1, followed by a more significant breakthrough likely attributed to the minor volume of CO_2 injected into Well #13 in attempt to increase CO_2 permeability and communication with Well CO2-I #1. A minor boost in oil production at the Colliver A7 Well northwest and outside the CO_2-EOR pilot lease was observed during the end of 2005 (Figure 2.22) prior to re-opening the LKCC zone in August 2006, which saw significant production increase attributed to CO_2-EOR. The small increase in production at Colliver A7 near the end of 2005 may coincide with the northerly loss of fluid within the pilot region as a result of significant pressure loss between Well #10 and Well CO2-I #1, noted by Willhite et al. (2010). Since M6 was acquired in July 2005, it is reasonable to assume the CO_2 plume was migrating towards, and potentially near, Colliver A7 during seismic

acquisition of M6. A 4D seismic anomaly may be observed at Well #10 due to water injection for pressure containment, especially between the Baseline and M2 survey due to a significant increase in injection rate, which was sustained relatively constant through M6. A response is less likely to be observed at water injection Well #18 compared to Well #10, since injection rate was maintained at a notably smaller scale, and injection was intermittent due limitations of water availability.

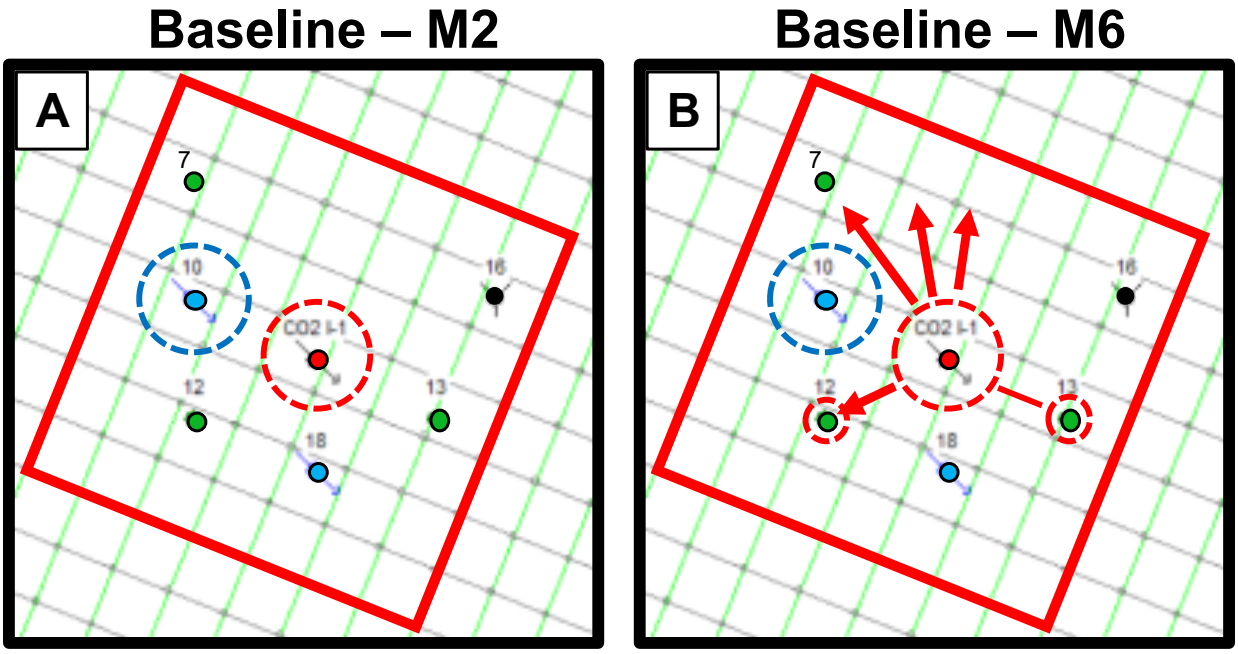

Figure 6.8: Potential spatiotemporal changes to expect in the seismic data based on injection and production data between acquisition of the (A) Baseline and M2 Surveys, and (B) Baseline and M6 Surveys. Potential sources of anomalies expected for both cases include a significant increase in water injection rate at Well #10 and immediate injection of CO_2 into Well CO2-I #1. CO_2 anomalies can be expected north and northwest of Well CO2-I #1 and to both production wells (#12, #13) between the Baseline and M6 Surveys.

Ambiguity of Tuning Phenomena from CO_2 Fluid Replacement

Amplitude tuning phenomena gain an additional degree of complexity when attempting to image zones of CO_2 fluid replacement in reservoirs fluctuating above and below tuning thickness. The LKC reservoir in this case study contains a higher impedance relative to its confining layers, so CO_2 fluid replacement of original reservoir fluid would decrease the

impedance contrast between these layers through a combined decrease of both velocity and density. The reduction of LKC interval velocity increases the time required for wave propagation through the CO_2-invaded zone, and therefore increases the time-thickness of the reservoir. For a simple case neglecting potential secondary effects of thickness variation on CO_2 fluid mixing models, saturation changes, and plume thickness – these physical changes in impedance remain the same regardless of reservoir thickness. Assuming these impedance changes are uniform, ambiguity arises in 4D seismic amplitude interpretation in zones with CO_2 fluid replacement, which is dependent upon reservoir thickness. Using a tuning curve of the wavelet extracted from the data (Figure 4.2), this phenomenon is plotted for scenarios above and below tuning thickness in Figure 6.9A and Figure 6.9B, respectively. Zones in which the LKC reservoir exceeds tuning thickness are expected to undergo amplitude dimming with CO_2 fluid replacement as the time-thickness increases away from the effect of constructive interference. The opposite effect of amplitude brightening is expected to occur for CO_2 replacement when reservoir thickness is below tuning thickness, as the time-thickness increase is driven toward maximum constructive interference.

The phenomenon of tuning ambiguity in 4D seismic amplitude interpretation for a reservoir fluctuating between conventional and thin-bed thickness is, however, variable by the effective bandwidth and dominant frequency of the full-band data. When analyzing full-band data, significant amplitude changes attributed to CO_2 fluid replacement in the LKC reservoir between 4D seismic surveys may be concealed at frequency sub-bands higher and lower than the dominant frequency. In theory, spectral decomposition for analysis of inter-survey (Baseline to Monitor) amplitude changes at frequency sub-bands can reveal this ambiguity and constrain a range of reservoir thickness. Similar to the approach of spectral decomposition for estimation

and relative variation of thickness, the frequencies used to investigate inter-survey changes in reflection strength were limited to the LKC, with consideration that physical changes onset from CO_2 fluid substitution – even if completely limited to the LKCC interval – would still contribute to changes in reflectivity strength of the LKC. Complex interplay between CO_2 tuning effects and changes in other reservoir properties (saturation, pressure, geomechanical) through injection and production activity must be considered, which can introduce uncertainty in 4D seismic amplitude tuning interpretation across frequency sub-bands. Additionally, non-repeatability introduced from data acquisition and seasonal near-surface variance can destroy subtle 4D seismic anomalies and/or introduce artifacts in the data suggestive of actual anomalies.

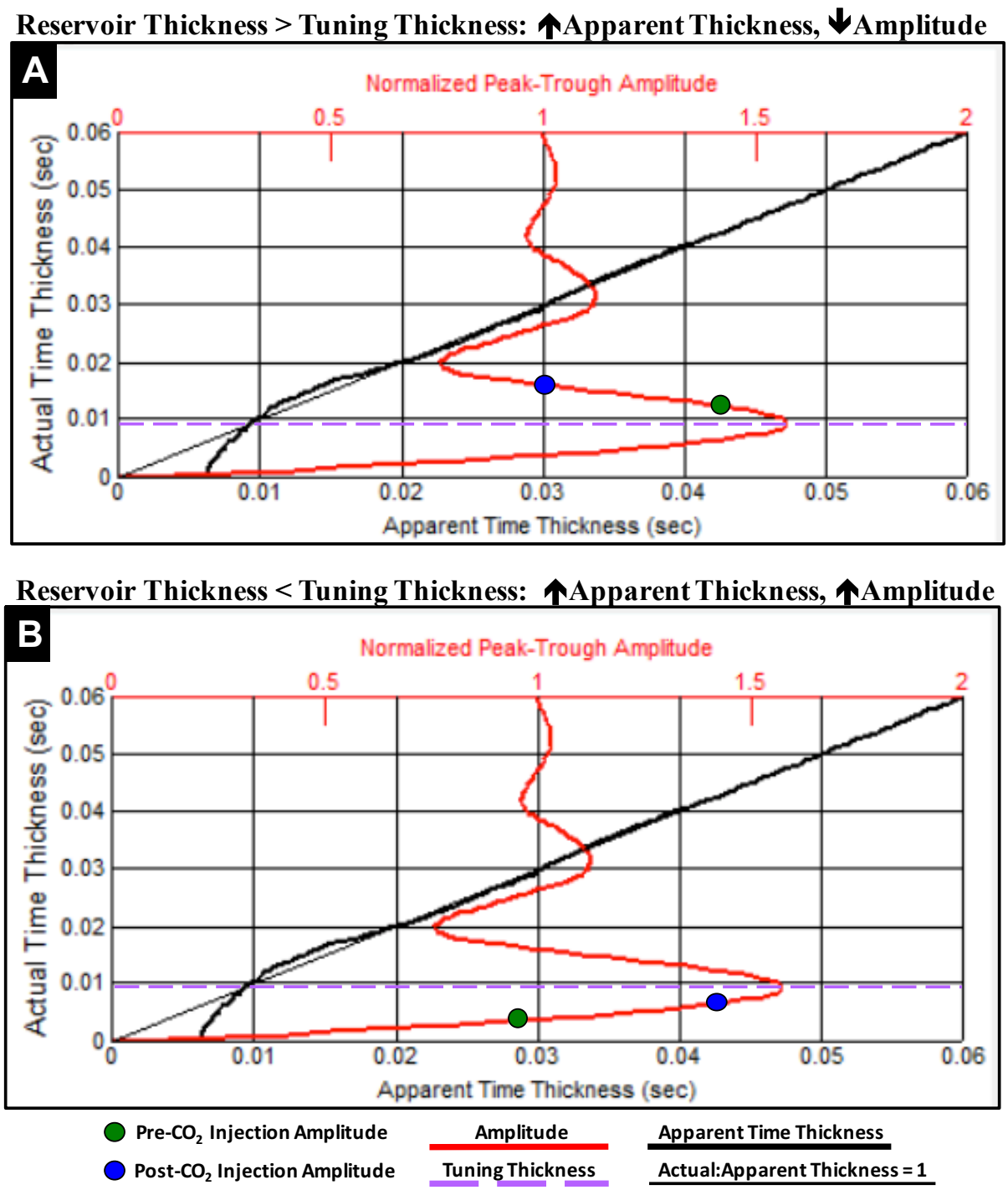

Figure 6.9: Theoretical, ambiguous effects of CO_2 fluid replacement on amplitude introduced by reservoir thickness variation. This tuning curve of a frequency-matched extracted wavelet demonstrates the potential of LKC amplitude to decrease or increase with CO_2 fluid replacement when the reservoir is (A) above and (B) below tuning thickness, respectively.

Observed Spectral and Tuning Changes Between Baseline and Monitor Seismic Surveys

Observed changes in spectral and tuning response were analyzed between the Baseline, M2, and M6 Surveys in consideration of potential pressure and saturation changes caused by injection and production. For this discussion, reference to frequency sub-bands' amplitude envelope response through spectral decomposition across the Baseline, M2, and M6 Surveys can be found in Figure 6.10.

As expected, an amplitude anomaly – dominated by a decrease in reflection strength – appears at the zone of CO_2 injection at Well CO2-I #1, which is obvious between 48.7-55.0 Hz. This anomaly is also significant in the amplitude envelope data filtered to 30-80 Hz bandwidth (Figure 6.6).

From Well CO2-I #1 to the north and northwest (toward Colliver A7 well) within the bounds of Shoal #2, a notable change in the amplitude envelope occurs in the M6 Survey relative to the Baseline and M2 Surveys between 46.7 and 50.8 Hz. This subtle, broad attenuation of amplitude reflection strength is likely caused from the presence of CO_2, which was interpreted through PPB analysis (Raef et al., 2005a) to reach this extent in the M6 Survey but not in the M2 Survey. Although a loss of reflection strength in the general extent of Shoal #2 north of the CO_2 is observed, a series of lineaments develop within the CO_2 contacted region in the M6 Survey, which are not present in the Baseline and M2 Surveys. An east-west trending lineament stands out immediately north of Well CO2-I #1 in the M6 Survey, which develops subtly at 44.6 Hz, is most prominent between 48.7-50.8 Hz, and persists through 55.0 Hz. This anomaly is also present in the amplitude envelope data spanning 30-80 Hz bandwidth (Figure 6.6). Two subtler lineaments trending parallel to this anomaly also appear between 50.8-52.9 Hz in the M6 Survey – both north of the more obvious lineament. This effect of amplitude brightening in the zone of

CO_2 fluid replacement suggests CO_2 has contributed to tuning effects which highlight a series of lineaments, which may represent fractures, structural-stratigraphic features, or distinct facies' boundaries below tuning thickness (as seen in Figure 6.9B scenario).

An anomaly appears between Well CO2-I #1 and Well #12 across 48.7-52.9 Hz, in which amplitude brightening outside the eastern edge of polygon #5 occurs in the M6 Survey relative to the Baseline and M2 Surveys. This effect may be due to the presence of CO_2, which is known to have swept the region near Well #12 by the time of M6 Survey acquisition. Amplitude brightening highlights the interpreted edge of Shoal #3, suggesting this is a thin zone below tuning thickness as modeled in Figure 6.9B.

Observed tuning frequency of the low-frequency anomaly (polygon #1) associated with Well #10 is 40.4 Hz for the Baseline, M2, and M6 Surveys, but reflection strength increases substantially in the M2 and M6 Surveys relative to the Baseline. Associated with this increase in reflection strength in M2 and M6 Surveys is a slight increase in the spatial coverage of the low-frequency anomaly relative to the Baseline Survey, observed between 36.2-42.5 Hz. Both effects may be due to the significant increase in water injection rate between the Baseline and M2 Survey, which maintained a relatively constant rate between the M2 and M6 Surveys (Figure 6.2). Increased injection rates would yield an increase in pore pressure within the vicinity of Well #10 – as intended for pressure containment – resulting in a decrease in velocity within the affected area. Increased pore pressure may explain the amplitude brightening observed proximal to Well #10 if the amplitude envelope in this zone is responding to an anomalously thicker stratigraphic LKC interval than originally estimated, resulting in the onset of constructive interference as apparent thickness approaches tuning thickness.

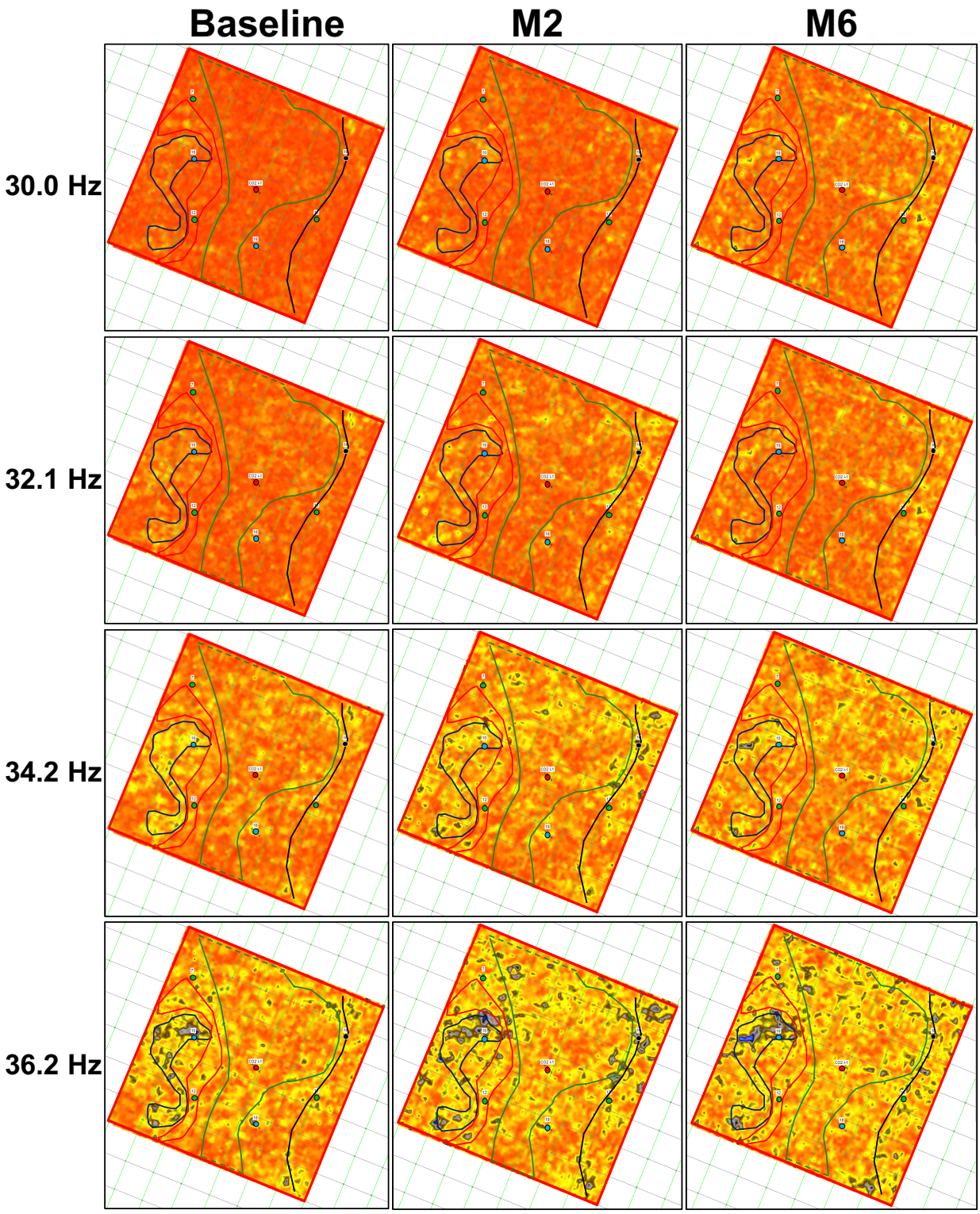
Baseline
M2
M6
30.0 Hz
32.1 Hz
34.2 Hz
36.2 Hz

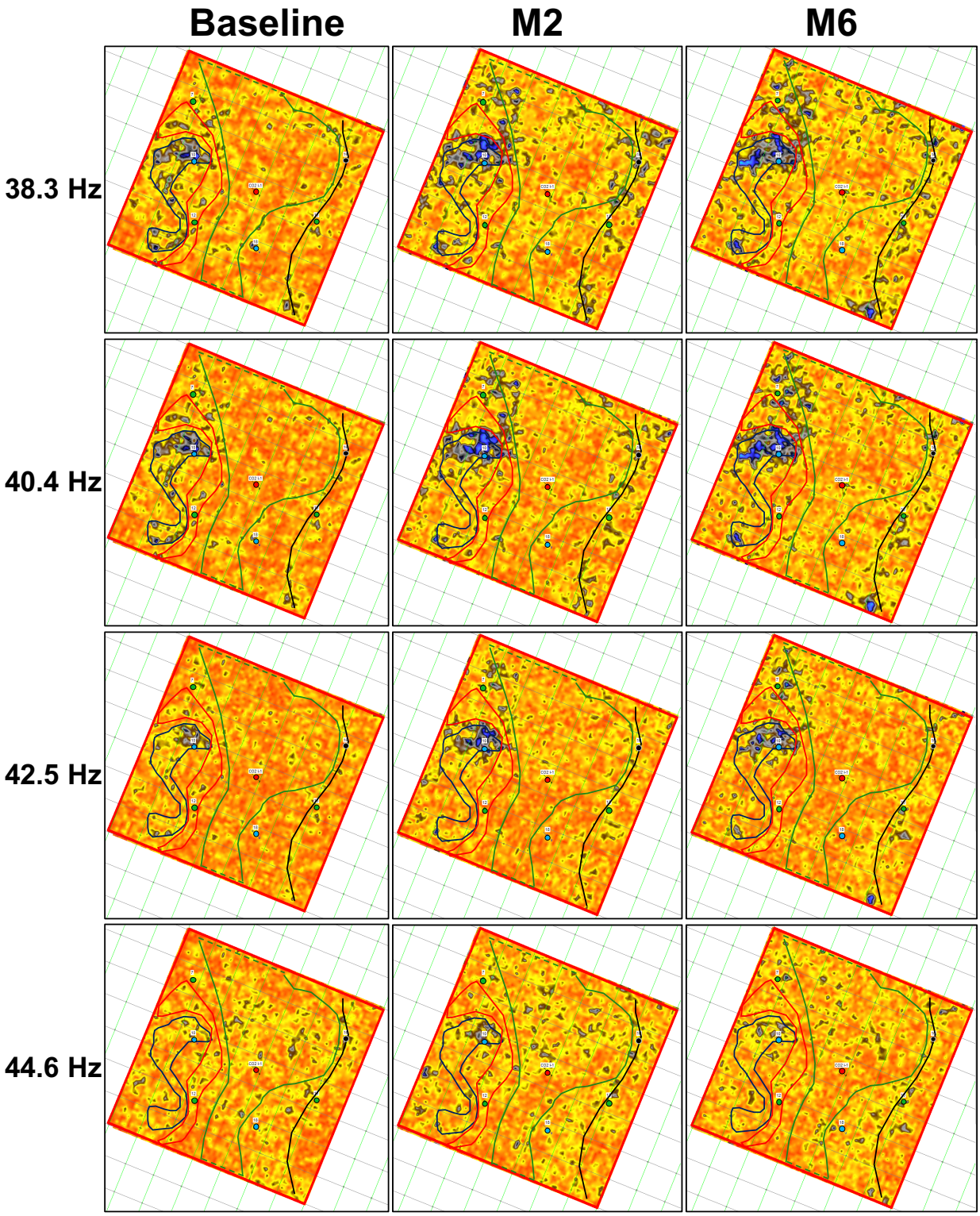
Baseline
M2
M6
38.3 Hz
40.4 Hz
42.5 Hz
44.6 Hz

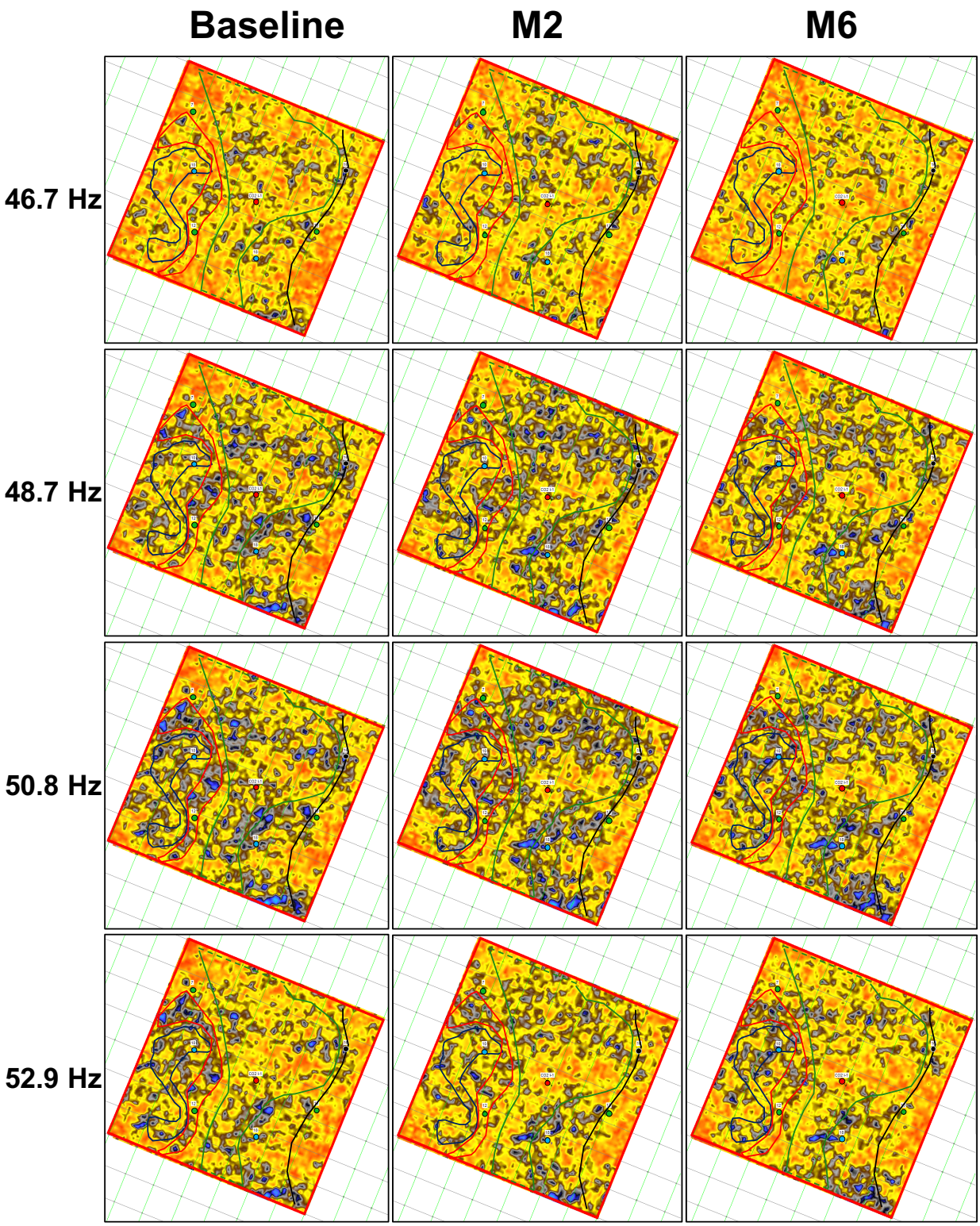
Baseline
M2
M6
46.7 Hz
48.7 Hz
50.8 Hz
52.9 Hz

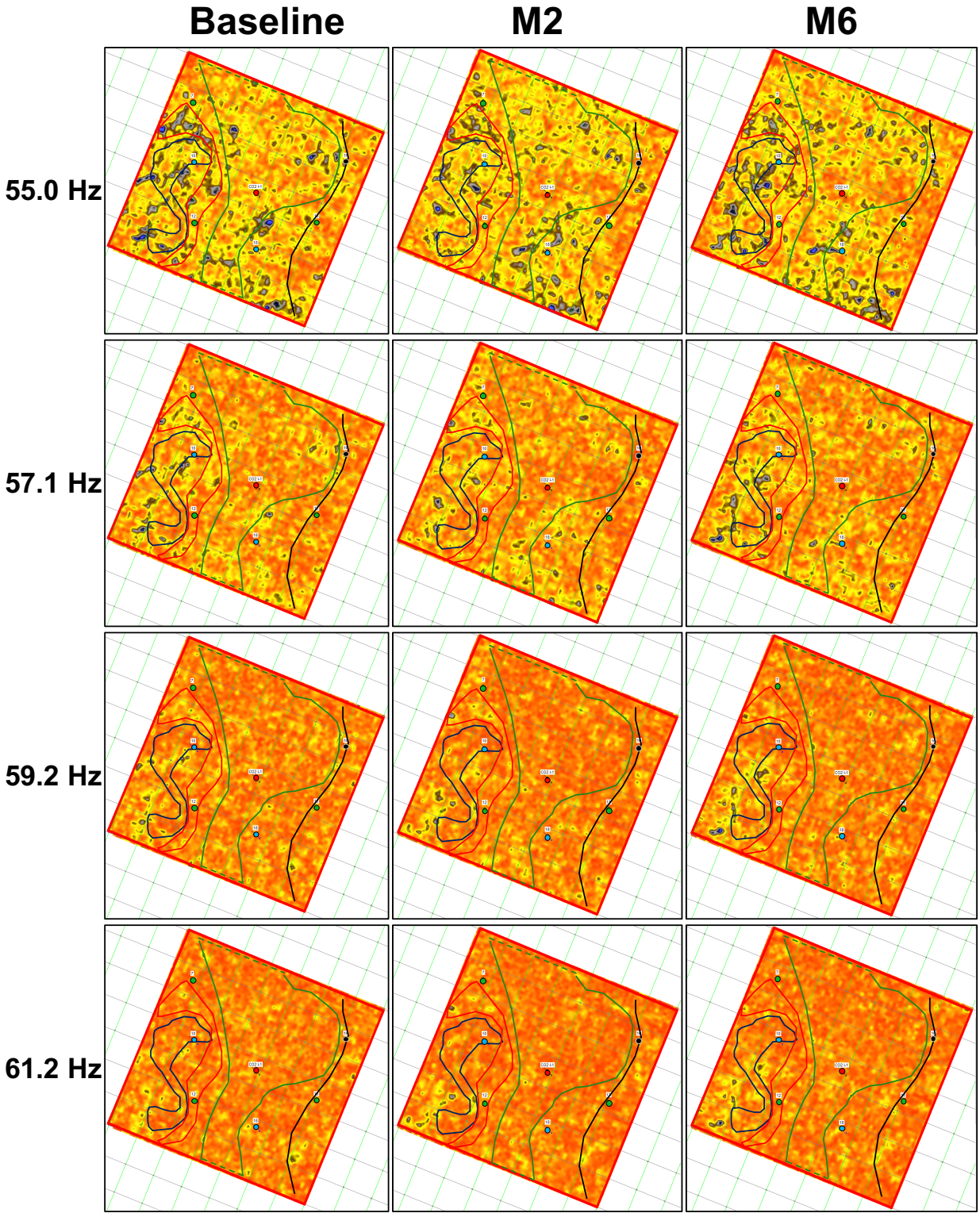
Baseline
M2
M6
55.0 Hz
57.1 Hz
59.2 Hz
61.2 Hz

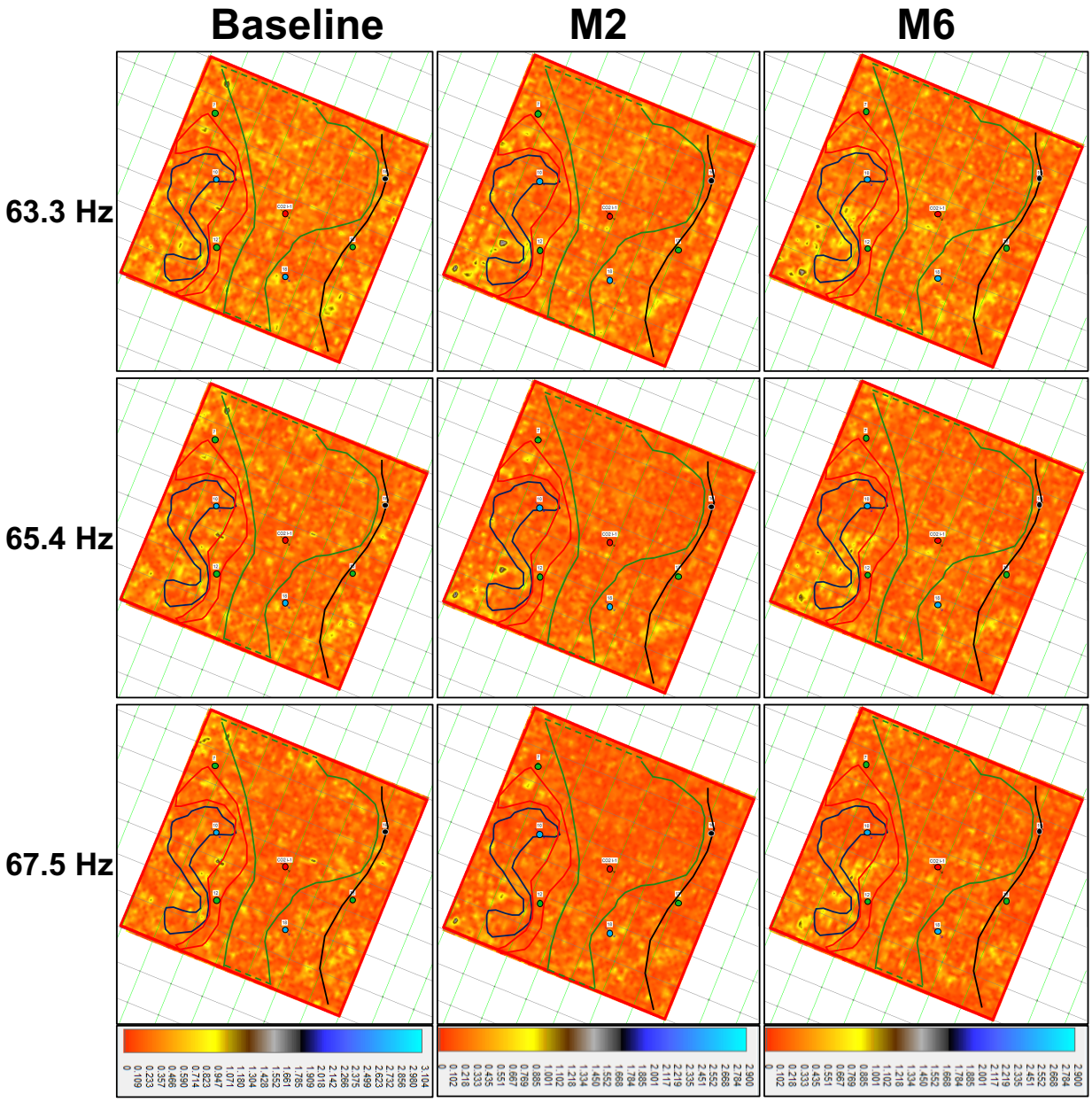

Figure 6.10: Spectral decomposition (30.0-67.5 Hz) of amplitude envelope data for the Baseline, M2, and M6 Surveys extracted to the LKC horizon. Polygons from Baseline Survey interpretation overlain on all Surveys.

Conclusions

Spectral decomposition of amplitude envelope data significantly enhanced the ability to reveal subtle differences and tuning ambiguity between the Baseline, and M2 and M6 Monitor Surveys. Through analysis of production and injection data at wells within the pilot region,

criteria were established in terms of spatiotemporal changes to expect within the M2 and M6 Surveys relative to the Baseline. Effects of both amplitude dimming and brightening were observed in zones of known CO_2 contact – near Well #12 and between Well CO2-I #1 and Colliver A7. Modeling of ambiguous changes in reflection strength from CO_2 fluid replacement of original reservoir fluid suggest zones undergoing amplitude attenuation exceed tuning thickness, whereas those containing brightening are zones below tuning thickness – or contain significant variance in physical properties from the surrounding lithology which place them below effective tuning thickness. Amplitude dimming was observed as a more spatially extensive, subtle effect on reflection strength between the Baseline and M2 and M6 Surveys. Amplitude brightening appeared to highlight lineaments suggestive of fractures and/or stratigraphic structures north of Well CO2-I #1, in addition to the interpreted eastern boundary of Shoal #3 proximal to Well #12. The east-west trending lineaments observed north of Well CO2-I #1 may serve as conduits for CO_2 flow between Shoal #2 and Shoal #3 and explain the loss of CO_2 outside the pilot pattern. As expected, these changes were observed in the M6 Survey following approximately 21 months of CO_2 injection, but not in the M2 survey acquired 6 months after the start of injection. Changes observed in amplitude envelope across frequency sub-bands between the Baseline and Monitor Surveys through this study may provide interpretation value to similar, future CO_2-EOR monitoring programs in shallow, onshore, thin carbonate reservoirs.

Chapter 7 - Conclusions

1. Resorting to horizon-based, windowed attributes is more dependable towards minimizing the effect of inconsistencies in horizon tracking – within surveys, and between surveys with 4D seismic data sets. This also accounts for minor survey misties between TWT, phase, and amplitude scaling created by, or remaining after, cross-equalization is applied to the 4D seismic data set.
2. The application of multiple horizon snapping operations within the low SNR seismic surveys in this data set proved more powerful in horizon tracking than single autotracking and snapping operations alone. This multi-step approach constrained horizon snapping within realistic bounds to maintain geologic integrity, reduced time required for horizon tracking of subsequent monitor surveys, and provided a quantitative, repeatable approach to horizon tracking of 4D seismic surveys.
3. Amplitude tuning phenomena should be considered as a factor within 4D seismic feasibility studies to monitor production and/or injection in thin reservoirs. The effect of CO_2 fluid replacement on the seismic character can yield complex responses of amplitude brightening and dimming, and introduce ambiguity into interpretation of 4D seismic anomalies.
4. Despite complexity and ambiguity introduced, CO_2-induced tuning phenomena can provide value in reservoir characterization. These observed effects may reveal heterogeneity across 4D seismic monitoring surveys, and allow flood patterns to be adjusted to optimize secondary and tertiary recovery operations.

Suggestions and Potential for Future Research

The additional 'fourth' dimension of time added in time-lapse seismic interpretation of 3D seismic volumes adds a significant number of avenues for additional research. The 4D

seismic monitoring program of the Hall-Gurney CO_2-EOR project contains a significant amount of data and reports, and uncertainty which can be fulfilled with further thesis research across disciplines of geophysics, geology, geomechanics, petroleum engineering, and additional geoscience sub-disciplines. Although the unexpected loss of CO_2 from the pilot pattern and early termination of the project were unfortunate, this outcome is a perfect example of how subsurface heterogeneity – especially that of carbonate systems – can frustrate and humble geoscientists in spite of excellent data and analysis. It is a reminder that although the oil and gas industry is constantly pushing and extending its limits through innovation, there is still progress to be made.

In terms of future research with this data set, I suggest the following as potential areas of research which could contribute to CO_2-EOR monitoring of onshore, shallow, thin carbonate reservoirs:

- AVO analysis of pre-stack data between surveys, and potentially the application of pre-stack inversion.
- RGB blending applied to spectral components and additional attributes for enhanced multi-attribute analysis
- Analysis of spectral ratios between the Baseline and Monitor Surveys to reveal anomalies associated with CO_2 fluid replacement
- Application of PPB method to the amplitude envelope data across frequency sub-bands through spectral decomposition.
- Application of self-organizing maps (SOM) and/or neural networks for hyperdimensional attributes analysis. This may include comparison between surveys, but a very intriguing area of interest is producing a SOM using differenced attributes' volume data.

- Geomechanical study to characterize the local stress field, which may vary from the regional stress regime. Results of this study may provide additional insight into the potential of fracture networks in CO_2 loss.
- A thorough investigation to compare the application of various spectral decomposition methods, and potentially further improve the amplitude-frequency analysis conducted in this study.
- Re-processing and data enhancement methods to boost the frequency content of the data.
- Statistical study to determine the optimal range of data to normalize for each surveys' attributes in order to difference the data between and obtain results representative of relative increases or decreases in attribute value.

References

Agile Geoscience. 2011. Tuning geology. Retrieved from: http://www.agilegeoscience.com/blog/2011/7/8/tuning-geology.html (accessed 6 December 2015)

Algeo, T.J., and Heckel, P.H. 2008. The Late Pennsylvanian Midcontinent Sea of North America: a review. Palaeogeography, Palaeoclimatology, Palaeoecology, **268**.

Baars, D.L., Watney, W.L., Steeples, D.W., and Brostuen, E.A. 1993. Petroleum: a primer for Kansas. Kansas Geological Survey, Education Series 7.

Blakey, R. 2005(a-e). Paleogeography and geologic evolution of North America: images that track the ancient landscapes of North America. Northern Arizona University, Ron Blakey webpage. (accessed 10 July 2015)

____2005a. Retrieved from: https://www2.nau.edu/rcb7/namM325.jpg

____2005b. Retrieved from: https://www2.nau.edu/rcb7/namM345.jpg

____2005c. Retrieved from: https://www2.nau.edu/rcb7/namPP290.jpg

____2005d. Retrieved from: https://www2.nau.edu/rcb7/namPP300.jpg

____2005e. Retrieved from: https://www2.nau.edu/rcb7/namPP315.jpg

Byrnes, A.P., Watney, W.L., Guy, W.J., and Gerlach, P. 2000. Oomoldic reservoir of Central Kansas: controls on porosity, permeability, capillary pressure and architecture. AAPG Annual Convention, New Orleans, LA. AAPG Search and Discovery Article #90914.

Byrnes, A.P, Franseen, E.K., Watney, W.L., and Dubois, M.K. 2003. The role of moldic porosity in Paleozoic Kansas reservoirs and the association of original depositional facies and early diagenesis with reservoir properties. Kansas Geological Survey Open File Report 2003-32.

Chen, G., Wrobel, K., Tiwari, A., Zhang, J., and Payne, M. 2008. 4D seismic in carbonates: from rock physics to field examples. International Petroleum Technology Conference, Kuala Lumpur, Malaysia.

DOE/NETL. 2008. Brief history of the reservoir depositional classification system.

DOE/NETL. 2010. Carbon dioxide enhanced oil recovery – untapped domestic energy supply and long term carbon storage solution.

Dubois, M.K., Byrnes, A.P., and Watney, W.L. 2001. Field development and renewed reservoir characterization for CO2 flooding of the Hall-Gurney Field, Central Kansas. AAPG Annual Convention, Denver, CO. AAPG Search and Discovery Article #90906.

Google Earth V 7.1.5.1557. (4 September 2013). Tongue of the Ocean, Bahamas. 23°16'11.91"N, 77° 9'44.71"W, Eye alt 19545 feet. Image Landsat 2015. http://www.earth.google.com [29 November 2015].

Heckel, P.H. 1994. Evaluation of evidence for glacio-eustatic control over marine Pennsylvanian cyclothems in North America and consideration of possible tectonic effects. Tectonic and Eustatic Controls on Sedimentary Cycles, SEPM Concepts in Sedimentology and Paleontology #4.

Heckel, P.H. 2008. Pennsylvanian cyclothems in Midcontinent North America as far-field effects of waxing and waning of Gondwana ice sheets. Resolving the Late Paleozoic Ice Age in Time and Space: Geological Society of America Special Paper 441.

Heckel, P.H., and Watney, W.L. 2002. Revision of stratigraphic nomenclature and classification of the Pleasanton, Kansas City, Lansing, and lower part of the Douglas groups (Lower Upper Pennsylvanian, Missourian) in Kansas. Kansas Geological Survey Bulletin 246.

Higley, D.K. 1995. Cambridge Arch/Central Kansas Uplift Province (053). 1995 National Assessment of United States Oil and Gas Resources – Results, Methodology, and Supporting Data. U.S. Geological Survey Digital Data Series 30.

Johnston, D.H. 2013. Practical applications of time-lapse seismic data. Distinguished Instructor Series No. 16, SEG, Tulsa, OK.

Kansas Geological Survey (KGS). 1996a. Geologic provinces in Kansas. Kansas Digital Petroleum Atlas. Retrieved from: http://www.kgs.ku.edu/DPA/Plays/ksProv.html (accessed 10 July 2016)

____1996b. Map of geologic provinces in Northern Mid-Continent. Kansas Digital Petroleum Atlas. Retrieved from: http://www.kgs.ku.edu/DPA/NMC/nmcProv.html (accessed 10 July 2016)

____1997. Generalized oil and gas fields of Kansas. Kansas Digital Petroleum Atlas. Retrieved from: http://www.kgs.ku.edu/DPA/Plays/ksOGMap.html (accessed 10 July 2016)

____1998. Statewide production maps – Lansing-Kansas City – oil production. Kansas Digital Petroleum Atlas. Retrieved from: http://www.kgs.ku.edu/DPA/Plays/ProdMaps/lgkc_oil.html

____1999. Potential for CO2 enhanced oil recovery in Kansas. Energy Research Center. Retrieved from: www.kgs.ku.edu/CO2/evaluation/slide16.html (accessed 12 July 2016)

____2000. Oil and gas – county oil & gas production – Russell County. Kansas Digital Petroleum Atlas. Retrieved from: http://www.kgs.ku.edu/PRS/County/rs/russell.html (accessed 10 July 2016)

____2011. Oil and gas wells and fields; interactive oil and gas well maps. Retrieved from: http://maps.kgs.ku.edu/oilgas/index.cfm (accessed 10 July 2016)

____2016. Hall-Gurney Field general information. Digital Petroleum Atlas. Retrieved from: chasm.kgs.ku.edu/ords/gemini.dpa_general_pkg.build_general_web_page?sFieldKID=1000146629 (accessed 12 July 2016)

Kelly, L. 2014. An investigation into the effects and implications of gamma radiation on organic matter, crude oil, and hydrocarbon generation. Kansas State University MS Thesis.

Lee, G.H., Lee, K., and Kim, H.J. 2009. Tuning effects' impact on seismic. AAPG Explorer, October, 32.

Lumley, D.E., Behrens, R.A., and Wang, Z. 1997. Assessing the technical risk of a 4-D seismic project. The Leading Edge, **16**.

Merriam, D.F. 1963. The geologic history of Kansas. Kansas Geological Survey Bulletin 162.

Miller, R.D., Raef, A.E., Byrnes, A.P., and Harrison, W.E. 2007. 4-D high-resolution seismic reflection monitoring of miscible CO2 injected into a carbonate reservoir. Final Report, September 2007.

Newell, K.D., Watney, W.L., Cheng, S.W.L., and Brownrigg, R.L. 1987. Stratigraphic and spatial distribution of oil and gas production in Kansas. Kansas Geological Survey, Subsurface Geology Series 9.

O'Brien, J., Moran, J., Wilbourn, G., Morris, S., Andersen, J., and Quezada, O. 2010. Monitoring a CO2 flood with fine time steps: Salt Creek 4D. The Leading Edge, **29**.

Palaz, I., and Marfurt, K.J. 1997. Carbonate seismology: an overview. In: *Carbonate Seismology*, I. Palaz and K.J. Marfurt (Eds.), Geophysical Development Series No. 6, SEG, Tulsa, OK.

Partyka, G., Gridley, J., and Lopez, J. 1999. Interpretational applications of spectral decomposition in reservoir characterization. The Leading Edge, **18**.

Raef, A.E., and Miller, R.D. 2006. A non-differencing approach to seismic monitoring: implications for difficult carbonate reservoirs. SEG Annual Meeting, New Orleans, LA.

Raef, A.E., Miller, R.D., Byrnes, A.P., and Harrison, W.E. 2004. 4D seismic monitoring of the miscible CO2 flood of Hall-Gurney Field, Kansas, U.S. The Leading Edge, **23**.

Raef, A.E., Miller, R.D., Byrnes, A.P., Franseen, E.K., Watney, W.L., and Harrison, E.H. 2005a. A new approach for weak time-lapse anomaly detection using seismic attributes: geology and production data integrated monitoring of miscible EOR-CO2 flood in carbonates. SEG Annual Meeting, Houston, TX.

Raef, A.E., Miller, R.D., Byrnes, A.P., and Harrison, W.E. 2005b. Rock physics and seismic modeling guided application of 4D-seismic attributes to monitoring enhanced oil recovery CO2-flood in a thin carbonate reservoir, Hall Gurney Field, Kansas, U.S.A.

AAPG Annual Meeting, Calgary, Alberta, Canada. AAPG Search and Discovery Article #90039.

Raef, A.E., Miller, R.D., Byrnes, A.P., Harrison, W.E., and Franseen, E.K. 2005c. Time-lapse seismic monitoring of enhanced oil recovery CO2-flood in a thin carbonate reservoir, Hall-Gurney Field, Kansas, U.S.A. AAPG Annual Meeting, Calgary, Alberta, Canada.

Raef, A.E., Miller, R.D., Franseen, E.K., Byrnes, A.P., and Watney, W.L. 2005d. 4D seismic to image a thin carbonate reservoir during a miscible CO2 flood: Hall-Gurney Field, Kansas, U.S.A. The Leading Edge, **24**.

Raef, A.E., Miller, R.D., Byrnes, A.P., and Harrison, W.E. 2006a. Impact of improved seismic resolution and signal-to-noise ratio on monitoring pore-fluid composition changes: CO2-injection, Hall Gurney Field, Kansas, U.S.A. Search and Discovery Article #90052.

Raef, A.E., Miller, R.D., Byrnes, A.P., and Harrison, W.E. 2006b. Pore-fluid composition oriented 4-D seismic data processing and interpretation: implications for monitoring EOR and/or sequestration of CO2. AAPG Rocky Mountain Section Meeting, Billings, MT. AAPG Search and Discovery Article #90055.

Riggs, C.H., Heath, L.J., Ward, D.C., and Huff, R.V. 1963. Petroleum-engineering study of the Hall-Gurney oilfield, Russell County, Kansas. Bureau of Mines Report of Investigations 6134. United States Department of the Interior.

Sarg, J.F., and Schuelke, J.S. 2003. Integrated seismic analysis of carbonate reservoirs: from the framework to the volume attributes. The Leading Edge, **22**.

Skirius, C., Nissen, S., Haskell, N., Marfurt, K., Hadley, S., Ternes, D., Michel, K., Reglar, I., D'Amico, D., Deliencourt, F., Romero, T., D'Angelo, R., and Brown, B. 1999. 3-D seismic attributes applied to carbonates. The Leading Edge, **3**.

Stammeijer, J.G.F., and Hatchell, P.J. 2014. Standards in 4D feasibility and interpretation. The Leading Edge, **33**.

Taner, M.T. 1983. Joint time/frequency analysis, Q quality facor and dispersion computation using Gabor-Morlet wavelets or Gabor-Morlet transform. Rock Solid Images.

Verma, M.K. 2015. Fundamentals of carbon dioxide-enhanced oil recovery (CO2-EOR) – a supporting document of the assessment methodology for hydrocarbon recovery using CO2-EOR associated with carbon sequestration. U.S. Geological Survey Open-File Report 2015-1071.

Wang, Z. 2001. Fundamentals of seismic rock physics. Geophysics, **66**, No. 2.

Watney, W.L. 1980. Cyclic sedimentation of the Lansing-Kansas City Groups in Northwestern Kansas and Southwestern Nebraska: a guide for petroleum exploration. Kansas Geological Survey Bulletin 220.

Watney, W.L. 1994. Depositional sequence analysis and sedimentologic modeling for improved prediction of Pennsylvanian reservoirs. Final Report, U.S. DOE Contract DOE/BC/14434-13.

Watney, W.L. 2015. Reservoir lithofacies and their recent analogs. AAPG Education Course: Petrophysical Analysis and Integrated Approaches to the Study of Carbonate Reservoirs. April 21-23, 2015. Austin, TX.

Watney, W.L., Franseen, E.K., Byrnes, A.P., Miller, R., Raef, A.E., Reeder, S.L., and Rankey, E.C. 2006. Characterization of seismically-imaged Pennsylvanian ooid shoal geometries and comparison with modern. AAPG Annual Convention, Houston, TX. Search and Discovery Article #20038.

Watney, W.L., Byrnes, A.P., Franseen, E.K., Dubois, M.K., Miller, R., Raef, A.E., Reeder, S.L., Rankey, E.C., Cruz, F.E., and Eberli, G.P. 2007. Characterization of seismically-imaged Pennsylvanian ooid shoal geometries and comparison with modern.

Widess, M.B. 1973. How thin is a thin bed? Geophysics, **38**, No. 6.

Willhite, G.P., Byrnes, A.P., Green, D.W., Pancake, R., Tsau, J.S., Watney, W.L., Doveton, J., Guy, W., Reynolds, R., Murfin, D., Daniels, J., Marin, R., Flanders, W., Griend, D.V., Mork, E., and Cantrell, P. 2010. Field demonstration of carbon dioxide miscible flooding in the Lansing-Kansas City Formation, central Kansas. Final Report, March 7, 2010.

Willhite, G.P., Byrnes, A.P., Dubois, M.K., Pancake, R.E., Tsau, J.S., Daniels, J.R., and Flanders, W.A. 2012. A pilot carbon dioxide test, Hall-Gurney Field, Kansas. SPE Reservoir Evaluation & Engineering.

Xu, S., and Payne, M.A. 2009. Modeling elastic properties in carbonate rocks. The Leading Edge, **28**.

Yam, H., and Schmitt, D.R. 2011. CO2 rock physics: a laboratory study. Canadian Well Logging Society Insite Magazine, **30**.